

Metabolic Regulation of the Ubiquitin-Proteasome System

Inaugural-Dissertation

zur

Erlangung des Doktorgrades

der Mathematisch-Naturwissenschaftlichen Fakultät

der Universität zu Köln



vorgelegt von

Sonia Ravanelli

aus Trento, Italien

Köln, 2021

Referees / Gutachter:

Prof. Dr. Thorsten Hoppe

Institut für Genetik, CECAD Forschungszentrum

Universität zu Köln

Prof. Dr. Elena I. Rugarli

Institut für Genetik, CECAD Forschungszentrum

Universität zu Köln

Chair/ Vorsitzende/r :

Prof. Dr. Jan Riemer

Institut für Biochemie

Universität zu Köln

Tag der mündlichen Prüfung: 26.01.2022

The work described in this dissertation was conducted during May 2016 and September 2021 under the supervision of Prof. Dr. Thorsten Hoppe at the CECAD Research Center, University of Cologne, Joseph-Stelzmann Str. 26, 50931 Cologne, Germany.

Die in dieser Dissertation beschriebenen Arbeiten wurden zwischen Mai 2016 und September 2021 unter der Betreuung von Prof. Dr. Thorsten Hoppe am CECAD Research Center, Universität zu Köln, Joseph-Stelzmann Str. 26, 50931 Köln, Deutschland

Parts of this thesis project have been published or accepted for publication:

Ravanelli, S., den Brave, F., and Hoppe, T. Mitochondrial Quality Control Governed by Ubiquitin. *Front Cell Dev Biol.* (2020).

Ravanelli, S., Li Q., Annibal A., Trifunovic A., Antebi A., Hoppe T. Reprogramming of Proteasomal Degradation by Branched Chain Amino Acid Metabolism. *Aging Cell.* (2022).

Efstathiou S., Ottens F., Schütter L., Ravanelli S., Charmpilas N., Gutschmidt A., Le Pen J., Gehring N. H., Miska E. A., Bouças J., Hoppe T. ER-Associated RNA Silencing Promotes ER Quality Control. *Nature Cell Biology.* (2022).

Table of contents

1.1	Acknowledgements	6
1.2	List of abbreviations.....	7
1.3	Summary	9
1.4	Zusammenfassung.....	10
2	Introduction	11
2.1	Proteostasis.....	12
2.1.1	The ubiquitin-proteasome system (UPS).....	13
2.1.2	The 26S proteasome	16
2.1.3	UPS regulation through adaptive gene expression	17
2.1.4	Proteasomal adaptation to cellular needs	19
2.2	Mitochondrial protein quality control.....	21
2.2.1	Mitochondrial unfolded protein response.....	21
2.2.2	The role of the UPS in mitochondrial quality control	23
2.3	Metabolic Regulation of Proteostasis	26
2.3.1	Branched chain amino acid metabolism	27
2.3.2	BCAAs: biomarkers or supplements?.....	28
2.4	Rationale and aim of the project.....	29
3	Results	31
3.1	Mitochondrial stress can modulate UPS substrate specificity without UPR ^{mt} induction	32
3.2	<i>acs-19</i> allele-specific phenotypes reveal the presence of background mutations	33
3.3	Defective leucine catabolism integrates known stress response pathways.....	38
3.4	Specific types of mitochondrial stress regulate the UPS.....	41
3.5	Transamination of BCAAs is physiologically essential.....	43
3.6	<i>C. elegans</i> BCAT-1 is the ancestor of both mammalian BCAT paralogs.....	47
3.7	BCAA transamination and downstream catabolic steps play opposing roles in proteostasis.....	48
3.8	Multi-omics analysis reveals cooperative and antagonistic roles of IVD-1 and BCAT-1	51
3.9	Impaired BCAA metabolism defines transcriptional programs.....	56
3.10	Changes in the BCAA metabolism induce an adaptive metabolic regulation.....	59
3.11	Isovaleric acid directly affects proteostasis.....	63
4	Discussion.....	67
4.1	The BCAA metabolism takes on distinct roles in proteostasis regulation	69
4.2	BCAA-derived intermediates influence proteostasis	70
4.3	BCAA metabolism regulates UPS specificity	72

4.4	<i>C. elegans</i> model system to study the physiological roles of BCAA metabolism	73
4.5	Disease relevance and possible novel therapies	74
4.6	Outlook	75
5	Materials and Methods	79
5.1	<i>C. elegans</i> techniques	80
5.1.1	Solutions and reagents	80
5.1.2	Strains and cultivation methods	80
5.1.3	Strain generation by crossing	81
5.1.4	Strain generation by CRISPR-Cas9	82
5.1.5	Population synchronization	83
5.1.6	Gene knock-down by RNAi feeding	84
5.1.7	Targeted metabolic RNAi screen	84
5.1.8	Embryonic lethality quantification	85
5.1.9	Generation time quantification	85
5.1.10	Viable progeny quantification	86
5.1.11	Chemical supplementation	86
5.2	Molecular biology	87
5.2.1	Solutions and reagents	87
5.2.2	Genotyping	88
5.2.3	Western blot	89
5.2.4	RNA extraction	90
5.2.5	qRT-PCR	90
5.3	Microscope imaging	91
5.3.1	Live imaging	91
5.3.2	Imaging quantification	92
5.4	Multi-omics analysis	93
5.5	Data processing, statistical analysis and bioinformatics	94
5.5.1	Software, databases, and online resources	94
5.5.2	Subcellular localization prediction	95
5.5.3	Multi-omics data processing	95
5.5.4	Phylogenetic analysis	96
	References	98
	Appendix	119
	Declaration for the doctoral thesis / Erklärung zur Dissertation	128
	Curriculum vitae	129

1.1 Acknowledgements

First of all, I would like to thank my supervisor Prof. Thorsten Hoppe for mentoring me during the entire PhD project and giving me the opportunity to work independently in the lab, learn how to write a scientific review and also help revising scientific manuscripts. I'm also glad he was always open to share his professional experience, talking about career choices and details about the academic life.

I'm grateful to my thesis referees Prof. Elena Rugarli and Prof. Jan Riemer who have supported me throughout the PhD project from the start till the end.

It was a pleasure and an honor to be part of the mito-RTG (SFB 1218). This research training group was incredibly helpful to develop as scientist, in addition to great scientific discussions, I learned how to organize retreats and conferences. Particularly, I would like to express my deep gratitude to our coordinator Katerina, who accompanied me during this entire journey.

A special thank goes to all members, present and past, of the Hoppe lab. I really enjoyed the relaxed atmosphere and the constant collaborative attitude of all members. In particular, I would like to mention Laylan, Vishnu, Kavya, Ricardo, and Carl with whom I had great scientific and non-scientific discussions and together we crafted awesome PhD hats and wagons. I also had fun in sharing with Soto my enthusiasm in the basic bioinformatics I learned in these years while analyzing RNAseq data together. I'm thankful to Fabian with whom I collaborated closely to write the mitochondrial quality control review, that was a really nice and constructive experience.

I'm grateful to Qiaochu, who joined the lab only recently and in few weeks greatly enhanced the potential of the manuscript we recently submitted. I sincerely thank Andrea not only for performing the metabolomics analysis but also for discussing the whole project several times. I also would like to thank Alex for fruitful discussions and all the other people that contributed to the manuscript.

A special thanks is dedicated to the technicians and secretaries Agata, Ela, Gaby, Karoline and Kerstin. Their kindness and availability to help me was of great support during my time in the lab. In particular, Agata, with her positive attitude, was really a good companion and a fantastic psychological support also during the most stressful times.

I would like to express my deep gratitude to André for being always there, ready to help, explain, and collaborate in any occasion. He always found time even when it was really short, also to read my thesis and to write the protocol. I really learned a lot from him and enjoyed working together.

Last, but not least, I would like to thank my family and friends in Italy who supported me from there and made my holidays always nice and recharging. Martin also contributed to this PhD project by discussing scientific concepts, teaching me a little of the obscure world of structural biology. Then of course I thank Mathias, who was incredibly important to cope with stressful moments and to share scientific thoughts that greatly contributed to my PhD project.

1.2 List of abbreviations

AAA+	ATPases associated with various cellular activities
ACS-19	acetyl-CoA synthetase 19
AMP	adenosine monophosphate
AMPK	AMP-activated kinase
ATF4	activating transcription factor 4
ATFS-1	activating transcription factor associated with stress
ATP	adenosine triphosphate
BCAA	branched chain amino acid
BCAT	branched chain amino acid transaminase
BCKA	branched chain α -keto acid
BCKDH	branched chain amino acid dehydrogenase
C-terminal	carboxy-terminal
CGC	Caenorhabditis Genetics Center
CoA	Coenzyme A
DAF-16	abnormal dauer Formation 16
DNA	deoxyribonucleic acid
DTT	dithiothreitol
DUB	de-ubiquitylating enzyme
E1	ubiquitin-activating enzyme
E2	ubiquitin-conjugating enzyme
E3	ubiquitin ligase
E4	ubiquitin-chain elongation factor
eIF2 α	eukaryotic translation initiation factor 2
EMS	ethyl methane sulfonate
ER	endoplasmic reticulum
ERAD	ER-associated degradation
ETC	electron transport chain
FPKM	fragments per kilobase of transcript per million
GABA	γ -aminobutyric acid
GFP	green fluorescent protein
HECT	homologous to E6-AP C-terminus
HIF	hypoxia inducible factor
HSD	Tukey's Honest Significant Difference
Hsf	heat shock transcription factor
Hsp	heat shock protein
HSR	heat shock response
IMM	inner mitochondrial membrane
IMS	intermembrane space
ISR	integrated stress response

IVA	isovaleric acid
IVD	isovaleryl-CoA dehydrogenase
Lys-C	lysyl endopeptidase
MAD	mitochondria-associated degradation
MAPK	mitogen-activated protein kinase
MHC	major histocompatibility complex
mtDNA	mitochondrial DNA
mTOR	mechanistic target of rapamycin
N-terminal	amino-terminal
Nrf	Nuclear factor erythroid 2-related factor
OMM	outer mitochondrial membrane
polyQ	polyglutamine
PQC	protein quality control
PSC	premature stop codon
RING	really interesting new gene
RNA	ribonucleic acid
RNAi	RNA interference
ROS	reactive oxygen species
Rpn	Regulatory particle non-ATPase subunit
SKN-1	skinhead 1
TCA	tricarboxylic acid
TEAB	triethylammonium bicarbonate
UFD	ubiquitin fusion degradation
Unc	unchoordinated
uORF	upstream open reading frame
UPR	unfolded protein response
UPR ^{mt}	mitochondrial unfolded protein response
UPS	ubiquitin-proteasome system
UTR	untranslated region
WT	wild-type
YFP	yellow fluorescent protein

1.3 Summary

Metabolic and protein networks are highly dynamic and flexible; therefore, efficient surveillance of both networks is required to maintain cellular and organismal integrity. The ubiquitin-proteasome system (UPS) ensures selective turnover of damaged proteins, avoiding accumulation of potentially toxic proteins and restoring the amino acid pool. Previously, our lab demonstrated that metabolic defects reduce the UPS function without activating the mitochondrial unfolded protein response (UPR^{mt}). Depletion of the leucine catabolic enzyme isovaleryl-CoA dehydrogenase (IVD) impaired the turnover of a fluorescently tagged UPS substrate both in *C. elegans* and in mammalian cells, identifying a previously unknown link between proteostasis loss and the metabolic disorder isovaleric acidemia. However, the mechanistic regulation of the UPS by leucine catabolism remained to be determined. Combining genetic and multi-omics approaches in *C. elegans*, I demonstrated that altered BCAT-1, the enzyme responsible for the first step of the branched chain amino acid (BCAA) metabolism, can restore UPS defects observed upon defective IVD-1. Particularly, the transcription of proteasome regulatory subunits is reduced in *ivd-1* loss-of function mutants, which might reflect an adaptive response mechanism. Conversely, the *bcat-1(hh58)* mutant allele promoted the expression of proteasome subunits in *ivd-1* loss-of-function mutants suggesting a recovery of the proteasomal capacity. Supplementation of isovaleric acid (IVA), an intermediate metabolite accumulating in the body fluids of isovaleric acidemia patients, impaired the UPS and enhanced aggregation of metastable proteins. Collectively, my work contributes to the current knowledge related to the etiology of the metabolic disorder isovaleric acidemia, identifying proteostasis loss as a contributing pathological event and the BCAA transamination as a novel potential therapeutic target. Since impaired BCAA metabolism has been linked to a multitude of pathological states, the identified connection between BCAA metabolism and the UPS might also be relevant for the development of clinical interventions for the treatment of cardiovascular diseases, diabetes, cancer, and neurodegenerative disorders.

1.4 Zusammenfassung

Stoffwechsel- und Proteinnetzwerke sind dynamisch und flexibel; daher ist eine effiziente Überwachung beider Netzwerke erforderlich, um die zelluläre Integrität zu erhalten. Das Ubiquitin-Proteasom-System (UPS) sorgt für den selektiven Umsatz geschädigter Proteine und verhindert dadurch die Anhäufung toxischer Proteine. Frühere Ergebnisse aus unserem Labor haben gezeigt, dass Stoffwechselddefekte die Funktion des UPS verringern, ohne die mitochondriale Reaktion auf ungefaltete Proteine (UPR^{mt}) zu aktivieren. Die Deletion des Enzyms Isovaleryl-CoA-Dehydrogenase (IVD) verhinderte den Umsatz eines fluoreszenzmarkierten UPS-Substrats sowohl in *C. elegans* als auch in Säugetierzellen, wodurch eine bisher unbekannt Verbindung zwischen dem Verlust von Proteostase und der Stoffwechselstörung Isovalerianazidämie identifiziert wurde. Die mechanistische Verbindung zwischen der UPS-Regulierung und dem Leucin-Katabolismus war jedoch noch nicht geklärt. Durch die Kombination von Genetik und Multi-omics in *C. elegans* konnte ich zeigen, dass eine Veränderung von BCAT-1, das für den ersten Schritt des Stoffwechsels der verzweigtkettigen Aminosäuren (BCAA) verantwortliche Enzym, die UPS-Defekte wiederherstellen kann. Insbesondere ist die Transkription der regulatorischen Untereinheiten des Proteasoms in *ivd-1*-Funktionsverlustmutanten reduziert, was einen adaptiven Reaktionsmechanismus darstellen könnte. Umgekehrt förderte das *bcat-1(hh58)*-Mutantenallel die Expression von Proteasom-Untereinheiten in *ivd-1*-Funktionsverlustmutanten, was auf eine wiederhergestellte proteasomale Kapazität hinweist. Die Verabreichung von Isovaleriansäure, die sich in den Körperflüssigkeiten von Isovalerianazidämie-Patienten anreichert, führte zu einer direkten Beeinträchtigung des UPS und einer verstärkten Aggregation metastabiler Proteine. Insgesamt trägt meine Arbeit zum aktuellen Wissensstand über die Ätiologie der Isovalerianazidämie bei, indem sie den Verlust der Proteostase als pathologisches Ereignis nahelegt und die BCAA-Transaminierung als neues potenzielles therapeutisches Ziel identifiziert. Da ein gestörter BCAA-Stoffwechsel mit einer Vielzahl von pathologischen Zuständen in Verbindung gebracht wird, könnte die identifizierte Verbindung zwischen BCAA-Stoffwechsel und UPS auch für die Entwicklung klinischer Interventionen zur Behandlung von Herz-Kreislauf-Erkrankungen, Diabetes, Krebs und neurodegenerativen Störungen von Bedeutung sein.

2 Introduction

2.1 Proteostasis

Proteins constitute biological core elements that are important for cellular structure, motility, communication, and energy production. The entire set of all proteins of an organism, termed the proteome, is highly dynamic and flexible in order to adapt in response to endogenous and exogenous insults. A sophisticated network of protein quality control (PQC) pathways surveils the proteome in a joint effort to maintain protein homeostasis, or proteostasis (Hipp et al., 2019; Hoppe and Cohen, 2020; Kaushik and Cuervo, 2015; Klaipe et al., 2018; Pilla et al., 2017). The concept of proteostasis was first described in 2008 (Balch et al., 2008) and refers to the cooperative action of multiple molecular mechanisms that adapt the proteome by surveilling concentration, conformation, binding interactions and location of proteins. In other words, the entire protein life cycle is assisted by specialized PQC machineries. Protein synthesis is regulated by coupling transcriptional and translational processes (Pakos-Zebrucka et al., 2016; Richter et al., 2010; Shpilka and Haynes, 2018; Walter and Ron, 2011). Folding of the nascent polypeptide chains and mature proteins is facilitated by molecular chaperones, which counteract misfolding and the possible formation of protein aggregates (Balchin et al., 2016; Hartl et al., 2011). Molecular chaperones and several binding partners contribute also to the correct protein localization or their targeting for degradation (Kriegenburg et al., 2012). Ultimately, damaged or superfluous proteins are degraded either by the ubiquitin-proteasome system (UPS) or the autophagy-lysosome pathway (Pilla et al., 2017; Pohl and Dikic, 2019). In optimal conditions, all these PQC machineries ensure dynamic proteome adaptations in response to changing physiological conditions. Whereas, various types of stress that might impact proteostasis are compensated by the activation of alternative protective mechanisms that foster the capacity of the PQC system restoring proteostasis (Pilla et al., 2017). Loss of proteostasis has been associated with several pathologies, including aging-related diseases, neurodegeneration, cancer, and metabolic disorders (Balchin et al., 2016; Hipp et al., 2019; Hoppe and Cohen, 2020; Labbadia and Morimoto, 2015; Ottens et al., 2021). Consequently, molecular mechanisms involved in proteostasis maintenance have been extensively studied due to their relevance for medical research.

2.1.1 The ubiquitin-proteasome system (UPS)

Eukaryotic cells are equipped with two conserved protein degradation systems: the autophagy-lysosome pathway and the UPS (Dikic, 2017). The autophagy-lysosome pathway is responsible for the removal of large cellular components such as protein aggregates or organelles. The UPS ensures selective degradation of soluble short-lived proteins as well as misfolded and damaged proteins (Pilla et al., 2017; Pohl and Dikic, 2019; Vilchez et al., 2014). Autophagy is strongly induced by starvation, providing recycled molecular building blocks that ensure cell survival under nutrient deprivation; whereas, in optimal conditions cells can survive without autophagy (Nakatogawa et al., 2009; Ohsumi, 2014; Tsukada and Ohsumi, 1993). In contrast, numerous genes encoding for UPS components, such as proteasome subunits or ubiquitin, are essential, because the protein turnover by the UPS is required also upon nutrient availability (Finley, 2009; Rousseau and Bertolotti, 2018; Ryu et al., 2007). Although autophagy and the UPS are characterized by distinct degradation mechanisms and specialized substrate specificity, both degradation systems share ubiquitin as a common degradation signal (Pohl and Dikic, 2019). Ubiquitin is a 76-residue peptide which is highly conserved among eukaryotes and its conjugation to a protein substrate is termed ubiquitylation. Ubiquitylation is catalyzed by an enzymatic cascade of three steps: (I) in a first ATP-dependent reaction (Kipreos, 2005), a high-energy thioester bond is formed between the catalytic cysteine of a ubiquitin-activating enzyme (E1) and the C-terminal glycine residue of ubiquitin (Gly76); (II) the ubiquitin is then transferred to the catalytic cysteine of a ubiquitin-conjugating enzyme (E2); (III) finally, specific ubiquitin ligases (E3) facilitate the covalent attachment of ubiquitin to the selected substrate, mostly to a lysine residue (Figure 1A) (Kerscher et al., 2006; Passmore and Barford, 2004; Schulman and Wade Harper, 2009; Ye and Rape, 2009).

Repeated ubiquitylation cycles result in numerous combinations of either multiple mono-ubiquitylation of different lysine residues on a substrate protein or formation of ubiquitin chains by targeting lysine residues within ubiquitin itself, a process that is assisted by ubiquitin-chain elongation factors or E4 enzymes (Hoppe, 2005). Ubiquitin contains 7 different lysine residues and depending on the lysine residue targeted for

further ubiquitylation (K6, K11, K27, K29, K33, K48, or K63), several types of ubiquitin chains, linear or branched, can be formed (Akutsu et al., 2016; Haakonsen and Rape, 2019; Komander and Rape, 2012). Importantly, deubiquitylating enzymes (DUB) reverse the ubiquitylation reaction by either completely removing ubiquitin from substrates or by trimming/editing ubiquitin chains to alter their composition (Clague et al., 2019; Kuhlbrodt et al., 2005). The numerous combinations, termed the “ubiquitin code” (Komander and Rape, 2012), serve as specialized signals for various downstream events mediated by specialized binding partners. Well described ubiquitin chains are the linear K63-, K11-, and K48-linked chains. K63-linked ubiquitin chains coordinate the assembly of machineries involved in autophagy, DNA repair, translation, and immune response; whereas the K11- and K48-linked ubiquitin chains are typically associated with UPS degradation. However, several ubiquitin chains are not linear and characterized by a more heterotypic nature. For example, substrates expressed in yeast, which are N-terminally fused with ubiquitin and termed ubiquitin fusion degradation (UFD) substrates, are initially modified by the E3 UFD4, before the E4 UFD2 assembles K29/K48-branched chains (Johnson et al., 1995; Koegl et al., 1999; Liu et al., 2017).

The UPS is physiologically relevant not only for the removal of damaged proteins, but also for the turnover of regulatory proteins involved in several cellular processes including apoptosis, stress response, and cell cycle progression (Bard et al., 2018; Rousseau and Bertolotti, 2018; Schmidt and Finley, 2014; Vilchez et al., 2014). Consequently, UPS malfunction, occurring at multiple levels of the pathway, is associated with numerous age-related and genetic diseases, including neurodegeneration and cancer (Deshaies and Joazeiro, 2009; Franz et al., 2014; Nalepa and Wade Harper, 2003; Rousseau and Bertolotti, 2018; Wang et al., 2020). The high versatility of the system relies mainly on the hierarchical structure of the UPS components (Glickman and Ciechanover, 2002): one single E1 can activate ubiquitin for several E2 enzymes, most of which interact with more than one E3 ligase, which in turn ubiquitylate multiple substrates. Accordingly, lower eukaryotes, including yeast, worms and flies, possess only one E1, while higher organisms, from zebrafish to humans, express two E1s (Schulman and Wade Harper, 2009). Conversely, at least 13, 20, and 38 genes encode for E2s in yeast, worms, and humans, respectively (Jones et al., 2001; Kipreos, 2005; Ye and Rape, 2009); whereas,

the E3 protein family comprises 80 members in yeast and more than 600 in mammals (Li et al., 2008).

Not only this hierarchical structure consents versatile degradation of myriad of substrates but also a high degree of substrate selectivity, which is mostly driven by the pairing of E2s and E3s. One class of E3, the homologous to E6-associated protein C-terminus (HECT) E3s, form a thioester bond with ubiquitin, determining the specificity of ubiquitin-linkage to the substrate independently of E2s (Komander and Rape, 2012; Wang et al., 2020). However, most E3 ligases contain a really interesting new gene (RING) domain or a RING-related U-box domain and bind simultaneously to the ubiquitin-E2 thioester complex and the substrate. Consequently, both E3s and E2s participate actively in the selective recognition of substrates and in the determination of specialized ubiquitin chains (Komander and Rape, 2012; Ye and Rape, 2009). The UPS versatility and selectivity is further complemented by numerous interacting partners, participating in the substrate recognition and shuttling to the proteasome (Franz et al., 2014; Komander and Rape, 2012; Kriegenburg et al., 2012). Moreover, the complex and dynamic structure of the 26S proteasome holoenzyme contributes to the UPS flexibility (Bard et al., 2018) (Figure 1B).

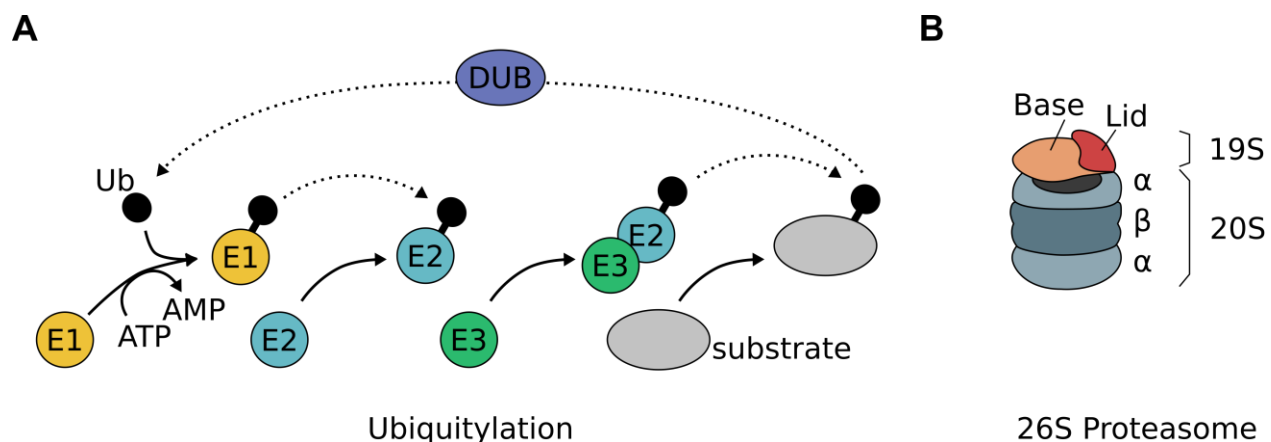


Figure 1 Ubiquitin-proteasome system

(A) Ubiquitylation is a protein post-translational modification that occurs through an enzymatic cascade involving E1, E2, and E3 enzymes and can be reversed by the deubiquitylating enzymes (DUB), only the first step requires ATP (B) The 26S proteasome is constituted by a core catalytic subunit (20S), composed of four stacked heptameric rings (2 external α and 2 internal β), and a

regulatory particle (19S), which is formed by a lid and a base (details in Chapter 2.1.2).

2.1.2 The 26S proteasome

The proteolytic active sites of the 26S proteasome reside inside the chamber of a barrel-shaped multicatalytic complex, named the 20S core particle, which is assembled of four stacked heptameric rings, 2 external and 2 internal, each composed of α and β subunits, respectively. Recognition, unfolding, and translocation of the substrate into the narrow pore of the 20S particle is mediated by the 19S regulatory particle, which contains a base and a lid structure (Figure 1B). The base constitutes a hexameric complex of ATPases of the AAA+ (ATPases associated with various cellular activities) family (Sauer and Baker, 2011) and four additional non-ATPase subunits. The lid contains nine non-ATPase subunits and acts as a scaffold that braces one side of the base. Among these nine subunits, the DUB Rpn11, together with other stably associated DUBs, is responsible for the substrate de-ubiquitylation before its contact with the AAA+ ATPase subunits (Bard et al., 2018; Collins and Goldberg, 2017; Rousseau and Bertolotti, 2018). The standard proteasome composition is reported in Table 1, where proteasome subunits and their functions are reported following the systematic nomenclature (Coux et al., 1996; Finley et al., 1998).

Table 1 Proteasome composition

PARTICLE	SUBUNITS	FUNCTION
20S	α 1- α 7	Gating
	β 1- β 7	Proteolysis
19S - Base	Rpt1-Rpt6	AAA-ATPase activity
	Rpn1, Rpn2, Rpn10, Rpn13	Substrate docking by ubiquitin binding (Rpn2 has more structural function)

19S - Lid	Rpn3, Rpn5-9, Rpn12, Sem1	Structural
	Rpn11	Deubiquitylation

2.1.3 UPS regulation through adaptive gene expression

In response to changing environmental conditions, UPS capacity and substrate specificity are promptly regulated through a plethora of molecular mechanisms, including programs that adapt gene expression of UPS components, both at the transcriptional and the translational level. Adaptive gene expression regulation represents a highly conserved cellular strategy to compensate fluctuations in the cellular environment. The heat shock response (HSR) represents one of the first adaptive gene expression regulation extensively studied; it was discovered in the early '60 in flies, and later observed in multiple organisms, including both prokaryotes and eukaryotes (Lindquist and Craig, 1988; Morimoto, 1993; Richter et al., 2010; Ritossa, 1962). The preferred expression of certain genes in response to heat led to coin the term heat shock proteins (Hsps), although it became soon clear that other types of stress could also induce this response (Ashburner and Bonner, 1979). The Hsps encompass mostly molecular chaperones and components of the proteolytic system including several UPS factors, but also other regulatory proteins involved in the maintenance of cellular integrity such as metabolic enzymes, transcription factors, kinases, and DNA/RNA modifying proteins (Richter et al., 2010). In eukaryotes, the HSR is triggered by the activation of the conserved heat shock transcription factor Hsf1. Under normal conditions, Hsf1 is kept in an inactive monomeric form by interacting with the chaperones Hsp70 and Hsp90. Whereas during stress, accumulated unfolded proteins sequester the available chaperones, including Hsp70 and Hsp90, facilitating the formation of Hsf1 homotrimers, which translocate to the nucleus to activate gene expression (Morimoto, 1993; Richter et al., 2010). Other specialized adaptive mechanisms apply a similar gene regulatory strategy to flexibly remodel the cellular physiology to variable needs and efficiently combat stress, like for example the unfolded protein responses in the endoplasmic reticulum (ER) and mitochondria—UPR and UPR^{mt},

respectively (more details in Chapter 2.2.1).

In response to multiple stress conditions, eukaryotic cells couple transcriptional activation of protective genes with reduction of global protein translation, favoring synthesis of specialized proteins required for cell recovery and survival. This adaptive mechanism has been proposed as the integrated stress response (ISR), which central hub consists in the phosphorylation of the eukaryotic translation initiation factor 2 (eIF2 α), leading to global translation reduction and induction of particular proteins, including the ER-stress induced transcription factor ATF4 (Ron, 2002). Mechanistically, phosphorylation of the eIF2 α inhibits translation of 5'-capped mRNAs favoring translation of selected mRNAs containing a short upstream open reading frame (uORF) in their 5' untranslated region (UTR), such as ATF4 (Pakos-Zebrucka et al., 2016; Ron, 2002; Sonenberg and Hinnebusch, 2009). Several kinases phosphorylate the eIF2 α and multiple uORF-containing transcription factors were identified as part of individual stress responses such as the UPR or the UPR^{mt}, demonstrating that this molecular mechanism of translation regulation is a common node for various stress response pathways. Both hyperactive and hypoactive ISR are causally linked with disease, indicating that precise balance of the ISR activity is crucial for cell and tissue integrity. Consequently, compounds that either induce or inhibit the ISR have been proposed as clinical interventions for a variety of diseases including neurodegenerative diseases, cancer, and metabolic disorders (Costa-Mattioli and Walter, 2020).

A complementary biological approach to reduce translation in response to stress is the inhibition of the mechanistic target of rapamycin (mTOR), also mentioned as mammalian target of rapamycin (Saxton and Sabatini, 2017). mTOR is a protein kinase that coordinates cell growth with fluctuating environmental conditions. In optimal state, mTORC1 fosters protein synthesis through phosphorylation of several substrates, including the activation of the p70S6 kinase 1 (S6K1) and the suppression of the eIF4E-binding protein (4EBP). mTOR is also a major coordinator of energy metabolism and protein degradation. Besides the well-known activation of autophagy upon nutrient deprivation, inhibition of the mTOR pathway fosters UPS-dependent degradation, either by enhancing ubiquitylation (Zhao et al., 2015) or by upregulating the translation of

proteasome subunits and the assembly of chaperones via inhibition of the mitogen-activated protein kinase (MAPK) MPK1/Erk5 (Rousseau and Bertolotti, 2016).

2.1.4 Proteasomal adaptation to cellular needs

Proteasome abundance is not only regulated by the cellular energy state via mTOR (Rousseau and Bertolotti, 2016), but also by transcriptional and post-transcriptional mechanisms that regulate the expression of proteasome subunits according to cellular needs. Particularly, 26 out of the 32 yeast genes encoding for proteasome subunits share a common sequence element in their promoter regions (GGTGGCAA) termed proteasome associated control element (PACE), which is recognized by the transcription factor Rpn4 (Mannhaupt et al., 1999), previously called Son1 or Ufd5. Rpn4 stands for regulatory particle non-ATPase subunit 4, since it was found to interact with the 19S regulatory particle (Finley et al., 1998; Fujimuro et al., 1998). Besides basal transcription of proteasome subunits, Rpn4 participates in their induced expression in response to proteotoxic stress. Several stress-induced transcription factors, including Hsf1, mediate the expression of Rpn4 upon various stress conditions, ultimately promoting the proteasome abundance (Dohmen et al., 2007). Additionally, Rpn4 is a proteasome substrate and normally has a half-life of 2 min in unstressed cells. Consequently, Rpn4 protein levels directly reflect the current proteasomal degradation capacity and mediate a feedback regulation of the proteasome concentration (Dohmen et al., 2007; Fujimuro et al., 1998; Kruegel et al., 2011; Xie and Varshavsky, 2001). In higher organisms, a similar feedback loop is conducted by the nuclear factor erythroid 2-related factor 1 (Nrf1) in mammals (Koizumi et al., 2016) and its homologue SKN-1A in *C. elegans* (Lehrbach and Ruvkun, 2016). In normal conditions, Nrf1/SKN-1A is produced in the ER, retrotranslocated to the cytosol and degraded by the proteasome. Conversely, when the proteasome degradation efficiency is lower, Nrf1/SKN-1A is cleaved by the aspartyl protease DNA-damage inducible 1 (DDI2 in mammals and DDI-1 in *C. elegans*), becoming an active transcription factor that enhances proteasome production (Koizumi et al., 2016; Lehrbach and Ruvkun, 2016).

Although the transcriptional regulation of proteasome subunits is an efficient method to

modulate proteasome concentration and composition, it represents a time-consuming process compared with the more rapid post-translational modifications. Numerous proteasome subunits undergo reversible post-translational modification, among which phosphorylation is the most frequent and studied. More than 400 phospho-sites have been identified in the human proteasome and can influence the proteasome activity, composition, localization, and substrate specificity (Guo et al., 2017). Complementing the intricate transcriptional and post-transcriptional regulation programs, the intrinsically dynamic structure of the proteasome contributes to the UPS flexibility (Collins and Goldberg, 2017; Mayor et al., 2016; Rousseau and Bertolotti, 2018). Numerous assembly chaperones have been identified but we are still far from resolving the complexity of the proteasome assembly. Tissue-specific types of proteasomes have been observed to contain different combinations of 20S core subunits in order to fulfill specialized functions. One example is the mammalian immunoproteasome, which major role is to generate antigenic peptides for presentation on major histocompatibility complex (MHC) class I molecules. Together with the fact that the regulatory subunits bind to one or both ends of the 20S core subunits, a consistent number of possible hybrid compositions with alternative regulatory complexes further increases the number of available combinations (Rousseau and Bertolotti, 2018). Moreover, the proteasome has been reported to disassemble upon oxidative stress (Grune et al., 2011; Livnat-Levanon et al., 2014; Wang et al., 2010) or metabolic impairment (Meul et al., 2020), maintaining free 20S core subunits, possibly to reduce the specificity of substrate degradation and protect the proteasome complex from challenging conditions (Livnat-Levanon et al., 2014). Since modulation of the proteasome activity has major impact on the cellular proteostasis, targeting the proteasome and its assembly factors to boost the UPS capacity represents a promising therapeutic approach to counteract the aging-related progressive loss of proteostasis (Mayor et al., 2016; Rousseau and Bertolotti, 2018). Conversely, reduction of the proteasome activity can prevent the proliferation of cancer cells, as demonstrated by proteasome inhibitors, such as bortezomib, which are clinically administered to treat multiple myeloma (Grigoreva et al., 2015; Nalepa and Wade Harper, 2003).

2.2 Mitochondrial protein quality control

The UPS degrades proteins in the cytosol and in the nucleus; however, other cellular compartments rely on the UPS for protein clearance. Particularly, cytosolic UPS and mitochondrial protein quality control systems are tightly interconnected to ensure the dynamic regulation of the mitochondrial biomass in response to variable cellular conditions (Andréasson et al., 2019; Ravanelli et al., 2020; Song et al., 2021). Perturbations in cytosolic proteostasis affect the mitochondrial import system; conversely, mitochondrial dysfunction leads to accumulation of mistargeted proteins overloading the cytosolic proteostasis capacity. Along with constitutive protective mechanisms, operating to surveil physiological processes, numerous quality control pathways are exclusively activated in response to certain stressful conditions and are integrated with several adaptive gene regulatory programs. Deriving from α -proteobacterial ancestors, mitochondria are subdivided by an outer mitochondrial membrane (OMM) and an inner mitochondrial membrane (IMM), which separate the lumen into intermembrane space (IMS) and matrix. Mitochondria provide the cell with energy in form of ATP, but also with essential molecules such as amino acids, nucleotides, and iron-sulfur clusters (Lill and Mühlenhoff, 2008). However, the endosymbiotic integration of this organelle into eukaryotes generated also a series of evolutionary challenges, such as the complex logistics of two independent genomes (Youle, 2019). In fact, mitochondria retained their own DNA (mtDNA); however, 99% of mitochondrial proteins are nuclear-encoded proteins that need to be imported from the cytosol through sophisticated import machineries (Schmidt et al., 2010; Wiedemann and Pfanner, 2017). Consequently, expression, folding, and import of nuclear-encoded proteins into mitochondria are finely balanced with the organelle's gene expression.

2.2.1 Mitochondrial unfolded protein response

Several signaling pathways ensuring efficient mitochondria-nucleus communication have been investigated (Andréasson et al., 2019; Eisenberg-Bord and Schuldiner, 2017). One example is represented by the mitochondrial unfolded protein response (UPR^{mt}), which promotes the expression of nuclear genes to promote the mitochondrial proteostasis upon

stress (Jovaisaite and Auwerx, 2015; Melber and Haynes, 2018; Shpilka and Haynes, 2018). The name UPR was first proposed for the molecular mechanism triggered by ER stress, consisting in a first step of sensing the accumulation of unfolded proteins in the ER lumen, later extended to other ER stressors, and the subsequent signal transduction leading to gene expression regulation that, in turn, fosters the recovery of organellar proteostasis (Walter and Ron, 2011). Similarly, activation of the UPR^{mt} was reported for several different mitochondrial stress conditions, including mtDNA depletion, respiratory deficiency or accumulation of unfolded proteins (Jovaisaite and Auwerx, 2015; Melber and Haynes, 2018; Shpilka and Haynes, 2018). Even though first identified in mammalian cells (Martinus et al., 1996; Zhao et al., 2002), the UPR^{mt} mechanism has been characterized in *C. elegans* (Haynes et al., 2010; Nargund et al., 2012; Yoneda et al., 2004). UPR^{mt} activation is mediated by redirected transport of the activating transcription factor associated with stress (ATFS-1) into the nucleus as a consequence of mitochondrial import defects, thus serving as sensor of mitochondrial stress. Having both a nuclear and a mitochondrial localization sequence, ATFS-1 is normally imported into the mitochondrial matrix and degraded by the LON protease. Conversely, import defects favor the nuclear localization of ATFS-1, which in turn activates the transcription of UPR^{mt}-downstream genes (Nargund et al., 2012) (Figure 2). Although the downstream transcriptional regulation induced in case of mitochondrial stress is similar to *C. elegans*, the regulatory signaling of the mammalian UPR^{mt} is more complex and a general consensus model is still far from being delineated (Münch, 2018). The canonical mammalian UPR^{mt} axis, activated upon protein misfolding in the mitochondria, relies on the activation of the three bZIP transcription factors ATF4, ATF5, and CHOP, which expression depends on the ISR central event—the phosphorylation of the eIF2 α —highlighting the interconnection of different adaptive mechanisms (Münch, 2018; Shpilka and Haynes, 2018). Interestingly, ATF5 was suggested to be the mammalian orthologue of ATFS-1, since ATF5 could rescue the UPR^{mt} activation in *atfs-1*-depleted worms (Fiorese et al., 2016).

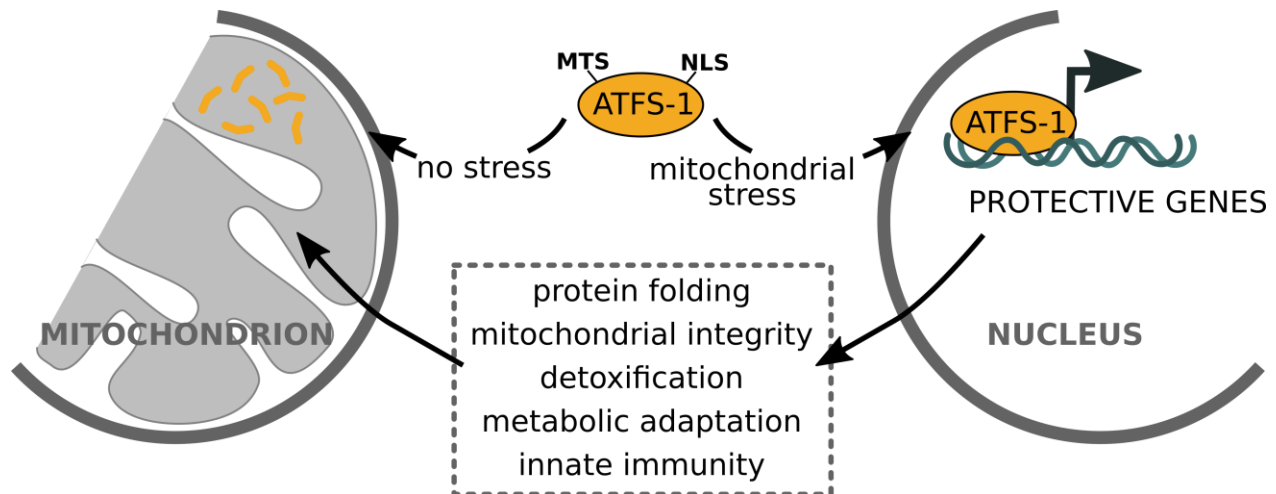


Figure 2 The mitochondrial unfolded protein response (UPR^{mt}) in *C. elegans*

Having both a mitochondrial targeting sequence (MTS) and a nuclear localization sequence (NLS), ATFS-1 is normally imported in the mitochondrial matrix and degraded by proteases. However, upon mitochondrial stress and subsequent defects in the mitochondrial import system, ATFS-1 is preferentially targeted to the nucleus where it induces the expression of protective genes, that in turn fosters PQC machineries restoring organismal homeostasis.

2.2.2 The role of the UPS in mitochondrial quality control

Mitochondria are equipped with an elaborate set of proteases acting both in the matrix and in the IMS to surveil the mitochondrial proteome from the inside (Glynn, 2017; Quirós et al., 2015). Nevertheless, the quality of the mitochondrial proteome is largely dependent on protein degradation conducted by the UPS (Escobar-Henriques et al., 2020; Ravanelli et al., 2020; Song et al., 2021). About 62% of the human mitochondrial proteome is ubiquitylated and hundreds of UPS components were predicted or experimentally proved to localize to the mitochondria and in many cases interact with mitochondrial matrix proteins. The presence of ubiquitylated proteins in the intact mitochondrial matrix was also confirmed; however, no evidence so far indicates that ubiquitylation can occur inside this compartment (Lehmann et al., 2016). In contrast, cytosolic protein degradation by the UPS emerged as a crucial process in the maintenance of mitochondrial integrity both in hormetic conditions as well as during stress (Escobar-Henriques et al., 2020; Lavie et al., 2018; Ravanelli et al., 2020; Song et al., 2021). The mitochondrial mass is efficiently regulated by the balanced regulation between biogenesis and degradation, two events

that are largely influenced by the UPS. In fact, not only is the UPS responsible for the degradation of damaged mitochondrial proteins, but also for the turnover of short-lived proteins, participating in the dynamic mitochondrial protein biogenesis (Bragoszewski et al., 2017; Song et al., 2021). Moreover, cytosolic protein degradation by the UPS participates in the surveillance of protein import into mitochondria, a process that is finely tuned to ensure mitochondrial functionality both under normal and stressed conditions (Song et al., 2021).

The best characterized organelle-specific branches of the UPS are the ER-associated degradation (ERAD) and the mitochondria-associated degradation (MAD), which specifically degrade proteins from ER and mitochondria, respectively. The basic mechanism consists of the ubiquitylation of the target proteins, the translocation to the cytosol and the subsequent degradation by the proteasome (Braun and Westermann, 2017; Franz et al., 2015; Guerriero and Brodsky, 2012; Heo and Rutter, 2011; Mehrtash and Hochstrasser, 2018; Ruggiano et al., 2014; Vembar and Brodsky, 2008). Mitochondria are tightly interconnected with other cellular organelles, especially the ER (Phillips and Voeltz, 2016; van Vliet et al., 2014). Accordingly, a certain degree of cooperation has been observed between the protein quality control machineries of these two tubular organelles. One great example was reported in two independent recent studies in yeast, which observed that mistargeted tail anchored (TA) proteins are extracted from the OMM by the AAA+ Msp1 and subsequently ubiquitylated by Doa10, an E3 ligase residing in the ER (Dederer et al., 2019; Matsumoto et al., 2019).

Increasing number of studies suggest a certain degree of interconnection among compartment-specific adaptive gene expression programs (Pakos-Zebrucka et al., 2016; Ravanelli et al., 2020). Along with the already mentioned overlap between UPR^{mt} and ISR, several components identified for the UPR^{mt}, emerged to be required in *C. elegans* for the transcriptional activation of the HSR-induced *hsp16.2* in response to changes in lipid homeostasis (Kim et al., 2016). Similarly, SKN-1 is an important player in the response to oxidative stress and proteasome impairments, but represents also a downstream target of the UPR and UPR^{mt} in *C. elegans* (Blackwell et al., 2015; Lehrbach and Ruvkun, 2016; Nargund et al., 2012). Multiple sub-branches of the UPR^{mt} and MAD have been described

(Boos et al., 2019; Braun and Westermann, 2017; Mårtensson et al., 2019; Shpilka and Haynes, 2018; Weidberg and Amon, 2018; Wrobel et al., 2015); however, besides specialized quality control factors, the ubiquitin-dependent mitochondrial surveillance machinery could be summarized into a series of common mechanistic events: stress sensing, substrate ubiquitylation, translocation, and degradation by the proteasome. Upon stress, this general proteolytic mechanism is sustained by the regulation of both nuclear transcription and cytosolic translation (Figure 3). Overall, this strategy is highly flexible and efficiently adapts the mitochondrial proteome to changing cellular conditions, including stressful situations (Ravanelli et al., 2020).

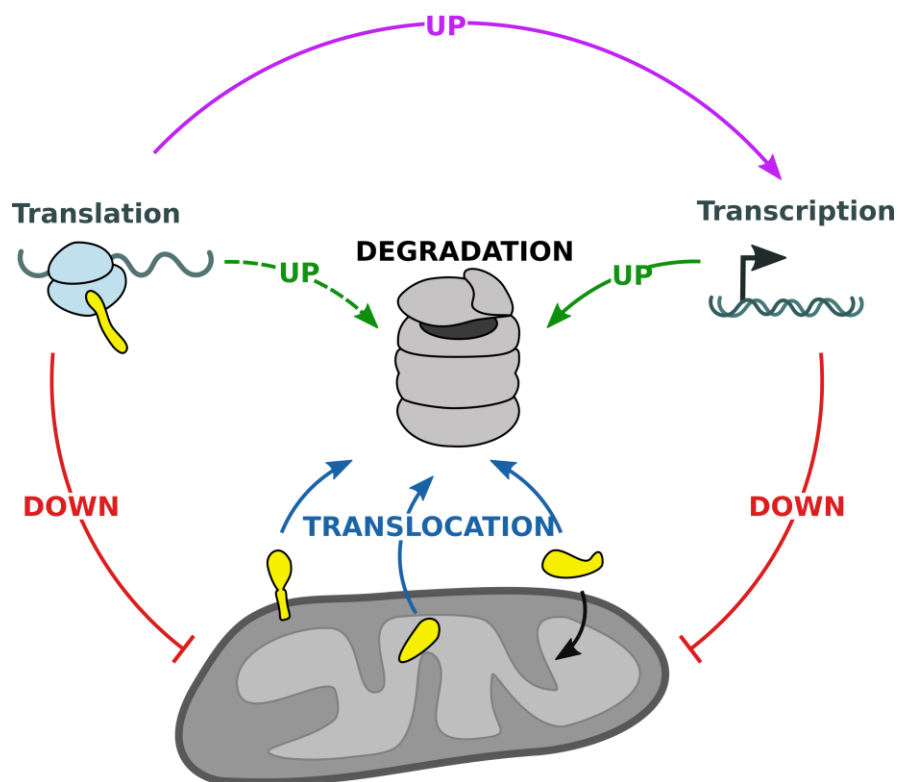


Figure 3 Mitochondrial protein quality control governed by the UPS

Misfolded, damaged, mistargeted, not successfully imported, or not required mitochondrial proteins are translocated (blue arrows) from the mitochondria to the cytosolic proteasome, which provide for their degradation. Upon stress, global translation is downregulated and protective genes are transcriptionally upregulated, reducing the load of proteins to be imported into the mitochondria and the overall mitochondrial stress (red arrows). The translational downregulation by phosphorylation of eIF2 α leads to translation of uORF-containing genes that directly support

proteasomal degradation (dashed green arrow) or indirectly foster downstream transcriptional responses (violet arrow), which in turn improve the UPS capacity (solid green arrow).

2.3 Metabolic Regulation of Proteostasis

The flexible and adaptive nature of the UPS allows efficient regulation of the proteome in multiple cellular compartments both in homeostatic and in stressful conditions. In response to a changing environment cells require constant and efficient adaptations of their proteome, as well as their metabolism. Accordingly, some of the aforementioned regulatory pathways (Chapters 2.1.3, 2.2.1, and 2.2.2) are tightly bound to the cellular metabolic state. The proteome integrity is governed by the coordinated action of four interconnected metabolically-regulated pathways: the insulin/insulin-like growth factor (IIS/IGF), the mTOR, the AMP-activated protein kinase (AMPK), and the NAD-dependent deacetylases (Sir2-like proteins, also known as sirtuins) (Ottens et al., 2021). While the IIS/IGF signaling and the mTOR pathway are activated upon nutrition availability and promote anabolic reactions, the AMPK and the sirtuins are important regulators at low energy states and promote catabolism. Insulin/IGF binds to the insulin/IGF receptor upon high glucose level, activating the serine/threonine kinase AKT, which in turn phosphorylates forkhead box-O class (FOXO) transcription factors preventing their nuclear translocation. FOXO-mediated transcription is not only activated upon IIS inhibition, but also supported by the activity of AMPK and sirtuins; whereas, AKT and AMPK antagonistically regulate TOR signaling (Ottens et al., 2021). IIS is regulated mostly by glucose levels (James et al., 2017), AMPK by ATP/AMP ratio (Salminen and Kaarniranta, 2012), sirtuins by NAD, and mTOR by amino acids. The amino acid concentration is tightly linked with the UPS activity. In fact, ubiquitylated proteins are digested by the proteasome into short peptides, which, once released in the cytosol are normally degraded by peptidases, recovering free amino acids, which are required for the survival of yeast, mammalian cells, and flies (Suraweera et al., 2012). Therefore, the UPS directly influences the metabolism of amino acids and mTOR, which in turn is interconnected with other metabolic regulators and stress response pathways.

2.3.1 Branched chain amino acid metabolism

As protein building blocks, amino acids are important nutrients and their metabolism is crucial for organismal physiology on multiple levels. Particularly, the branched chain amino acids (BCAAs) are essential amino acids and can only be synthesized by bacteria, plants, and fungi. Conversely, the BCAA catabolism is highly conserved and the first two steps are the same for all three BCAAs (leucine, isoleucine, valine) (summarized in Figure 4): (I) reversible transamination to form branched chain α -ketoacids (BCKAs) and glutamate, conducted by the branched chain amino acid transaminase (BCAT); (II) irreversible decarboxylation of BCKAs and covalent binding to coenzyme A (CoA), conducted by the branched chain amino acid dehydrogenase (BCKDH) complex. Ultimately, complete oxidation of leucine, valine and isoleucine leads to the production of acetyl-CoA, succinyl-CoA, or both (Neinast et al., 2019). Once bound to CoA, catabolic BCAA intermediate metabolites are retained inside the mitochondrial matrix, where all the oxidative steps following the BCAA transamination occur. In contrast, the first transamination step has been observed to take place both inside mitochondria as well as in the cytosol. In fact, mammals possess two forms of BCAT: BCAT1 or BCATc, which is present in the cytosol of nearly exclusively neuronal tissues, and BCAT2 or BCATm, which localizes in the mitochondria of most tissues (Sperringer et al., 2017; Toyokawa et al., 2021) (Figure 4). BCAAs represent not only an important carbon source for the TCA cycle, but also a nitrogen source and, together with BCKAs, can be flexibly transported among different tissues, through an intricate inter-tissue shuttling system. BCAT is not expressed in the adult rodent liver, although in this organ the BCKDH activity is high; conversely, around 50% of BCAAs is taken up by skeletal muscles, where the BCKDH activity is limited (Biswas et al., 2019; Sperringer et al., 2017). Beside its catabolic role, BCAT1 has crucial neurological functions, directly influencing the levels of the neurotransmitters glutamate and γ -aminobutyric acid GABA in neurons (Sperringer et al., 2017). Although numerous biochemical and physiological studies contributed to the current exhaustive knowledge about the BCAA metabolism, many details are still missing, especially in regard to the tissue-specific regulation and the secondary roles other than the tricarboxylic acid (TCA) cycle supply (Neinast et al., 2019; Sperringer et al., 2017).

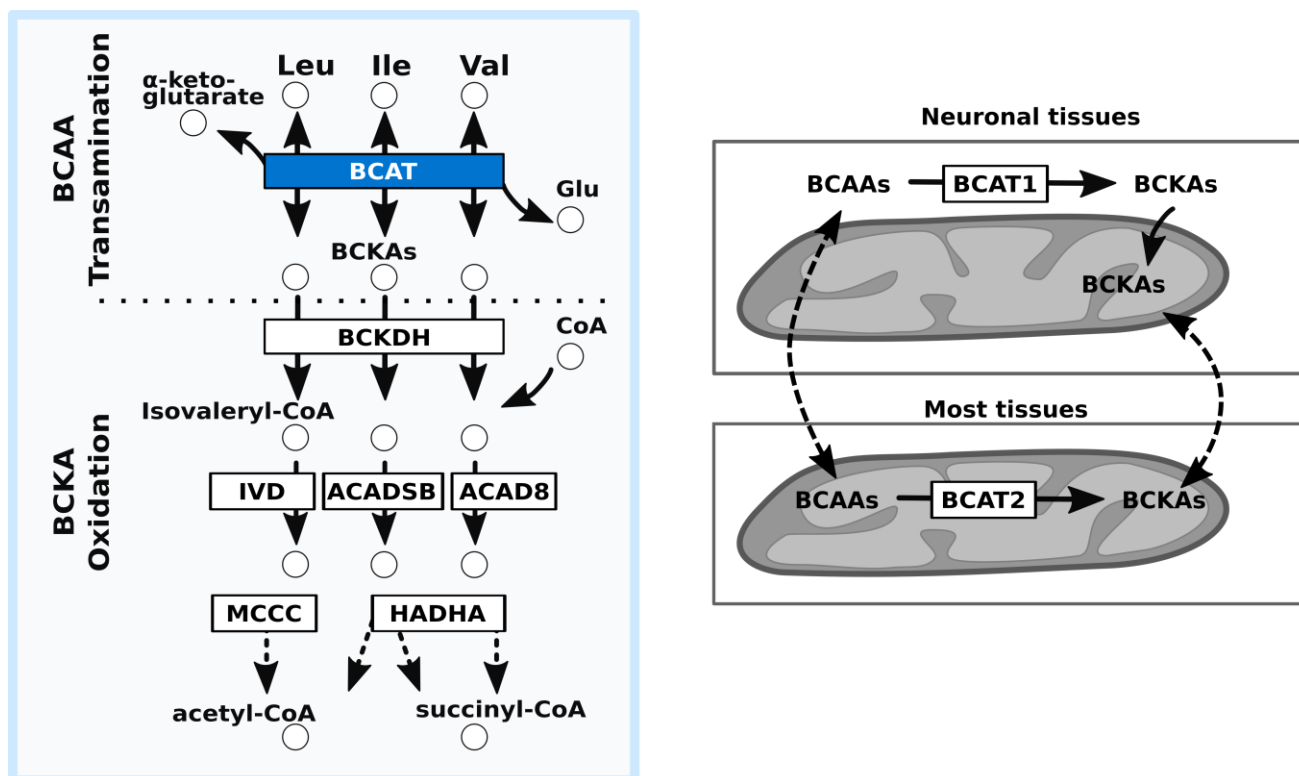


Figure 4 The BCAA metabolism

The BCAA metabolism comprehends a first reversible step of transamination, multiple oxidative steps, and final conversion to acetyl-CoA or succinyl-CoA. While the oxidation of BCKA occurs exclusively inside the mitochondrial matrix, the BCAA transamination reaction can occur both in the cytosol as well as in mitochondria. In mammals, BCAT1 localizes in the cytosol and is expressed mostly in the neuronal tissues (right, top), while BCAT2 localizes to mitochondria in most tissues (right, bottom). Both BCAAs as well as BCKAs are reported to be exchanged among different tissues (dashed arrows).

2.3.2 BCAAs: biomarkers or supplements?

Along with the biochemical characterization of BCAA metabolic reactions, numerous clinical studies focused on the role of free BCAAs in processes besides protein synthesis and catabolic energy production. BCAAs are important macronutrients and since many years they have been supplemented to the diet to improve muscle mass and protein synthesis during exercise or to mitigate cachexia (muscle wasting), although their efficacy is under debate (Holeček, 2018; Lysenko et al., 2018; Valerio et al., 2011; Wolfe, 2017). Conversely, BCAAs have been frequently identified as biomarkers and possibly causal

agents of numerous pathologies, such as metabolic diseases associated with obesity and insulin resistance (White, 2021). BCAAs are reported to stimulate the mTOR and IIS/IGF, which suppression has been associated with prolonged longevity (Souloukis and Partridge, 2016). Protein restriction, with a particular relevance for the BCAAs, is reported to increase lifespan and healthspan in various organisms (Babygirija and Lamming, 2021; Green et al., 2021; Souloukis and Partridge, 2016). However, elevated BCAAs have been reported to prolong lifespan (Fuchs et al., 2010; Mansfeld et al., 2015; Martin et al., 2011; Valerio et al., 2011). Although a consensus is still not reached, it is possible that in conditions of negative energy balance the supplementation of BCAAs is beneficial; whereas, chronic increase of BCAAs is clearly deleterious and potentially pathogenic (Holeček, 2018; White and Newgard, 2019).

As observed for the level of BCAAs, also intermediate metabolites generated in this pathway or altered function of the involved enzymes represent potential pathological triggers. For example, genetic mutations in the gene encoding the leucine catabolic enzyme isovaleryl-CoA dehydrogenase (IVD) underlie the metabolic disorder called isovaleric acidemia. Deficiency of IVD leads to the accumulation of several organic acids, including derivatives of isovaleryl-CoA, including isovaleric acid (IVA) (Chinen et al., 2017). Conventional treatments for isovaleric acidemia consist in leucine restriction and carnitine and/or glycine supplementation, which convert IVA into non-toxic isovalerylcarnitine and isovalerylglycine, respectively (Chinen et al., 2017). Besides inborn metabolic disorders directly related to the biochemical pathway, the BCAA metabolism has also been linked to neurodegeneration and cancer (Arany and Neinast, 2018; Manoli and Venditti, 2016; Neinast et al., 2019; Peng et al., 2020; Siddik and Shin, 2019; Sperringer et al., 2017), confirming the physiological relevance of this metabolic pathway.

2.4 Rationale and aim of the project

A cytosolic GFP-based UFD substrate under control of the ubiquitous *sur-5* promoter, later called UbV-GFP, was developed in our lab to monitor *in vivo* the UPS activity in *C. elegans* (Segref et al., 2011). UFD substrates are characterized by the N-terminal fusion of a ubiquitin moiety to the substrate, in which the glycine 76 of ubiquitin is converted to valine

(G76V), completely inhibiting the deubiquitylation of the UFD substrate (Johnson et al., 1995). Monitoring the level of the UbV-GFP, our laboratory observed that loss of metabolic genes or inhibition of the mitochondrial respiratory chain affect UPS efficiency (Segref et al., 2014). Moreover, accumulation of a UFD substrate in fibroblasts isolated from human patients of isovaleric acidemia confirmed the evolutionary conservation of the observed UPS regulation caused by impaired IVD and suggested a causal link between proteostasis loss and the pathology of this metabolic disorder (Segref et al., 2014). However, the mechanistic link between mitochondrial impairment and the reduced turnover of the UPS substrate remained to be determined. The aim of this PhD project was to investigate the molecular mechanisms underlying the observed regulation of cytosolic proteostasis in response to metabolic stress. Particularly, I addressed (I) which specific type of mitochondrial/metabolic stress triggers UPS impairment, (II) which physiological consequences derive from this response, and (III) how mitochondrial stress is transduced into a signaling pathway. Following a genetic approach, I analyzed the role of individual regulators and their role in UPS function, considering both known players in other stress-induced signaling pathways and possible novel components that might contribute to this process. A candidate RNAi approach targeting mitochondrion-related genes highlighted a key role of the BCAA metabolism in UPS regulation. Therefore, I genome engineered new BCAA metabolic enzyme mutants and combined phenotypic quantification with multi-omics analysis to investigate the physiological relevance of this metabolic pathway, particularly focusing on its role in proteostasis modulation. I supplemented IVA to the growth medium to study if accumulation of this metabolite is responsible for the UPS defects observed upon IVD impairment.

3 Results

3.1 Mitochondrial stress can modulate UPS substrate specificity without UPR^{mt} induction

Monitoring the level of UbV-GFP (Segref et al., 2011), our lab has shown that mitochondrial stress affects UPS-dependent degradation both in *C. elegans* and in human cells (Livnat-Levanon et al., 2014; Segref et al., 2014). However, while depletion of the metabolic enzymes acetyl-CoA synthetase 19 (ACS-19) or isovaleryl-CoA dehydrogenase (IVD-1) cause UPS defects, the amount of total ubiquitylated substrates is not affected, suggesting that metabolic impairments deriving from *ivd-1* or *acs-19* loss-of-function reprogram the substrate specificity of the UPS rather than reducing its global capacity. Accordingly, alteration of the proteasome composition through depletion of different proteasome subunits by RNAi showed differential accumulation of the UFD substrate reporter compared with the total amount of ubiquitylated substrates (Figure 5A). Treatment with increasing doses of the proteasome inhibitor bortezomib showed correlation between the level of total ubiquitylated proteins and of UbV-GFP (Figure 5B), excluding the accumulation of UbV-GFP upon proteotoxic stress levels that are too mild to induce increase of total ubiquitylated proteins.

Mitochondrial stress usually triggers the expression of the transcriptional reporter *hsp-6p::gfp*, indicating activation of the UPR^{mt} (Yoneda et al., 2004). Pharmacological inhibition of mitochondrial respiration with antimycin A was reported to activate the expression of the UPR^{mt} reporter *hsp-6p::gfp* (Bar-Ziv et al., 2020; Liu et al., 2014) and to reduce UbV-GFP turnover (Segref et al., 2014). However, neither depletion of *ivd-1* nor *acs-19* triggered the expression of *hsp-6p::gfp* (Segref et al., 2014). While I could confirm this result, I further observed that supplementing the worms with increasing doses of antimycin A induced a dose-dependent activation of both UPR^{mt} and UbV-GFP accumulation (Figure 5C). This result confirms that the nature of the stress caused by mitochondrial respiratory deficiency is substantially different from the one induced by *ivd-1* or *acs-19* depletion and suggests that certain types of mitochondrial defects activate a stress response that modulate the UPS activity independently of UPR^{mt}, ultimately influencing proteostasis.

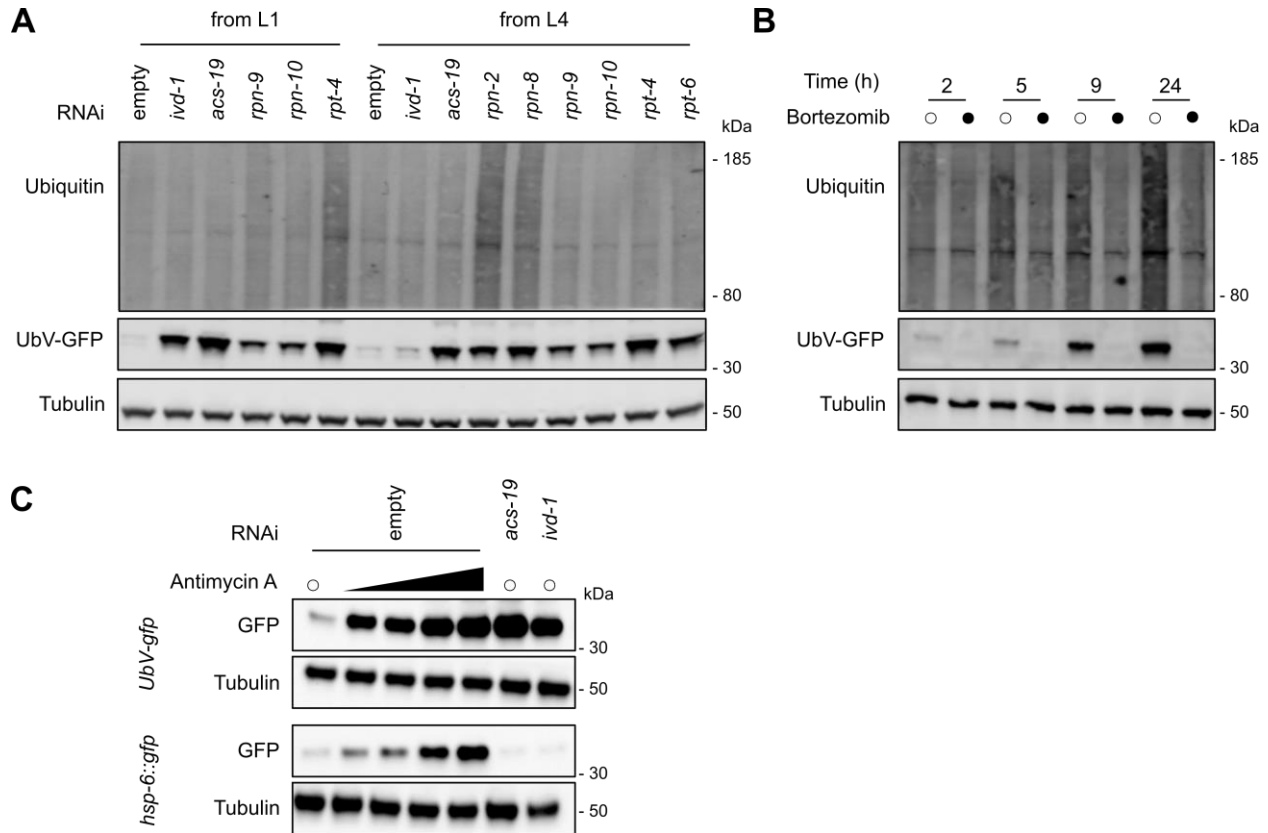


Figure 5 Metabolic stress reprograms UPS substrate specificity

(A, B) Western blot analysis of total ubiquitylated proteins and UbV-GFP level with tubulin as loading control. (A) Worms were treated with RNAi against *ivd-1*, *acs-19*, and indicated proteasome subunits, either starting from L1 or L4 larval stage. (B) L4-staged worms were treated with 10 μ M bortezomib and collected after increasing amount of time. DMSO was used as control. (C) Western blot analysis of UbV-GFP level and *hsp-6p::gfp* expression with tubulin as loading control. Worms were treated with increasing concentrations of antimycin A or RNAi against *acs-19* or *ivd-1*. (A, C) RNAi empty vector was used as control (empty).

3.2 *acs-19* allele-specific phenotypes reveal the presence of background mutations

Reactive oxygen species (ROS) emerged as key stressors in the UPS regulation observed upon mitochondrial stress, both in *C. elegans* and in mammalian cells. Accordingly, the master regulator of the oxidative stress response *skn-1* is required for functional turnover of ubiquitylated proteins (An and Blackwell, 2003; Segref et al., 2014).

Considering also the important role of SKN-1A in promoting the expression of proteasome subunits, like its homolog Nrf1 (Koizumi et al., 2016; Lehrbach and Ruvkun, 2016), I wondered if SKN-1 might play a specific role in the UPS regulation in the context of *acs-19* or *ivd-1* loss-of-function (for *ivd-1* see next chapter). Unexpectedly, *skn-1(RNAi)* caused different effects on the *acs-19(hh5)* point mutant worms in comparison to the *acs-19(tm4853)* deletion mutants (Figure 6A). Instead of the usually observed accumulation of UbV-GFP in the intestine, *acs-19(hh5)* treated with *skn-1(RNAi)* showed a reduced GFP fluorescence which was limited to certain tissues, visually identified as the hypodermis. The changed fluorescence pattern correlated with tissue degeneration (Figure 6B), which rapidly increased after adulthood and finally led to premature death in few days. This effect could be partly explained by the important role of SKN-1 in the development of the digestive tract; in fact, loss of *skn-1* is reported to prevent intestine and pharynx formation, which is compensated by extra hypodermal cells (Bowerman et al., 1992). However, upon *skn-1(RNAi)*, the *acs-19(tm4853)* deletion mutants retained tissue integrity and accumulated the UFD substrate in the intestine (Figure 6A and 6B). To test if the observed tissue degeneration and aberrant fluorescence pattern is linked to the expression of the UFD substrate, I crossed the *acs-19(hh5)* mutants with other two reporters driven by the same promoter of UbV-GFP: (I) *sur-5p::gfp*, which have longer half-life due to the absence of ubiquitin; (II) *sur-5p::^{K29/48R}UbV-gfp*, where the ubiquitin was modified on lysine 29 and 48 to prevent K29- and K48-linked ubiquitin chains (Segref et al., 2011). Surprisingly, none of the newly obtained strains showed tissue defects, nor a change in the fluorescence pattern (Figure 6C), suggesting that the *acs-19(hh5)* allele was not responsible for those effects and possibly background mutations introduced during the ethyl methane sulfonate (EMS) mutagenesis might have been involved.

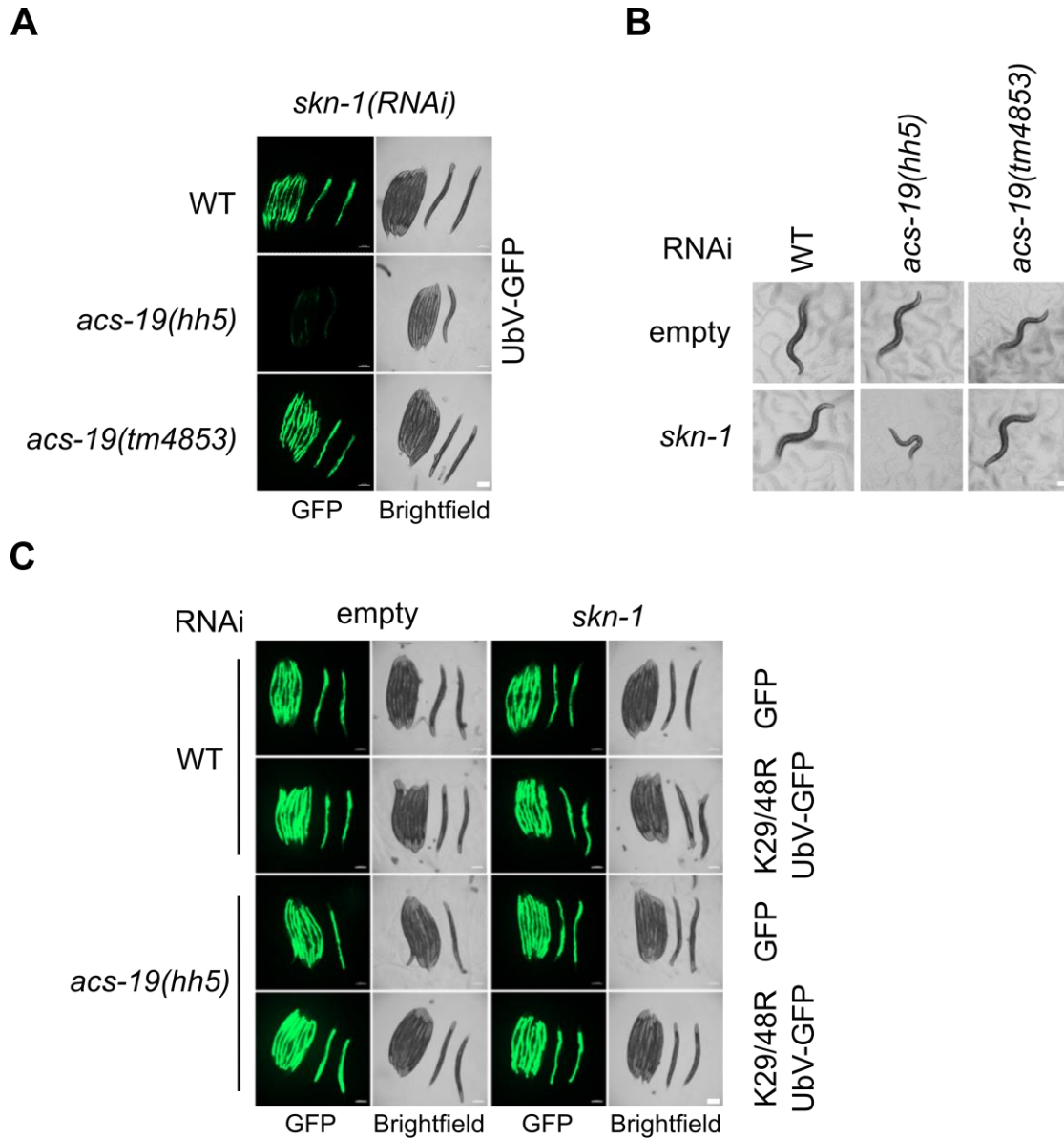


Figure 6 *skn-1(RNAi)* has different effects on *acs-19* alleles

(A, C) Fluorescent and brightfield microscopic images of immobilized worms expressing either *sur-5p::gfp* or *sur-5p::^{K29/48R}UbV-gfp*. (B) Brightfield microscopic images of representative worms. (A-C) RNAi empty vector was used as control (empty). Scale bars: 200 μ m.

To confirm if the observed phenotype was caused by background mutations, I compared the tissue integrity and the UbV-GFP accumulation upon *skn-1(RNAi)* of different *acs-19(hh5)* strains, including the strain originally isolated from the EMS screen and two other strains obtained after multiple cycles of outcrossing (Segref et al., 2014) (Figure 7A).

All three strains displayed a similar fluorescence pattern, but the original strain, *mut1*, was more susceptible to *skn-1(RNAi)*, displaying stronger and earlier tissue degeneration in comparison to the strains outcrossed more times, *mut2* and *mut3* (Figure 7B). This observation indicates that the outcrossing reduced the level of tissue degeneration, possibly deriving from the combined action of several genetic mutations. According to the whole genome sequencing performed after the EMS screen, the insertion locus of the *UbV-gfp* reporter resides in chromosome III, like the *acs-19* gene (data from Alexandra Segref). Consequently, some EMS-induced mutations near the inserted *UbV-gfp* were probably retained during the multiple outcrossing with wild-type worms bearing the *UbV-gfp* reporter. To exclude the mutations surrounding the *UbV-gfp* reporter, I outcrossed the *acs-19(hh5)* with wild-type worms to remove the reporter and crossed the resulting strain with wild-type worms containing the reporter, obtaining a new outcrossed line that lacks the background mutations (*new mut*, Figure 7A). I observed 5 recombination events out of 342, when combining all segregating progenies monitored during both crossing cycles to generate the *new mut* from *mut3*, which indicates 1.4 cM distance between the *acs-19* locus and the reporter insertion site. When treated with *skn-1(RNAi)*, the *new mut* worms display an UbV-GFP accumulation similar to wild-type and do not undergo tissue degeneration (Figure 7B), confirming that the phenotypes observed in *mut1*, *mut2*, *mut3* are caused by EMS mutations neighboring the *UbV-gfp* insertion locus. Although I did not investigate which specific background mutations interacted synergistically with *skn-1(RNAi)*, the generation of *new mut acs-19(hh5)* strain, which contains a substantially lower amount of background mutations, represents a valuable contribution for future studies related with ACS-19.

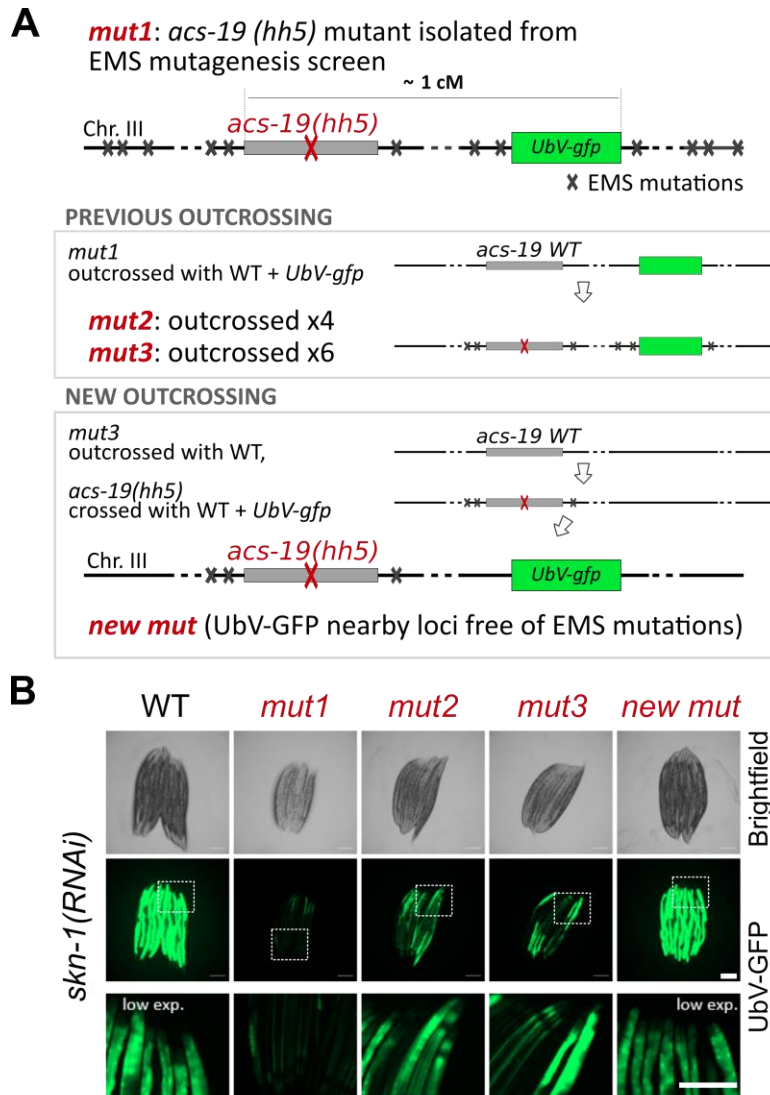


Figure 7 Background mutations were retained in the studied *acs-19(hh5)* strain despite outcrossing

(A) Schematic summary of outcrossing strategy to reduce the background mutation of *acs-19(hh5)* strain (*mut3*), previously used in this study. *mut1* was the original strain obtained by the EMS screen (Segref et al., 2014), *mut2* and *mut3* were previously outcrossed in our lab but always against wild-type worms expressing *sur-5p::UbV-gfp*. In the new crossing, *new mut* was obtained after crossing with wild-type worms, isolating *acs-19(hh5)* mutation without the reporter, which was then crossed to reintroduce the *sur-5p::UbV-gfp* reporter. (B) Fluorescent and brightfield microscopic images of immobilized worms treated with *skn-1(RNAi)* expressing *UbV-gfp* of the different strains reported in A. Scale bars: 200 μ m.

3.3 Defective leucine catabolism integrates known stress response pathways

The UbV-GFP stabilization detected upon *ivd-1* depletion is probably linked to defective leucine catabolism. In fact, RNAi-depletion of two enzymes involved in the degradation of leucine, one upstream and the other downstream of IVD-1, also induced the UbV-GFP stabilization (Segref et al., 2014). The first identified *ivd-1(hh6)* allele was suggested to be a loss-of-function allele (Segref et al., 2014), which I could confirm by measuring a lower *ivd-1* transcript level compared to wild-type (Figure 8A). The UbV-GFP stabilization occurred also in the complete knock-out mutant allele *ivd-1(tm6784)* (Figure 8B), further sustaining that interrupted leucine catabolism regulates the UPS.

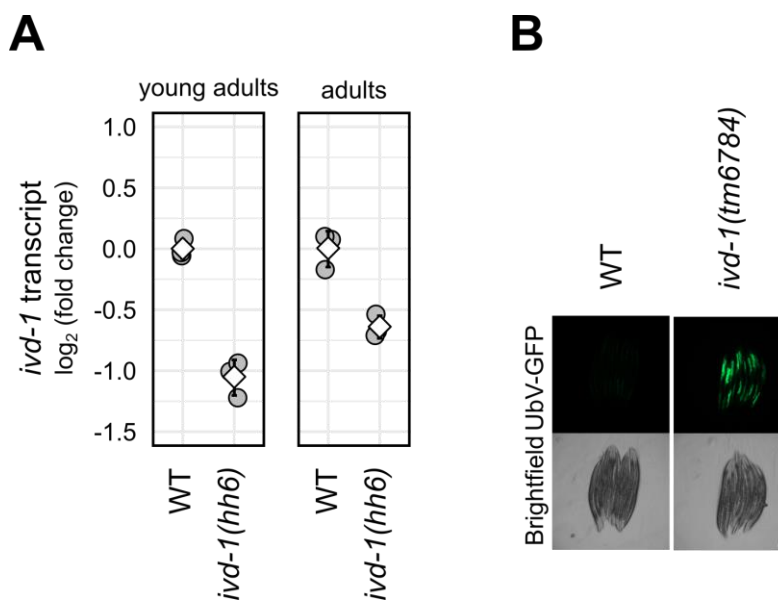


Figure 8 *ivd-1* loss-of-function reduces proteasomal degradation

(A) mRNA transcript level of *ivd-1* quantified with qRT-PCR relative to wild-type (WT). 3 technical replicates. Fold changes calculated as $2^{-\Delta\Delta Cq}$. Means as white squares and standard deviations as error bars. (B) Fluorescent and brightfield microscopic images of immobilized worms expressing UbV-GFP. Scale bar: 200 μ m.

To investigate if the metabolic stress caused by defective IVD regulates the UPS by triggering known stress signaling pathways, I analyzed the UFD substrate accumulation upon RNAi depletion of some transcription factors known to be involved in different stress

response mechanisms (Figure 9A). Particularly, I tested the effect on the UbV-GFP turnover by knock-down of the oxidative stress and proteasome regulator *skn-1*, the heat shock factor *hsf-1*, the hypoxia inducible factor *hif-1*, the FOXO homolog *daf-16*, and the key inducer of UPR^{mt} *atfs-1*. In wild-type worms, RNAi of *skn-1* or *atfs-1* led to stabilization of the UFD substrate, indicating a role of both transcription factors in support of the UPS functionality in physiological conditions. In *ivd-1(tm6784)* mutant worms, *skn-1(RNAi)* had a strong additive effect, especially in young adults, suggesting that the UPS regulation triggered by leucine catabolic stress is most likely independent of SKN-1. In general, none of the transcription factors tested here were required to stabilize the UFD substrate upon *ivd-1(tm6784)* mutation. However, depletion of *hif-1* enhanced the proteolytic defects of sexually mature *ivd-1(tm6784)* worms, without affecting the UbV-GFP turnover in wild-type worms. None of the RNAi-treated transcription factors affected the UbV-GFP level in the E3 ligase mutant allele *hecd-1(tm2371)*, suggesting that the observed UPS regulation requires ubiquitylation by HECD-1. In line with previous results of *ivd-1* depletion (Segref et al., 2014), multiple polyubiquitylated states of the UFD substrate indicate that SKN-1, ATFS-1, and HIF-1 are involved in the degradation of UPS substrates downstream of the ubiquitylation step (Figure 9A). The control ^{K29/48R}UbV-GFP substrate appears stable in all conditions, confirming that the UFD substrate turnover depends on K29- and/or K48-linked polyubiquitylation. Although these results are not conclusive and should be confirmed and further investigated, they suggest activation of the hypoxic stress response in case of defective leucine catabolism. On the other hand, they confirm an important role of SKN-1 in the normal UPS functionality, while a specific involvement during metabolic stress remains to be determined.

Since *skn-1* encodes multiple protein isoforms with different N-termini (Blackwell et al., 2015; Lehrbach and Ruvkun, 2016) and the *skn-1(RNAi)* suppression is not specific, I wondered if any of these isoforms are differentially regulated upon *ivd-1* loss-of-function. Using different sets of primers to target the *skn-1* transcripts encoding for the different protein isoforms (Figure 9B), I noticed that *skn-1b* was specifically upregulated in *ivd-1(hh6)* (Figure 9C), while it was comparable to wild-type in *skn-1a* mutant worms (Lehrbach and Ruvkun, 2016). These preliminary results represent a promising direction of study in the role of SKN-1B in the UPS regulation triggered by defective leucine

catabolism.

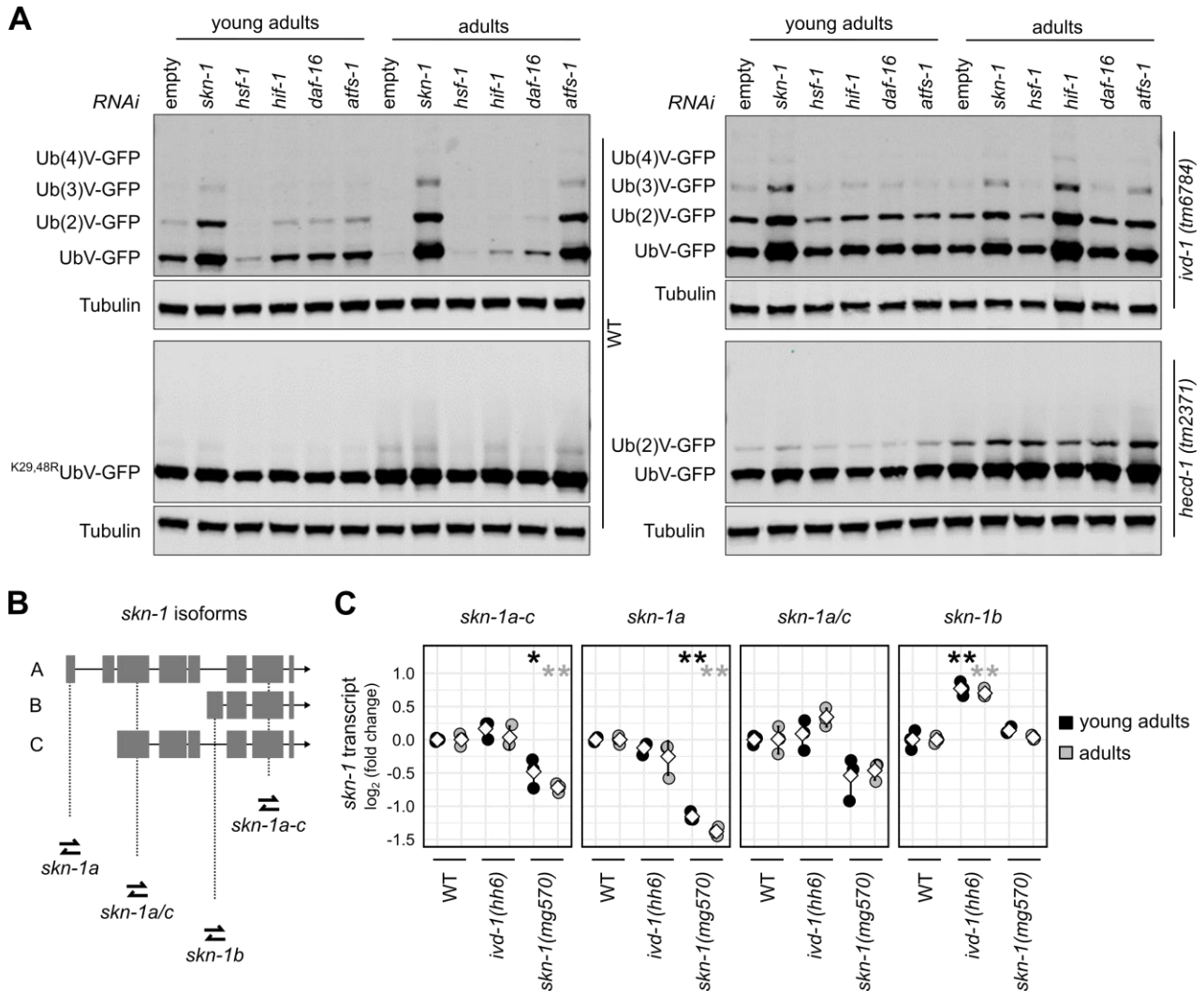


Figure 9 Defective leucine catabolism induces stress signaling

(A) Western blot analysis of UbV-GFP and ^{K29/48R}UbV-GFP levels with tubulin as loading control. RNAi empty vector was used as control (empty). (B) Schematic summary of the primer pairs used to amplify the different *skn-1* transcriptional isoforms by qRT-PCR, reported in C. (C) mRNA transcript level of *skn-1* different transcripts quantified with qRT-PCR relative to wild-type (WT). 3 technical replicates. Fold changes calculated as $2^{-\Delta\Delta Cq}$. Means as white squares and standard deviations as error bars. Statistically significant difference compared to WT calculated with Tukey's Honest Significant Difference (HSD) combined with one-way ANOVA performed in R and indicated in relation control with * for P-value ≤ 0.05 , ** for P-value ≤ 0.01 .

3.4 Specific types of mitochondrial stress regulate the UPS

To identify other mitochondrial stressors similar to *acs-19* or *ivd-1* depletion, I performed an RNA interference (RNAi) screen of 71 genes which encode metabolic enzymes connected to IVD-1 or ACS-19, respiratory chain elements, and mitochondrial transporters (Figure 10A). I conducted RNAi treatment on worms expressing either the UFD substrate *sur-5p::UbV-gfp* or the UPR^{mt} reporter *hsp-6p::gfp* and, after imaging, I quantified the transgene fluorescence using a semi-automated imaging method, which I validated by comparison with a manual qualitative assessment of fluorescence intensity (Figure 10A-10C). Only 7 RNAi-targeted genes caused accumulation of UbV-GFP without induction of the UPR^{mt} (Figure 10D), indicating that only specialized metabolic pathways regulate the UPS independently of the UPR^{mt}. Converting pyruvate into acetyl-CoA, pyruvate dehydrogenases are particularly interesting and might resemble a similar role in UPS regulation as ACS-19. On the other hand, the BCAA metabolism emerged as a crucial metabolic pathway in the context of ubiquitin-dependent degradation. RNAi against both *bckd-1B* and *mccc-1* led to UbV-GFP accumulation like *ivd-1(RNAi)*, confirming previous results (Segref et al., 2014). However, loss of BCAT-1, the enzyme responsible for the first step of the BCAA catabolism did not affect the UbV-GFP turnover (Figure 10D), indicating that only disruption of the downstream step of the pathway leads to a reduced turnover of UPS substrates. The specific conditions triggering UPS regulation upon defective BCAA catabolism only downstream of its first limiting step are particularly interesting to address in order to understand the nature of mitochondrial stress influencing the UPS.

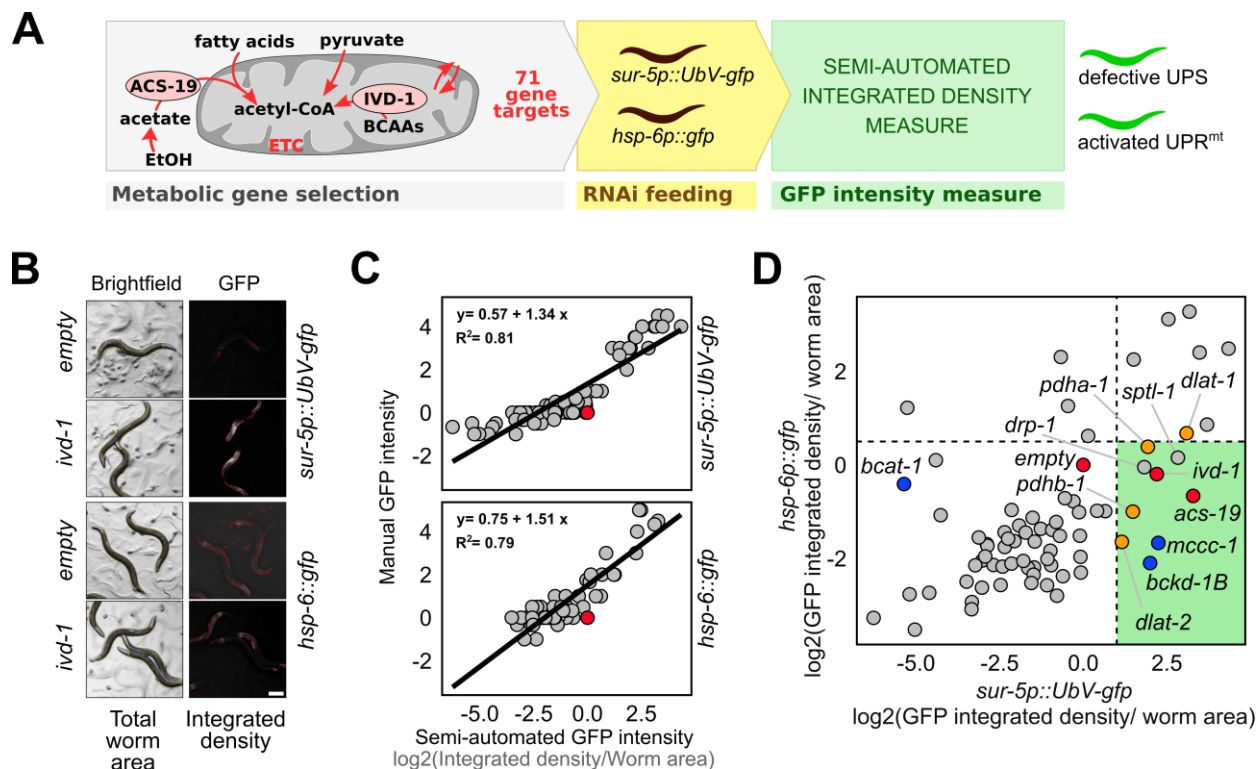


Figure 10 Specialized metabolic changes regulate the turnover of UPS substrates

(A) Metabolic RNAi screen schematic view. Selected 71 genes (red arrows) were RNAi-depleted in worms expressing the UFD substrate *sur-5p::UbV-gfp* or the UPR^{mt} sensor *hsp-6p::gfp*. After imaging, GFP intensity was quantified with ImageJ (B) Representative images of the RNAi screen quantification, showing *ivd-1*(RNAi) and empty RNAi control for both *sur-5p::UbV-GFP* and *hsp-6p::GFP* expressing worms. For both brightfield and GFP channels the thresholded areas used for quantification are indicated in yellow and red, respectively. Scale bar: 200 μ m. (C) Correlation analysis between manual and automated GFP intensity measure of the RNAi metabolic screen, respectively for *sur-5p::UbV-gfp* and *hsp-6p::gfp*. Linear regression with relative formula and R^2 are indicated in black. The GFP manual intensity was normalized on the empty control by subtraction, while the automated GFP integrated density/worm area was divided by the empty control (red) value and \log_2 transformed. (D) GFP integrated density of *sur-5p::UbV-gfp* and *hsp-6p::gfp* respectively for RNAi-depleted genes, normalized on the empty vector as RNAi control (red). RNAi-positive control genes *ivd-1* and *acs-19* in red; genes involved in the BCAA metabolism in blue.

3.5 Transamination of BCAAs is physiologically essential

The BCAA transamination reaction conducted by BCAT-1 represents the first limiting step of the BCAA metabolic pathway (Figure 4); therefore, it is surprising that *bcat-1(RNAi)* did not affect the UbV-GFP turnover, like depletion of the downstream enzymes *bckd-1B*, *ivd-1*, and *mccc-1* (Figure 10D). This result excludes UPS regulation upon general defects in the BCAA metabolism, as previously hypothesized (Segref et al., 2014), and suggests that specific molecular consequences influencing the UPS derive from the impairment of the BCAA catabolic pathway downstream of the initial step. To further analyze how specific alterations of the BCAA metabolism regulate the UPS, I opted to generate constitutive *bcat-1* knock-out mutants, that could then be combined with the *ivd-1(tm6784)* knock-out mutants. The goal was distinguishing the functional role of the first transamination step and the downstream catabolism of BCAAs. Since no mutant was available, I genetically modified the endogenous *bcat-1* gene using the CRISPR-Cas9 editing technique (Dickinson and Goldstein, 2016; Doudna and Charpentier, 2014; Paix et al., 2017). With introduction of a premature stop codon (PSC) and subsequent frameshift of the coding region I aimed to obtain *bcat-1* gene knock-out lines (Figure 11A). Knowing the high variability in efficiency reported for this technique, I designed two different guide RNAs (gRNAs) to increase the probability to get edited worms. During the identification of individual mutants, I could isolate only heterozygous worms for the *bcat-1(hh56)* and *bcat-1(hh57)* alleles, which, upon sequencing validation, demonstrated to carry the designed PSC and a 44bp insertion, respectively (Figure 11A, cyan). In line with partial embryonic lethality reported for *bcat-1(RNAi)* (Rual et al., 2004), the *bcat-1(hh56)* mutation resulted in 100% embryonic lethality. After balancing the *bcat-1(hh56)* (Dejima et al., 2018), the total progeny of a single heterozygous individual was composed of 25% phenotypically uncoordinated (Unc) worms (phenotypic marker for two copies of the balancer) and 50% phenotypically wild-type. The remaining 25% of total laid eggs did not hatch, which, according to the Mendelian segregation, represent the maximum proportion possible of homozygous mutant progeny (Figure 11B).

Interestingly, isolation of viable homozygous *bcat-1(hh58)* was possible, indicating at least partial viability, which could be explained by the position of the inserted PSC. Being

extremely close to the ATG (21 bp downstream), the PSC might escape recognition by the non-sense mediated decay machinery and induce translation re-initiation at the next start codon (Perrin-Vidoz et al., 2002), producing a truncated but functional protein (Figure 11A, violet). In line with this hypothesis, the *bcat-1* transcript was preserved in *bcat-1(hh58)* mutant worms (Figure 11C). In contrast, the *bcat-1(hh56)* allele was designed to have the PSC downstream of this alternative ATG, probably triggering the non-sense mediated mRNA decay and consequently the degradation of the *bcat-1* transcript.

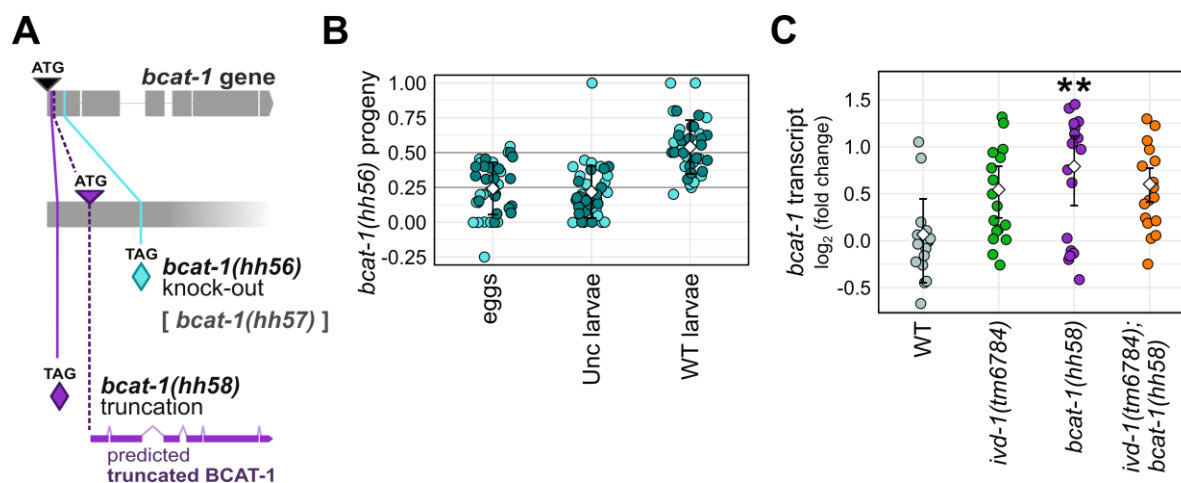


Figure 11 *bcat-1* gene is essential

(A) Overview of the CRISPR-Cas9 *bcat-1* mutations, with indicated PSCs (TAG) for *hh56* allele (light blue) and *hh58* allele (violet). *hh57* in brackets was obtained with the same gRNA as *hh56* but in this case a random 44bp insertion occurred, instead. (B) Quantification of *bcat-1(hh56)* lethality, as the number of unhatched eggs (*bcat-1(hh56)/bcat-1(hh56)*), viable larvae with Unc phenotype (*tmC24/tmC24*), and phenotypically wild-type larvae (*bcat-1(hh56)/tmC24*). Light and dark blue identify two independent isolates from crossing *bcat-1(hh56)/+* with balancer strain FX30253. 19 and 20 technical replicates for each line. (C) mRNA transcript level of *bcat-1* quantified with qRT-PCR relative to wild-type (WT). 5 independent experimental replicates with at least 3 technical replicates each. Fold changes calculated as $2^{-\Delta\Delta Cq}$. Means as white squares and standard deviations as error bars. Statistically significant difference compared to wild-type (WT) were calculated with Tukey's Honest Significant Difference (HSD) combined with one-way ANOVA performed in R and indicated in relation control with * for P-value ≤ 0.05 , ** for P-value ≤ 0.01 .

Considering the physiological relevance of the BCAA metabolism, I analyzed the general health of *ivd-1(tm6784)* and *bcat-1(hh58)* single mutants as well as the *ivd-1(tm6784); bcat-1(hh58)* double mutants. While motility was not impaired (Figure 12A), development and reproduction were greatly affected (Figure 12B-12D). Particularly, *bcat-1(hh58)* mutant worms required one day longer to reach adulthood in comparison to wild-type (Figure 12B), had a total viable progeny of approximately 50 worms compared with the 300 of wild-type (Figure 12C), and only 50% of the laid eggs eventually hatched (Figure 12D). Expression of the wild-type BCAT-1::GFP fusion reporter (Mansfeld et al., 2015) could efficiently recover all impairments caused by the *bcat-1(hh58)* mutation, indicating that these phenotypes derive from a *bcat-1* loss-of-function (Figure 12B-12D). The minor, but significant defects caused by *ivd-1(tm6784)*, further support a critical role of BCAA metabolism in development and reproduction. Interestingly, combination of *ivd-1(tm6784)* and *bcat-1(hh58)* mutations had different physiological outcomes. The partial recovery of the *bcat-1(hh58)* developmental delay by *ivd-1(tm6784)* suggests an adaptive regulation that supports development (Figure 12B). On the other hand, the epistasis of *bcat-1(hh58)* on the total viable progeny is in line with the BCAT-1 upstream position in the BCAA metabolic pathway (Figure 12C). Finally, the synergistic contribution of both mutations to the embryonic viability suggests possible compensatory effects of the available enzyme when only one is missing (Figure 12D). These results indicate a complex genetic interaction between *ivd-1* and *bcat-1*, which suggests multiple physiological roles of the BCAA metabolism, not limited to energy production, but also contributing to correct development and reproduction.

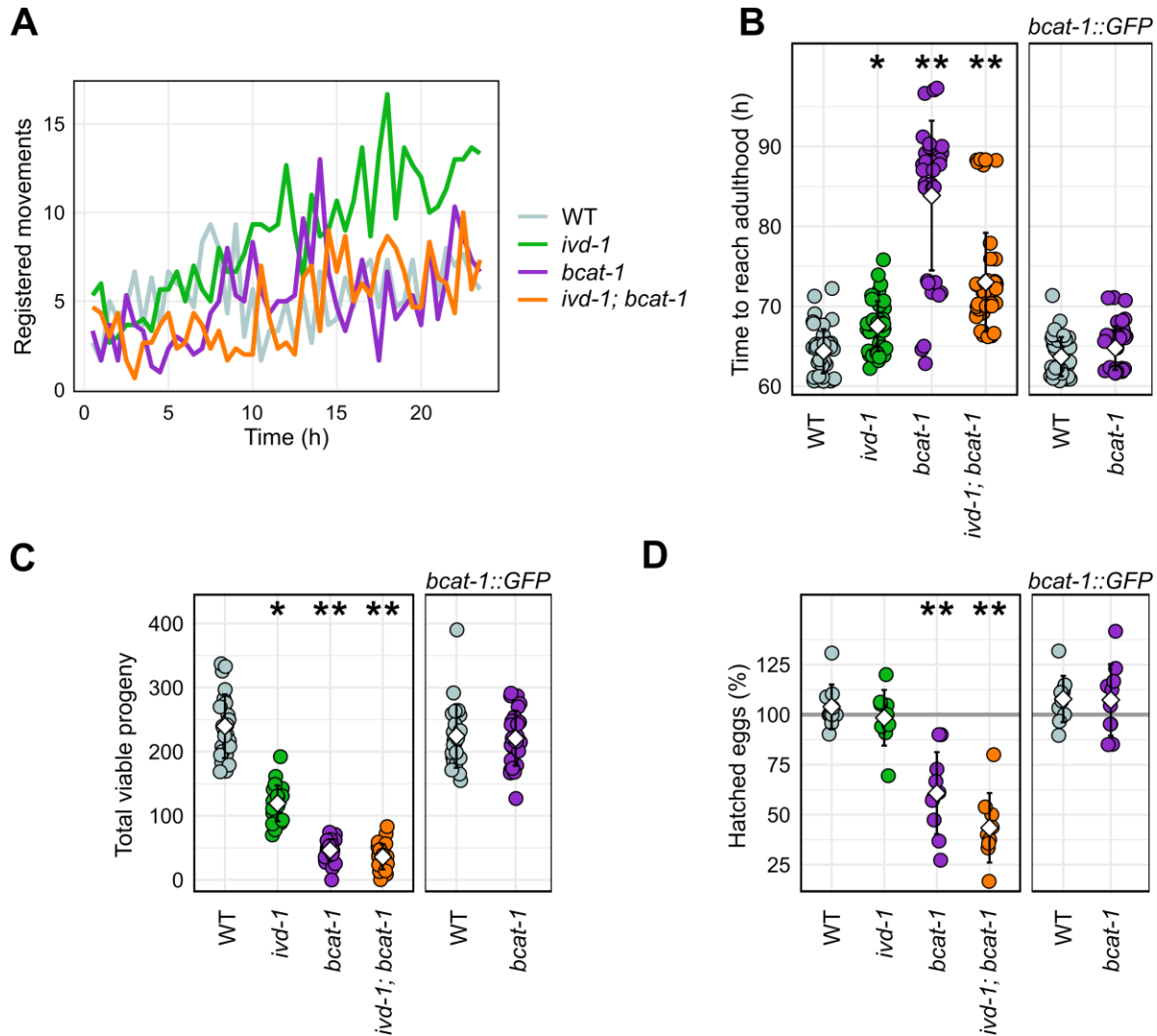


Figure 12 Functional BCAA metabolism is required for development and reproduction

(A) Population motility of 10 adult worms over time (hours), assessed with ARENA WMicrotracker (NemaMetrix) displayed as the average of 3 technical replicates after 30 min binning. Mean of 3 technical replicates. (B) Generation time of individual worms, considered as the time to reach adulthood from egg. 2 experimental replicates pooled together to have minimum 34 technical replicates for each strain. (C) Total number of viable progenies quantified for individual worms. 2 experimental replicates pooled together to have minimum 24 technical replicates for each strain (D) Viability quantification as proportion of viable progeny on the total number of eggs laid by 1 adult worm in 4 hours. 10 technical replicates for each strain. (B-D) Mean as white square and standard deviation as error bars are displayed for each strain. Statistically significant difference compared to wild-type (WT) were calculated with Tukey's Honest Significant Difference (HSD)

combined with one-way ANOVA performed in R is indicated with * for $p \leq 0.05$, ** for $p \leq 0.01$. The reported mutant alleles are *ivd-1(tm6784)* and *bcat-1(hh58)*.

3.6 *C. elegans* BCAT-1 is the ancestor of both mammalian BCAT paralogs

Given its physiological relevance, the BCAA metabolism is very well conserved; however, it is not clear how the *C. elegans* BCAT-1 is related to the two specialized mammalian homologs BCAT1 and BCAT2. Phylogenetic analysis revealed that BCAT-1 is the predicted ancestor of both mammalian BCAT1 and BCAT2 (Figure 13A), suggesting that BCAT-1 might be active both in mitochondria as well as in the cytosol, possibly differentially regulated in a time (developmental stage-specific) and/or space (tissue-specific) dependent manner. Although detailed information about *bcat-1* expression pattern is still missing, deposited data at Wormbase indicate that *bcat-1* is expressed in several tissues, including nervous system, reproductive system, muscle and intestine (<http://www.wormbase.org>). On the subcellular level, *bcat-1* is predicted to localize to the mitochondria by different prediction tools, including MitoProt, TargetP and iPSORT (Armenteros et al., 2019; Bannai et al., 2002; Claros and Vincens, 1996; Meissner et al., 2011). Accordingly, I quantified the proportion of the translational reporter BCAT-1::GFP (Mansfeld et al., 2015) localizing inside Mitotracker-stained mitochondria and observed approximately 75% of BCAT-1::GFP occurring inside the stained area (Figure 13B).

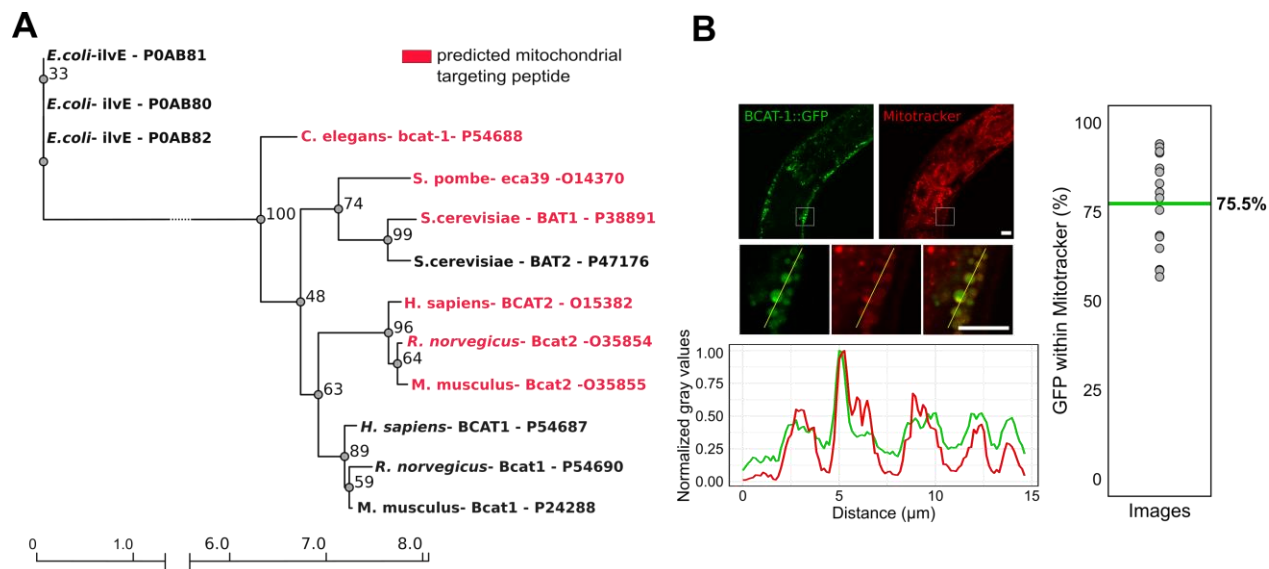


Figure 13 *C. elegans* BCAT-1 is the ancestor of mammalian BCAT1 (cytosolic) and BCAT2 (mitochondrial)

(A) Phylogenetic analysis of BCAT-1 protein, selecting homologous from Swiss-Prot records in the UniProt database, with bootstrap support values for each branch (100 bootstraps). The tree was obtained with the online tool PhyML (version 3.0) (Guindon et al., 2010) using the alignment computed by T-COFFEE EXPRESSO (Di Tommaso et al., 2011). Proteins predicted to have a mitochondrial targeting peptide by TargetP (Armenteros et al., 2019) are highlighted in red. (B) Quantification of BCAT-1::GFP localization inside mitochondria stained with Mitotracker DeepRed. On the left, representative image showing green, red and merged channels and the relative fluorescent histogram to compare BCAT-1::GFP and Mitotracker fluorescent intensity locally. On the right, quantification of 11 micrographs and relative proportion of GFP-positive area occurring inside the Mitotracker-stained area, with mean value indicated in green. Scale bars: 10 μ m.

3.7 BCAA transamination and downstream catabolic steps play opposing roles in proteostasis

Considering that *bcat-1(RNAi)* did not affect the turnover of the UFD substrate and that the BCAT-1 enzyme catalyzes the first step of the BCAA metabolism (Figure 4), one would expect a similar result also in combination with depletion of downstream enzymes. However, *bcat-1(RNAi)* did not suppress the accumulation of the UFD substrate induced by *ivd-1(tm6784)* (Figure 14A and 14B). qRT-PCR analysis confirmed that the *bcat-1*

transcript level was significantly reduced upon *bcat-1(RNAi)*, indicating efficient silencing (Figure 14C). *bcat-1(hh56)/+* showed similar results on the UbV-GFP turnover as *bcat-1(RNAi)*, confirming that knock-down of *bcat-1* has no effect on the UFD substrate degradation neither in wild-type nor in the *ivd-1(tm6784)* genetic backgrounds (Figure 14D and 14E). Intriguingly, the viable *bcat-1(hh58)* mutation was able to suppress the UPS defects of *ivd-1(tm6784)* (Figure 14D and 14E).

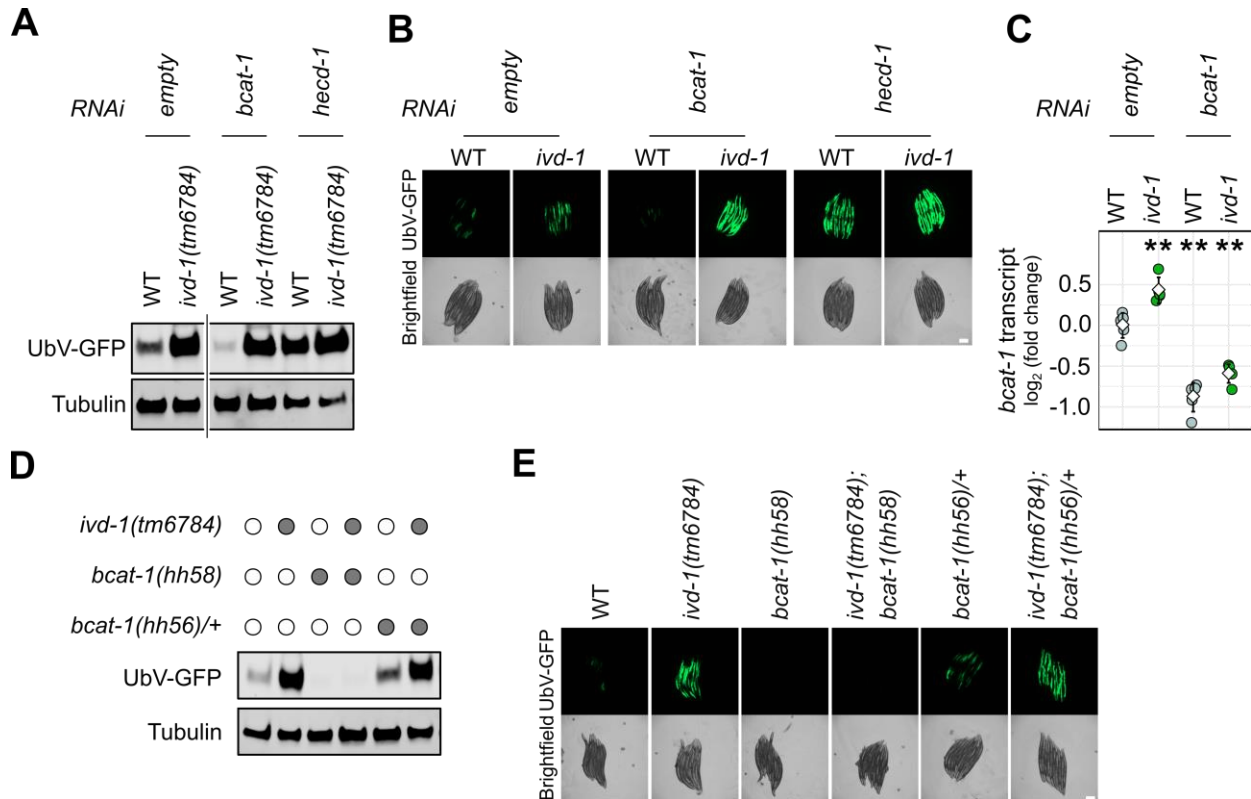


Figure 14 *bcat-1(hh58)* suppresses the proteolytic defects of *ivd-1(tm6784)*

(A, D) Representative Western blots of adult worm lysates showing UbV-GFP protein level with tubulin as loading control. *hecd-1(RNAi)* served as positive control. 3 and 2 experimental replicates respectively in A and D. (B, E) Fluorescent and brightfield microscopic images of immobilized worms expressing *UbV-gfp*, same samples and conditions as in A and D, respectively. Scale bars: 200 μ m. (C) Level of *bcat-1* mRNA transcript relative to wild-type (WT) treated with empty vector control measured by qRT-PCR, 5 technical replicates. Fold changes calculated as $2^{-\Delta\Delta C_q}$. Means as white squares and standard deviations as error bars. Statistically significant difference compared to WT was calculated with Tukey's Honest Significant Difference (HSD) combined with one-way ANOVA performed in R and indicated in relation control with * for

P-value ≤ 0.05 , ** for P-value ≤ 0.01 . (A-C) RNAi empty vector was used as control (empty).

The UbV-GFP stabilization caused by *ivd-1(tm6784)* mutation was restored in the *ivd-1(tm6784); bcat-1(hh58)* double mutants by expression of the BCAT-1::GFP translational reporter (Mansfeld et al., 2015) (Figure 15). To assure that the UFD substrate is not transcriptionally regulated, I crossed all mutants with the control reporter *sur-5p::mCherry* (Segref et al., 2011). Although *ivd-1(tm6784)* slightly upregulated the *sur-5p::mCherry* expression, this upregulation was not suppressed by *bcat-1(hh58)*, indicating that the lower UbV-GFP level in *ivd-1(tm6784); bcat-1(hh58)* derived from higher turnover, rather than lower expression (Figure 15A). In line with the observed rescue effect of *bcat-1::gfp* in the context of developmental and reproductive defects (Figure 12), this result indicates that the proteolytic defects caused by *ivd-1(tm6784)* is suppressed by *bcat-1* loss-of-function, suggesting a complex role of the BCAA metabolism in the regulation of ubiquitin-dependent protein degradation.

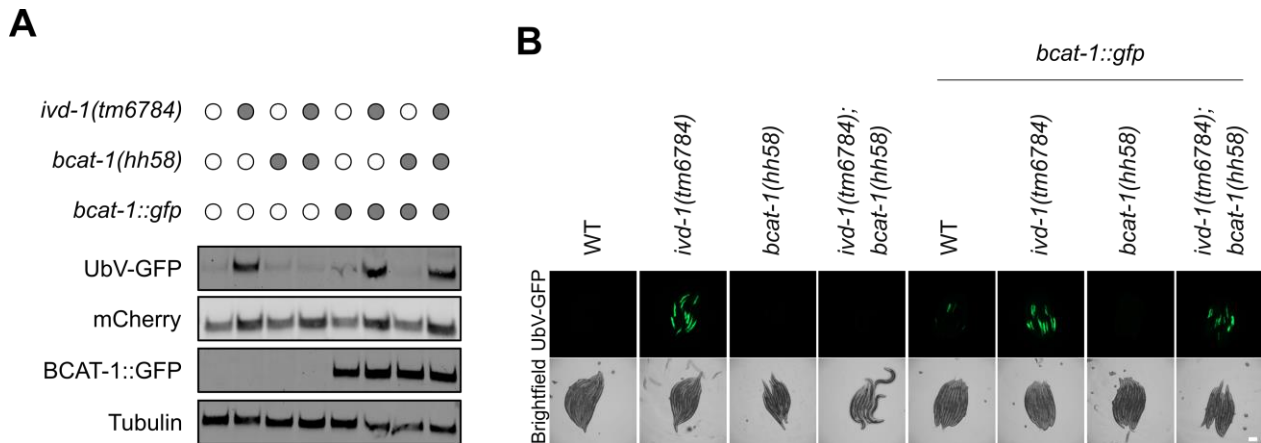


Figure 15 *bcat-1(hh58)* suppresses the UPS downregulation of *ivd-1(tm6784)*

(A) Representative Western blot of adult worm lysates showing UbV-GFP protein level compared with *sur-5p::mCherry* expression and with tubulin as loading control. 3 experimental replicates. (B) Fluorescent and brightfield microscopic images of immobilized adult worms expressing *sur-5p::UbV-gfp*. Same strains and conditions as in E. Scale bar: 200 μ m.

3.8 Multi-omics analysis reveals cooperative and antagonistic roles of IVD-1 and BCAT-1

To elucidate the complex genetic interaction between *ivd-1* and *bcat-1*, as well as their opposite role in the regulation of ubiquitin-dependent proteolysis, I decided to explore the underlying molecular mechanisms performing a multi-omics analysis. I compared transcriptomics, proteomics and metabolomics data derived from *ivd-1(tm6784)* and *bcat-1(hh58)*, both single and double mutants (Figure 16A and 16B). To specifically address the role of BCAA metabolism in proteostasis and particularly in the regulation of the UPS, I included the E3 ligase *hecd-1(tm2371)* mutants, which served as control of impaired UPS. Although both *ivd-1(tm6784)* and *hecd-1(tm2371)* mutants stabilized the UbV-GFP (Figure 9A), their transcriptome and proteome profiles differed greatly (Figure 16B), suggesting that the cellular compensation is distinct in the two mutants and most of the gene expression adaptation in *ivd-1(tm6784)* does not result from the stabilization of the UFD substrate. Frequency histograms of the fold changes detected stronger reprogramming associated with the *bcat-1(hh58)* mutation compared to *ivd(tm6784)*, both at transcript, protein and metabolite level (Figure 16C). This observation is in line with the previously described more drastic developmental and fertility defects of *bcat-1(hh58)* mutants compared with *ivd-1(tm6784)* mutants (Figure 12B-12D), and highlights the physiological relevance of the BCAA transamination.

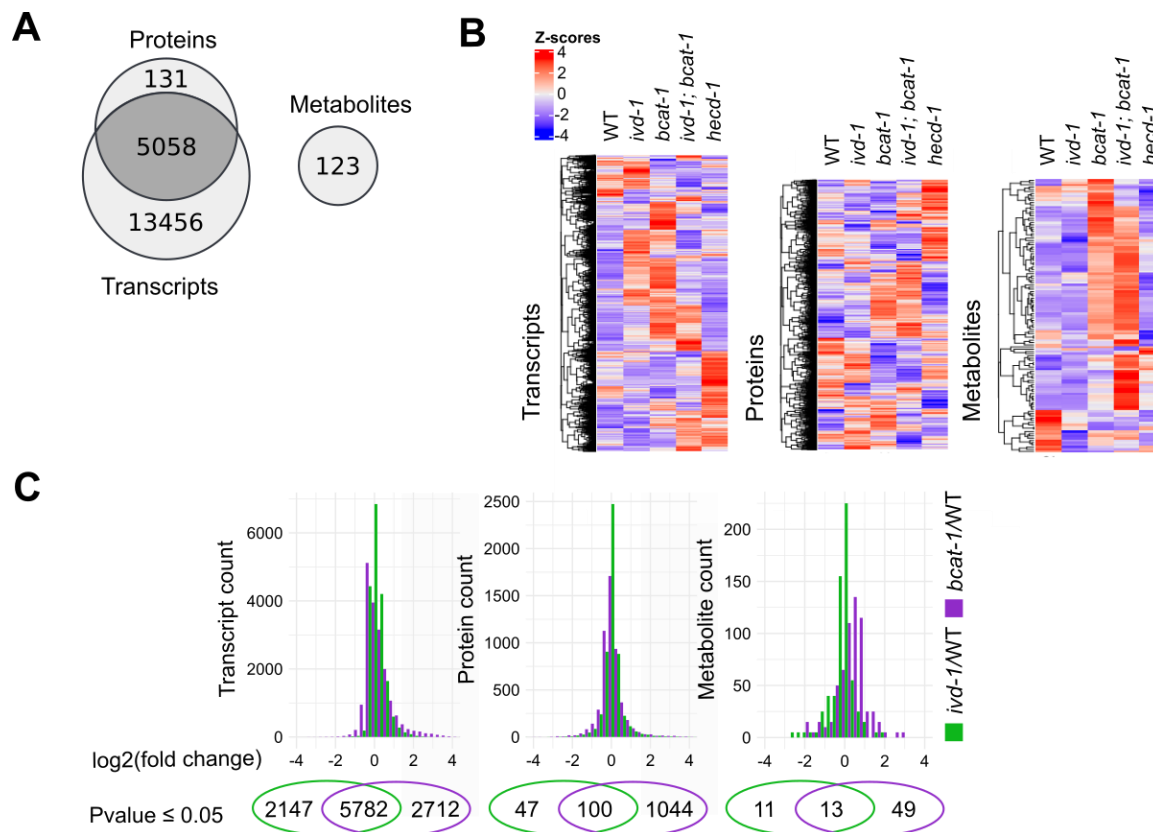


Figure 16 Multi-omics analysis highlights the broad physiological relevance of BCAA transamination

(A) Number of transcripts, proteins, and metabolites analyzed in the multi-omics analysis. 4 experimental replicates. (B) Heatmaps of Z-scores from the complete omics datasets (transcriptomics, proteomics, metabolomics). Means of 4 individual replicates. The reported mutant alleles are *ivd-1(tm6784)*, *bcat-1(hh58)*, and *hecd-1(tm2371)*. (C) Histograms of log₂(*ivd-1(tm6784)*/WT) (green) and log₂(*bcat-1(hh58)*/WT) (violet), with relative Venn diagrams displaying the number of significantly regulated transcripts, proteins, and metabolites, respectively (P-value ≤ 0.05). 0.3 bin width.

To identify the molecular mechanism underlying the defective turnover of the UFD substrate in *ivd-1(tm6784)*, I employed a filtering strategy, which was termed “*ivd-1* response”, selecting transcripts and proteins that were significantly regulated by the *ivd-1(tm6784)* mutation and reversed by the *bcat-1(hh58)* mutation (Figure 17). To identify regulatory pathways that are causally linked and not a consequence of *ivd-1(tm6784)* proteolytic defects, only *ivd-1(tm6784)* changes compared to both wild-type and

hecd-1(tm2371) were considered. This filter identified 2778 transcripts and 44 proteins (Figure 17A and 17B), among which, a big proportion was upregulated by *ivd-1(tm6784)* and suppressed by *bcat-1(hh58)*, and includes the most drastically regulated hits (Figure 17C and 17D). This observation suggests the induction of a transcriptional stress response that, upon impaired leucine catabolism, promotes the expression of specific genes, which is suppressed when the BCAA transamination is defective.

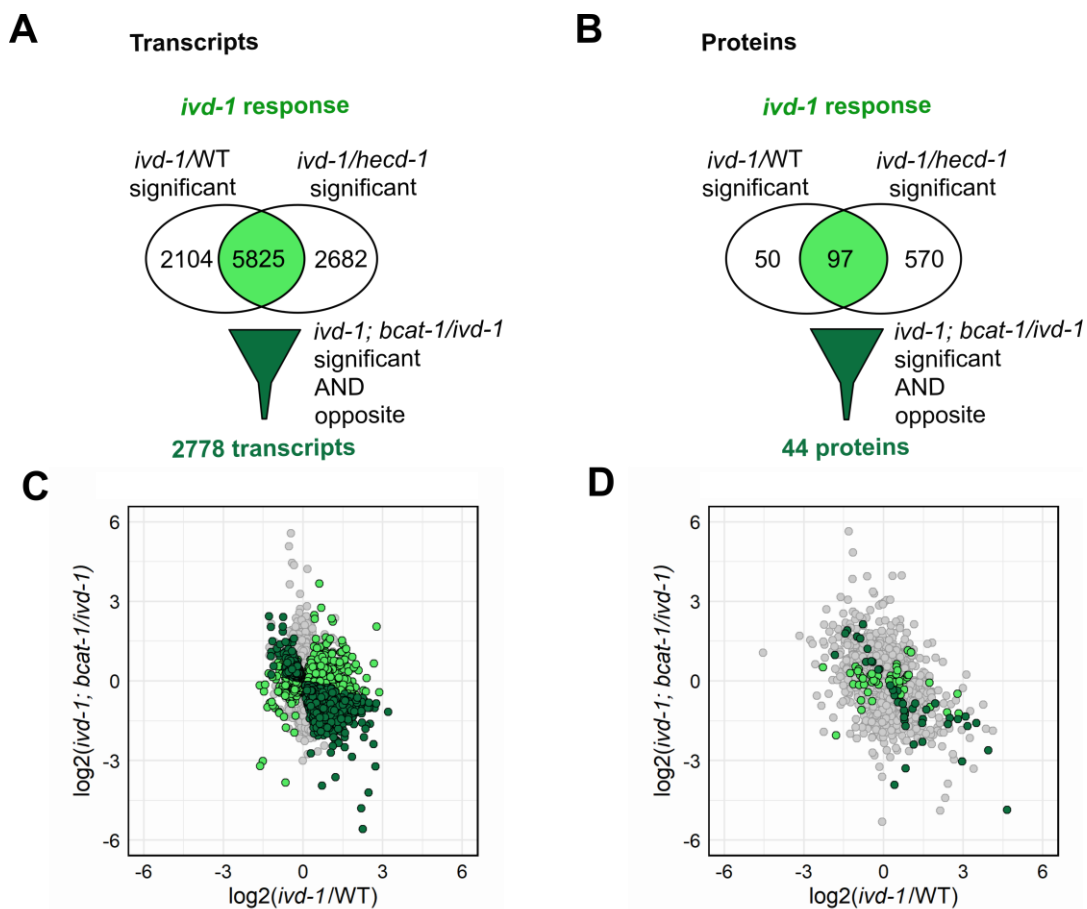


Figure 17 Filtering strategy to identify *ivd-1*-dependent regulation

(A, B) Venn diagrams of the regulated transcripts (A) and proteins (B) relative to the filtering for the “*ivd-1* response”: *ivd-1(tm6784)* significantly regulated genes compared to wild-type (WT) and *hecd-1(tm2371)* (light green), which are suppressed by *bcat-1(hh58)* (dark green) (P-value ≤ 0.05). (C, D) Scatterplots showing fold changes relative to A and B, respectively.

To distinguish the “*ivd-1* response” from the broad physiological changes caused by *bcat-1(hh58)*, I employed a second filtering strategy, termed “*bcat-1* response”, selecting

proteins and transcripts significantly regulated by *bcat-1(hh58)*, both in wild-type and *ivd-1(tm6784)* genetic backgrounds (Figure 18). In contrast to the “*ivd-1* response”, the “*bcat-1* response” filter identified a slightly lower number of transcripts, 2003 compared to 2778 and a higher number of regulated proteins, 399 compared to 44 (Figure 18A and 18B). This observation indicates that *bcat-1(hh58)* mutation has a more drastic effect on the proteome compared with *ivd-1(tm6784)*, which in turn seems to regulate gene expression mostly transcriptionally. In the scatterplots displaying filtered transcripts and proteins respectively filtered for the “*bcat-1* response” it is clear that the most drastic changes are similarly regulated by *bcat-1(hh58)* regardless of the background, once more highlighting the physiological relevance of the BCAA transamination (Figure 18C and 18D).

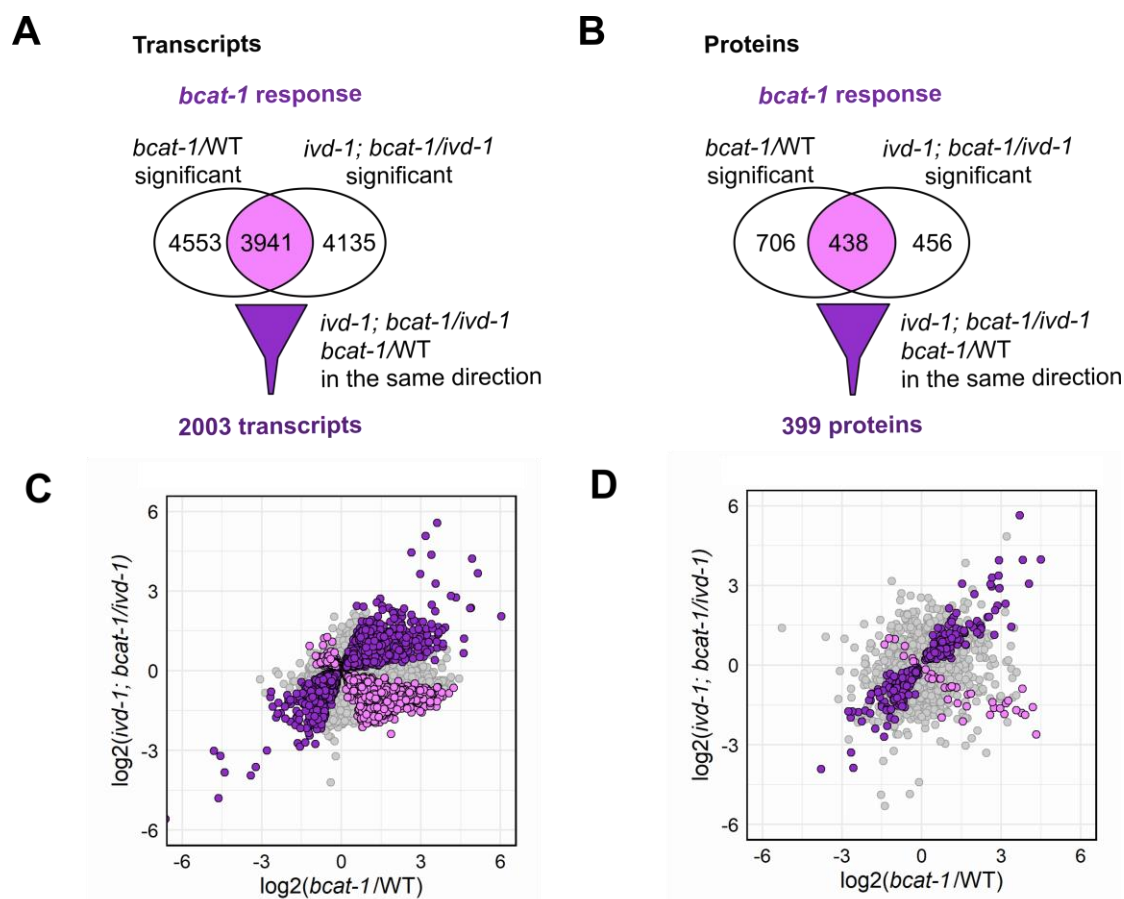


Figure 18 Filtering strategy to identify *bcat-1*-specific regulation

(A, B) Venn diagrams of the regulated transcripts (A) and proteins (B) relative to the filtering for the “*bcat-1* response”: *bcat-1(hh58)* significantly regulated genes in wild-type (WT) and

ivd-1(tm6784) background (pink) that follow the same direction (violet) (P -value ≤ 0.05). (C, D) Scatterplots showing fold changes relative to A and B, respectively.

Significant fold changes of genes regulated by *ivd-1(tm6784)* and *bcat-1(hh58)* single mutants, respectively compared to wild-type, displayed a good degree of linear correlation, with R^2 of 0.78 for transcripts and 0.61 for proteins (Figure 19A), suggesting that many changes induced by either single mutation follow the same direction. However, when comparing the changes induced in *ivd-1(tm6784)* mutants with the ones related to *ivd-1(tm6784); bcat-1(hh58)* double mutants, an inverse correlation is detected, although the low R^2 indicates that many fold changes deviate from the linear fitting (Figure 19B). In line with these observations, the regulations identified by “*ivd-1* response” and “*bcat-1* response” are clearly distinct, with only 82 common transcripts out of 4699 and 12 common proteins out of 431 (Figure 19C). The small overlaps suggest that the restored UPS activity in *ivd-1(tm6784); bcat-1(hh58)* double mutants is mediated by an adaptive response rather than broad *bcat-1(hh58)*-dependent regulation. The correlation studies reported here indicate that BCAA metabolic defects influence both proteome and transcriptome regardless of the specific catabolic step impaired. In contrast, the regulation induced by defective leucine catabolism is partly reversed by additional impairment in the BCAA transamination, revealing cooperative and antagonistic physiological roles relative to the different BCAA catabolic steps.

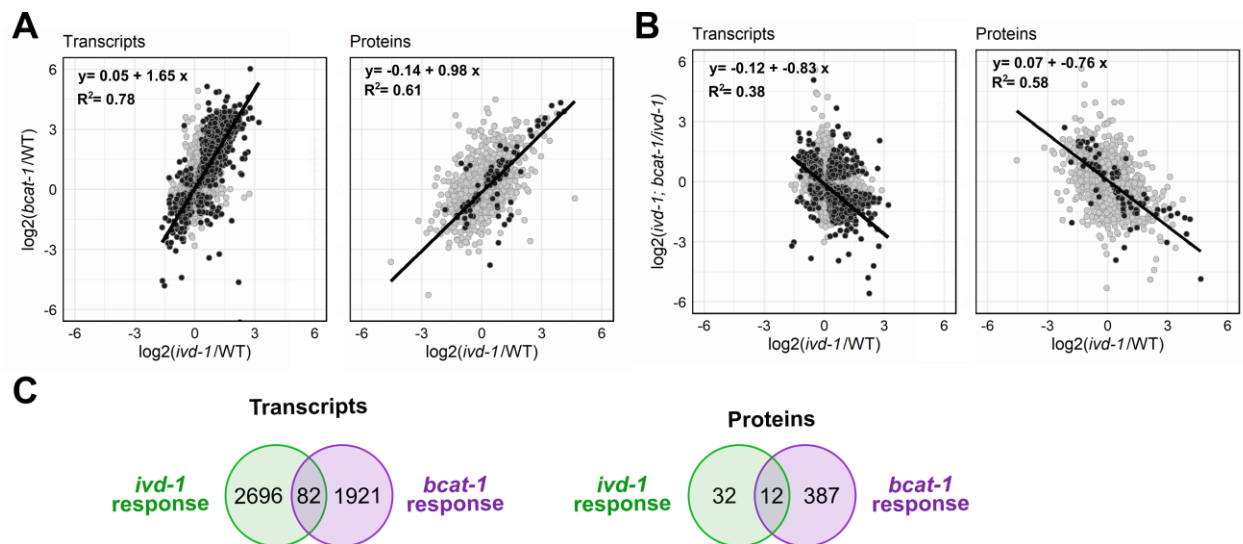


Figure 19 The *bcat-1(hh58)* suppression of *ivd-1(tm6784)* derives mainly by genetic interaction and not epistasis

(A, B) Scatterplots of fold changes relative to transcripts (left) and proteins (right), with darker fill indicating significantly different fold changes for both axes (P -value ≤ 0.05). Linear regression with relative formula and R^2 are indicated in black. (C) Intersection between the two filtering groups.

3.9 Impaired BCAA metabolism defines transcriptional programs

The general overview about transcriptome and proteome regulation reported in the previous paragraph suggests that *ivd-1(tm6784)* possibly induces a transcriptional stress response. To explore which transcriptional programs might be activated by *ivd-1(tm6784)*, I conducted a gene set enrichment analysis using the online tool WormCat (Holdorf et al., 2020). I included transcripts identified with the filtering strategies described above (Figure 17 and 18) and observed numerous categories enriched exclusively for the “*bcat-1* response”. In contrast, fewer categories were enriched for the “*ivd-1* response”, including metabolism, membrane transport, transcription factor, and stress response (Figure 20A). Proteostasis-related categories were also significantly enriched; particularly, the category “proteolysis proteasome” emerged as downregulated by the “*ivd-1* response” and upregulated by the “*bcat-1* response”, reflecting the UFD substrate turnover (Figure 14).

Focusing on the regulated transcripts of genes falling in the enriched categories “Proteolysis proteasome” and “Proteolysis general”, for which the relative proteins were

detected, a clear overall reduction of the former category and an increase of the latter category is visible for *ivd-1(tm6784)* mutants (Figure 14B). In contrast, *ivd-1(tm6784); bcat-1(hh58)* double mutants caused opposite regulation, while the *bcat-1(hh58)* mutants were more related to wild-type or *ivd-1(tm6784)*, supporting the idea that the restored UPS activity of *ivd-1(tm6784); bcat-1(hh58)* mutants is mediated by an adaptive response rather than general *bcat-1(hh58)* regulation. The UPS components downregulated by the *ivd-1(tm6784)* mutation include 19S proteasome subunits, E3 ligases, and DUBs (mentioned as ubiquitin peptidases in WormCat). Interestingly, no regulation of the 20S proteasome subunits was detected, supporting the idea that the BCAA metabolism regulates cytosolic proteolysis by reprogramming the substrate specificity of the proteasome, rather than its general activity. However, the RPN-6.1 overexpression has been reported to foster proteasome activity (Vilchez et al., 2014), indicating different levels of complexity in the molecular mechanisms underlying the UPS regulation by the BCAA metabolism.

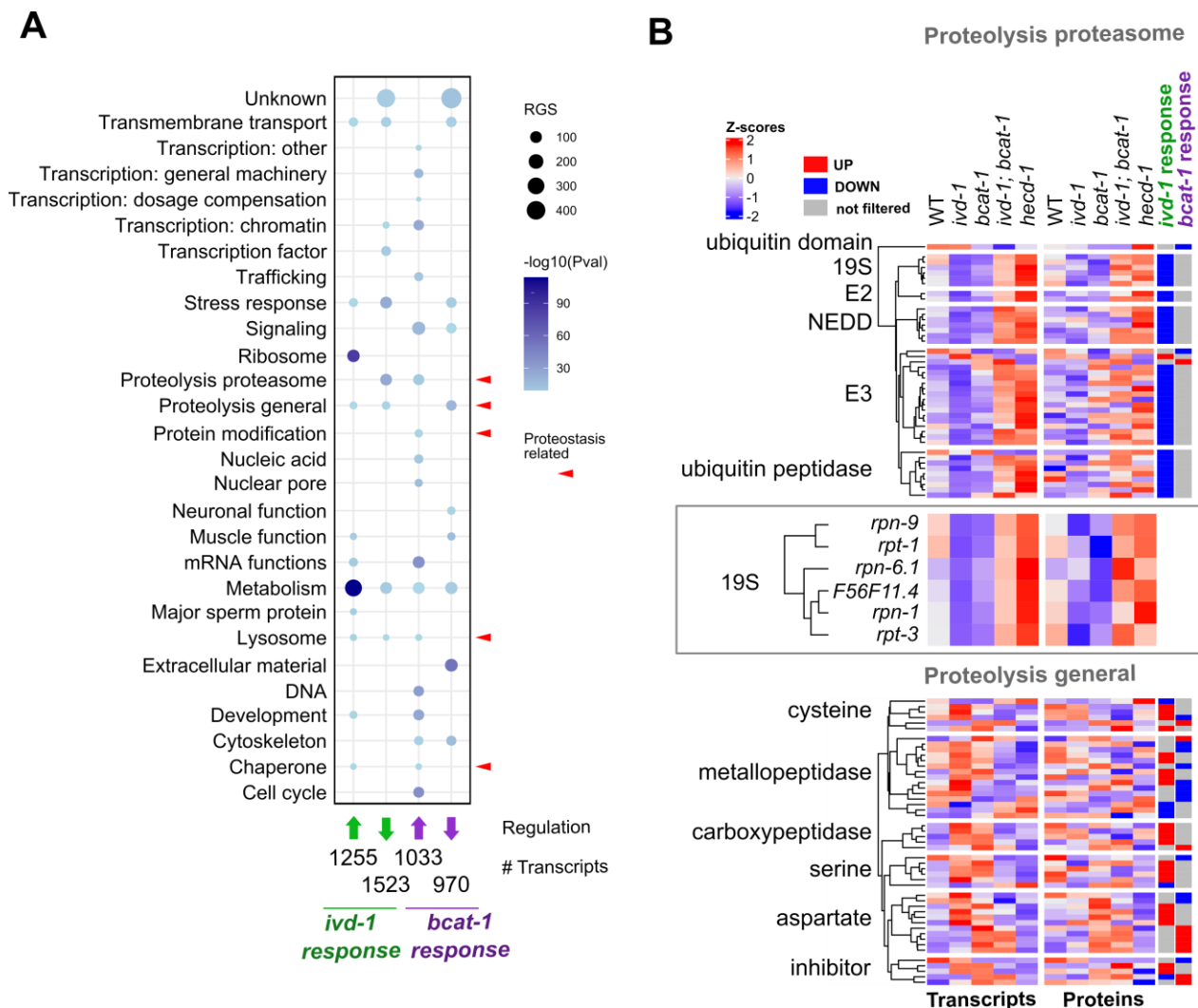


Figure 20 BCAA metabolism regulates the expression of UPS components

(A) Bubble chart of WormCat (Holdorf et al., 2020) gene enrichment analysis for Category 1. Number of regulated gene set (RGS, size of bubbles) and $-\log_{10}(\text{P-value})$ (color scale) of up- and down-regulated genes from “*ivd-1* response” and “*bcat-1* response” filtering. Proteostasis-related categories are indicated with red arrowheads. (B) Heatmaps with Z-scores relative to transcript and protein levels of genes within WormCat categories “Proteolysis general” and “Proteolysis proteasome”, with blow up of 19S subunits indicated by gene name. Clustering according to transcript levels and split according to WormCat category 2 (indicated on the left). All reported genes were filtered for either “*ivd-1* response” or “*bcat-1* response”, indicated on the right as up- (red) or down-regulated (blue) or not filtered (grey). The reported mutant alleles are *ivd-1(tm6784)*, *bcat-1(hh58)*, and *hecd-1(tm2371)*.

3.10 Changes in the BCAA metabolism induce an adaptive metabolic regulation

To further explore the link between BCAA metabolism and UPS regulation, I combined metabolomics data with transcriptomics and proteomics. Selecting the transcripts filtered for either “*ivd-1* response” or “*bcat-1* response”, nearly all metabolic genes connected with mitochondrial functions fell into the “*bcat-1* response” group (Figure 21A). Accordingly, transcription of these genes remained unaltered in *ivd-1(tm6784)* mutants; whereas, it was strongly reduced in *bcat-1(hh58)* single and in *ivd-1(tm6784); bcat-1(hh58)* double mutants, mostly reflected at the protein level. Genes involved in other pathways such as lipid, nucleotide, and amino acid metabolism were both up- and down-regulated by *ivd-1(tm6784)* and *bcat-1(hh58)* mutations, reflecting a more complex metabolic reprogramming (Figure 21A). In contrast, the *bcat-1(hh58)* mutation drastically reduced most metabolites, whereas the *ivd-1(tm6784)* metabolic profile resembled more that of the wild-type control (Figure 21B). Therefore, defective transamination of BCAAs induces a profound metabolic reprogramming, while leucine catabolic defects have milder effects on metabolism.

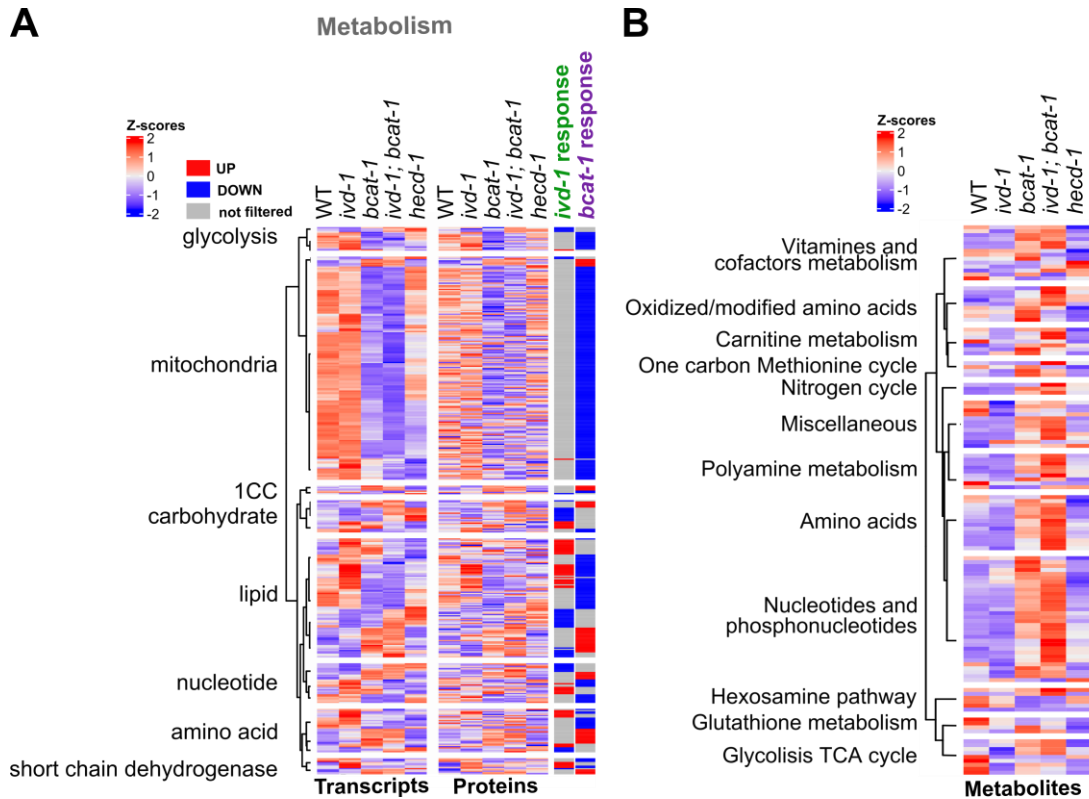


Figure 21 *bcat-1(hh58)* mutation downregulates mitochondrial genes and accumulates metabolites

(A) Heatmaps with Z-scores relative to transcript and protein levels of genes with WormCat gene category 1 “Metabolism”, filtered for either “*ivd-1* response” or “*bcat-1* response”, indicated on the right as up- (red) or down-regulated (blue) or not filtered (grey). Heatmaps were clustered according to transcript levels and split according to WormCat category 2 (indicated on the left). (B) Heatmap with Z-scores relative to the metabolite levels, split into categories (indicated on the left). (A-B) The reported mutant alleles are *ivd-1(tm6784)*, *bcat-1(hh58)*, and *hecd-1(tm2371)*.

Even though the metabolic regulation induced by *ivd-1(tm6784)* was very minor in comparison to *bcat-1(hh58)*, I combined transcriptomics and metabolomics data to visualize the *ivd-1(tm6784)* changes occurring in metabolic pathways directly or indirectly related to the BCAA metabolism (Figure 22). To visualize which of the regulations were reversed by *bcat-1(hh58)*, the regulation of *ivd-1(tm6784); bcat-1(hh58)* double mutants compared to *ivd-1(tm6784)* single mutants was also displayed. Although it is difficult to interpret the metabolic map as a whole, it is clear that *ivd-1(tm6784)* mutants downregulate glycolysis, electron transport chain (ETC) and TCA cycle. While glycolysis

seems restored by *bcat-1(hh58)*, ETC and TCA cycle is further reduced in the *ivd-1(tm6784); bcat-1(hh58)* double mutants, indicating complex metabolic adaptations due to the altered BCAA metabolism. BCAAs are significantly upregulated in the *ivd-1(tm6784); bcat-1(hh58)* double mutants compared to *ivd-1(tm6784)*, therefore I wondered if this regulation occurs also in the *bcat-1(hh58)* single mutants. Interestingly, *bcat-1(hh58)* upregulated most amino acids, including all three BCAAs, and this increase was enhanced in the double mutants. In contrast, *ivd-1(tm6784)* mutants maintained amino acid levels similar to with wild-type worms (Figure 22B).

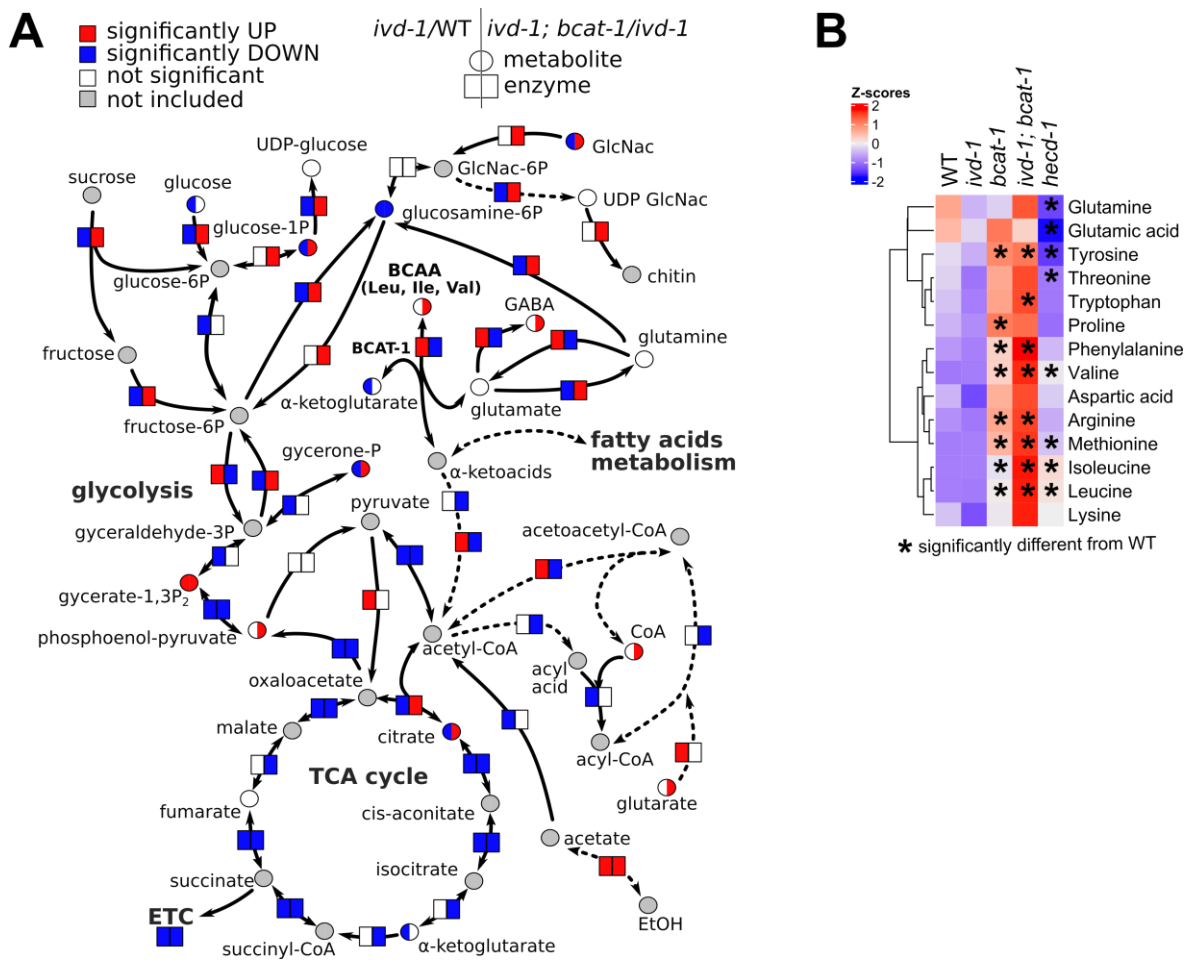


Figure 22 Impaired BCAA metabolism induces general metabolic adaptation

Simplified metabolic map with metabolites (circles) and enzyme transcripts (rectangles) relative to *ivd-1(tm6784)* changes compared to wild-type (WT) (left) and *ivd-1(tm6784); bcat-1(hh58)* changes compared to *ivd-1(tm6784)* (right). Colors indicate changes that are significantly increased (red, P-value ≤ 0.05), decreased (blue, P-value ≤ 0.05), not significantly changed (white,

P-value > 0.05), not present in the dataset (grey). Generated and modified from Pathview (Luo et al., 2017). (B) Heatmap with Z-scores relative to amino acid levels. Asterisks indicate significantly different changes compared to wild-type (P-value \leq 0.05). The reported mutant alleles are *ivd-1(tm6784)*, *bcat-1(hh58)*, and *hecd-1(tm2371)*.

The same filtering strategy employed for transcript and protein regulation (Figure 17 and 18) identified 46 regulated metabolites for the “*bcat-1* response”, and 4 metabolites for the “*ivd-1* response” (Figure 23). This result is in line with the drastic metabolic regulation caused by *bcat-1(hh58)* and the milder metabolic regulation of the *ivd-1(tm6784)* (Figure 21). Reducing the stringency of the “*ivd-1* response” filtering and including also changes possibly associated with the UPS impairment of *ivd-1(tm6784)* identified in total 9 metabolites that were significantly changed in *ivd-1(tm6784)* compared to wild-type and suppressed by *bcat-1(hh58)* (Figure 23D). Among those metabolites, acetyl-carnitine was particularly increased in the *ivd-1(tm6784); bcat-1(hh58)* double mutant compared to all other strains, emerging as a key metabolite for the genetic interaction between *ivd-1* and *bcat-1*, in contrast to the broad metabolic reprogramming induced by *bcat-1(hh58)*.

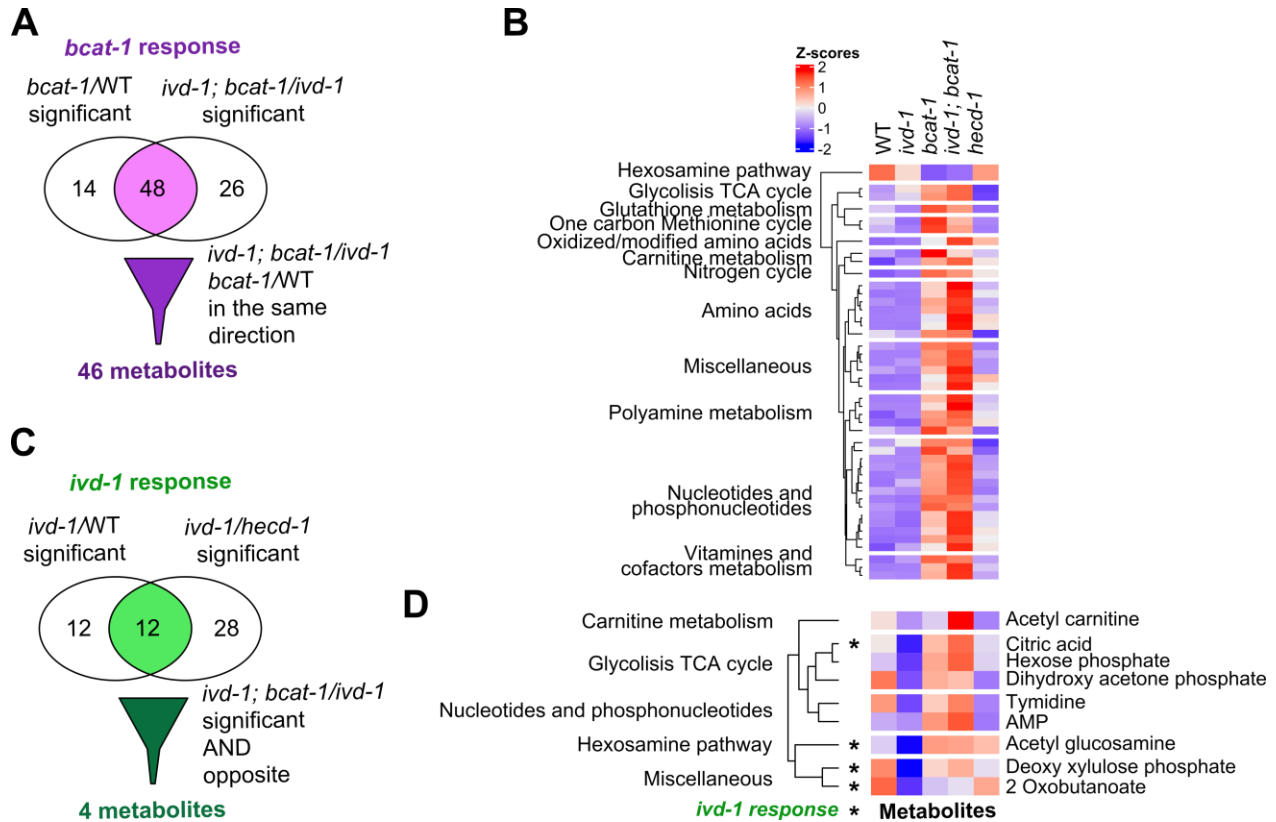


Figure 23 Acetyl-carnitine emerged as a key metabolite in the UPS regulation by the BCAA metabolism

(A) Filtering summary of metabolite changes relative to the “*bcat-1* response”, conducted as for transcripts and proteins (Figure 18) (B) Heatmap with Z-scores relative to the level of the 46 metabolites filtered for the “*bcat-1* response” reported in A. (C) Filtering summary of metabolite changes relative to the “*ivd-1* response” (Figure 17) (D) Heatmap with Z-scores of metabolites significantly changed in *ivd-1(tm6784)* compared to WT and suppressed by *bcat-1(hh58)* (P-value ≤ 0.05). Metabolites significantly different in *ivd-1(tm6784)* also compared with *hecd-1(tm2371)* are labeled with asterisks. (A-D) The reported mutant alleles are *ivd-1(tm6784)*, *bcat-1(hh58)*, and *hecd-1(tm2371)*.

3.11 Isovaleric acid directly affects proteostasis

Elevated acetyl-carnitine in *ivd-1(tm6784); bcat-1(hh58)* mutants (Figure 23D) might indicate an adaptive response induced by the *bcat-1(hh58)* mutation to enhance IVA clearance in case of impaired IVD-1. In fact, acetyl-carnitine has been reported as an indicator for sufficient concentration of carnitine clinically administered for the treatment

of isovaleric acidemia (Itoh et al., 1996). Consequently, I wondered whether IVA is the key metabolite which triggers the proteolytic defects of *ivd-1(tm6784)* mutants. Since direct quantification of isovaleric acid is challenging due to spontaneous conjugation with other compounds (Villani et al., 2017), I opted to supplement the growth medium with IVA to address its role in ubiquitin-dependent degradation. Indeed, IVA supplementation was sufficient to inhibit degradation of UbV-GFP in wild-type worms as well as in *ivd-1(tm6784); bcat-1(hh58)* double mutants, abrogating the suppression by *bcat-1(hh58)* (Figure 24A). The UbV-GFP level was unaltered in *bcat-1(hh58)* single mutants supplemented with IVA, possibly due to IVA catabolic oxidation after conversion into isovaleryl-CoA (Figure 4). In line with this hypothesis, IVA supplementation ameliorated *bcat-1* developmental defects which suggests that complete BCAA catabolism is required for organismal development (Figure 24C). Conversely, *ivd-1(tm6784); bcat-1(hh58)* developmental defects were exacerbated by IVA supplementation, since IVA catabolism is abrogated in worms lacking IVD-1. Although some degree of transcriptional regulation of the reporter depending on the *sur-5* promoter might occur, the mCherry protein levels confirm that elevated IVA reduces the turnover of the UFD substrate (Figure 24A). Protein ubiquitylation was not impaired by elevated IVA, neither due to *ivd-1(tm6784)* mutation nor direct IVA supplementation (Figure 24B), confirming that the ubiquitin-dependent degradation defects occur downstream of ubiquitylation.

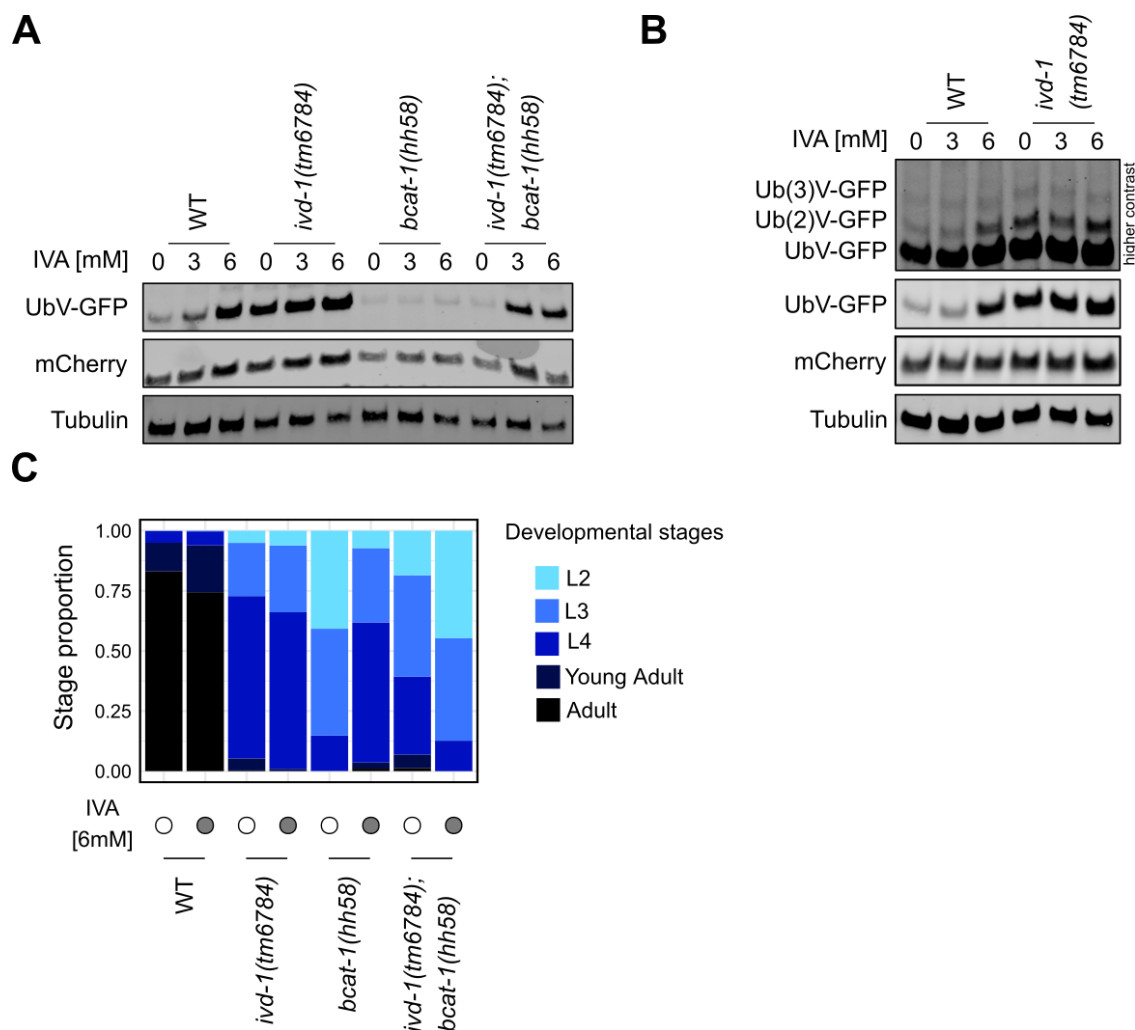


Figure 24 Isovaleric acid impairs ubiquitin-dependent protein degradation

(A) Representative Western blot of adult worm lysates showing UbV-GFP protein level compared with *sur-5p::mCherry* expression and with tubulin as loading control. Worms were treated with the indicated concentrations of IVA, H₂O as control. 4 experimental replicates (B) Representative Western blot following the same conditions as in A with higher contrast to observe UbV-GFP ubiquitylation. (C) Quantification of developmental stages after treatment with IVA. Means of 5 technical replicates.

IVA supplementation also aggravated the aging-induced protein aggregation in worms expressing Q40::YFP in the intestine (Figure 5C, data collected by Qiaochu Li) (Mohri-Shiomi and Garsin, 2008). Since polyglutamine (polyQ) expansions have been identified as causal agent for several neurodegenerative disorders due to their propensity to form aggregates, the expression of fluorophore-coupled polyQ expansion proteins in *C.*

elegans represents an effective model system to study the cytotoxic effect of protein aggregation (Satyal et al., 2000). The increased protein aggregation caused by IVA indicates a broader effect on protein homeostasis, not only limited to UPS substrates.

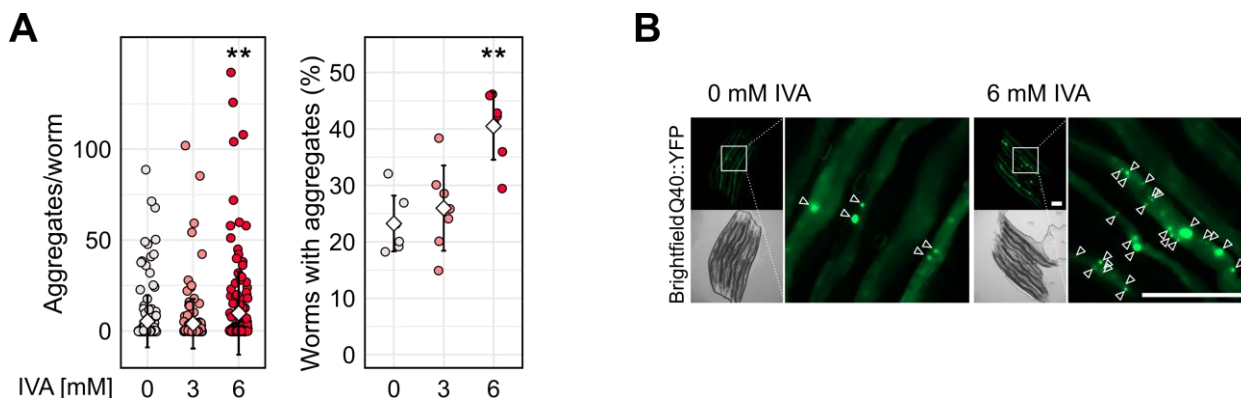


Figure 25 Isovaleric acid promotes aggregation of metastable proteins

(A) Manual quantification of protein aggregation in worms expressing Q40::YFP in intestine (Mohri-Shiomi and Garsin, 2008) upon IVA supplementation, reported as number of aggregates for each worm (left) and percentage of worms showing at least one aggregate (right). Means as white squares and standard deviations as error bars. 7 experimental replicates with 11 to 30 worms. Statistically significant difference was calculated with Wilcoxon rank sum test with Bonferroni P-value correction performed in R and indicated in relation to the control condition with * for P-value ≤ 0.05 , ** for P-value ≤ 0.01 . (B) Fluorescent and brightfield microscopic images of immobilized worms expressing Q40::YFP in the intestine. Arrowheads in the magnifications indicate protein aggregates. Scale bars: 200 μm . (A, B)

Data collected and images taken by Qiaochu Li.

4 Discussion

The BCAA metabolism is not only an important catabolic pathway for the production of energy, but also a central hub influencing multiple physiological processes. Previous data from our laboratory connected the catabolism of the BCAA leucine with the regulation of ubiquitin-dependent protein turnover in the cytosol of the intestine. This study confirmed a conserved UPS regulation also in mammalian cells, revealing a correlation between isovaleric acidemia symptoms with UPS defects (Segref et al., 2014). However, the mechanism underlying the connection between isovaleric acidemia and UPS defects remained to be determined. My data provide additional information indicating cooperative and antagonistic physiological roles relative to different BCAA catabolic steps. Particularly, depletion of IVD-1 leads to the accumulation of the intermediate metabolite IVA, which in turn negatively impacts organismal proteostasis. In contrast, altered BCAA transamination caused by the newly generated *bcat-1(hh58)* viable mutant restores the UPS capacity, coordinating a general metabolic adaptation which might prevent IVA accumulation and ultimately promotes general proteostasis.

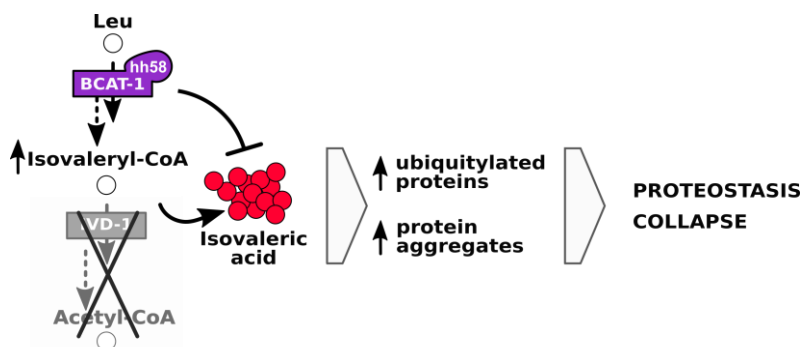


Figure 26 Proteostasis regulation by the BCAA metabolism: proposed model

ivd-1 depletion induces elevated IVA, which in turn inhibits the degradation of ubiquitylated proteins and aggravates aggregation of metastable proteins. Conversely, loss-of-function BCAT-1 prevents the accumulation of IVA and promotes proteostasis.

4.1 The BCAA metabolism takes on distinct roles in proteostasis regulation

BCAAs constitute approximately 35% of the total essential amino acid pool in mammals and their hydrophobic branched chain groups make them critical components for most proteins (Neinast et al., 2019). Breakdown of BCAAs is also a valuable source of energy; moreover, BCAAs and several intermediate metabolites produced during their catabolism are important signaling molecules activating the mTOR signaling pathway (Neinast et al., 2019; White et al., 2021). As important regulator of cell growth, mTOR might therefore be involved in the developmental and viability defects observed in the BCAA mutants (Figure 12). However, the significantly higher level of BCAAs in *bcat-1(hh58)* (Figure 22B) would theoretically activate mTOR signaling, promoting growth and instead *bcat-1(hh58)* mutant worms are slow-growing (Figure 12B). Moreover, *bcat-1(hh58)* resulted to be beneficial on organismal proteostasis and protective against toxic levels of IVA, either caused by *ivd-1* depletion or direct supplementation (Figure 14, 15, and 24). In contrast, mTOR is known to inhibit proteolytic systems, including autophagy and the UPS (Saxton and Sabatini, 2017), suggesting a regulatory mechanism distinct from the conventional mTOR induction by increased BCAAs. Alternatively, intracellular amino acid transporters might influence the amino acid sensitivity of mTOR in a compartment-specific manner (Goberdhan et al., 2016).

It is still under debate if elevated or reduced BCAAs promote longevity (Green et al., 2021; Mansfeld et al., 2015; Martin et al., 2011; Valerio et al., 2011; White et al., 2021). This contradictory effect of BCAAs on lifespan could be explained by the cooperation of multiple regulatory mechanisms that are influenced by the BCAA metabolism but not directly dependent on the absolute level of free BCAAs. In line with this hypothesis, my data suggest that changes in the BCAA metabolic flux influence proteostasis-related machineries along with numerous other molecular processes (Figure 20A) not necessarily affecting the total level of BCAAs, as observed for *ivd-1(tm6784)* (Figure 22B). Considering the role of the UPS in amino acid recycling (Suraweera et al., 2012), the UPS regulation by an altered BCAA metabolism might derive from the cellular need to regulate the free amino acid pool. Accordingly, the level of most amino acids is drastically

increased in the *ivd-1(tm6784); bcat-1(hh58)* double mutants, which also display higher UPS functionality compared with *ivd-1(tm6784)*.

The intriguing opposite role in proteostasis conducted by BCAT-1 and IVD-1 could derive from the specialized subcellular and tissue-specific activity of BCAT enzymes deviating from the catabolic roles of the downstream enzymes (Neinast et al., 2019; Sperringer et al., 2017). In fact, the BCAA transamination is crucial not only for catabolic generation of energy, but also for regulating the pool of neurotransmitters in neurons (Sperringer et al., 2017). The identified role of BCAT-1 in the regulation of ubiquitin-dependent proteolysis might be connected with the reported correlation between BCAT impairments and neurodegenerative diseases (El Hindy et al., 2013; Harris et al., 2020; Hull et al., 2015a; Sperringer et al., 2017; White and Newgard, 2019). Since the complete knock-out of *bcat-1* resulted in 100% embryonic lethality (Figure 11B), the *bcat-1(hh58)* mutation is predicted to produce a functional but mislocalized BCAT-1, due to a disrupted mitochondrial targeting peptide (Chapter 3.6). Consequently, BCAT-1 subcellular compartmentalization might be relevant for the regulation of proteostasis. Compartmentalization represents a general cellular strategy to finely regulate the self-inhibitory nature of metabolic reactions (Alam et al., 2017). Studying the specific roles of single metabolic enzymes is very challenging, not only due to dynamic metabolic adaptations, but also due to the tissue-specific expression of metabolic enzymes, such as BCAT or BKCD, and complex shuttling systems to flexibly move metabolites intra- and extra-cellularly (Alam et al., 2017; Biswas et al., 2019; Neinast et al., 2019; Sperringer et al., 2017).

4.2 BCAA-derived intermediates influence proteostasis

Intermediate metabolites accumulating in inborn genetic disorder associated with the BCAA metabolism are considered major pathological agents. As isovaleric acidemia is characterized by accumulation of toxic metabolic derivatives of isovaleryl-CoA, impairment in other steps of the pathway causes multiple metabolic disorders collectively called organic acidurias or acidemias due to the identification of small carboxylic acids in urine and blood (Manoli and Venditti, 2016). Organic acidurias are connected with a large

spectrum of clinical symptoms, from asymptomatic to life-threatening. Current therapies consist in diet restriction of the respective precursor and removal or conversion of the toxic metabolites (Knerr et al., 2019; Manoli and Venditti, 2016). Besides ROS production and alteration of the cellular pH, the mechanistic link between metabolic intermediates and organic aciduria symptoms remains elusive. My results demonstrate that elevated IVA directly reduces the turnover of UPS substrates (Figure 24). Moreover, the increased aggregation of metastable proteins upon IVA supplementation indicates a more general proteostasis loss, not only limited to UPS functionality (Figure 25). Notably, intermediate metabolites can spontaneously modify proteins with acylation reactions, which are counteracted by sirtuins (Houtkooper et al., 2012; Keller et al., 2015; Piedrafita et al., 2015; Wagner et al., 2017). Particularly, acylation of BCAA enzymes has been proposed as a feedback loop that regulate the relative enzymatic reactions according to the level of produced intermediate metabolites (Anderson et al., 2017). Consequently, IVA might affect proteostasis through protein acylation, either regulating the activity of transcription factors or directly modifying components involved in the proteolytic system, such as proteasome subunits.

Elevated levels of acetyl-carnitine have been reported to reflect efficient detoxification of accumulated isovaleric acid through carnitine binding (Chinen et al., 2017; Itoh et al., 1996). Carnitines are important detoxifying molecules, which sequester acyl groups from acyl-coenzyme A esters, thanks to the action of carnitine acyltransferases (Adeva-Andany et al., 2017). Therefore, the increased level of acetyl-carnitine in *ivd-1(tm6784)*; *bcat-1(hh58)* mutants suggests an adaptive metabolic reprogramming aiming to reduce the level of toxic IVA. Although accumulation of toxic metabolites is causally linked to pathology, other secondary effects might be involved, like for example downstream metabolite deprivation or regulation of other metabolic pathways such as the TCA cycle or the oxidative phosphorylation. ATP levels were not reduced in the *ivd-1* loss-of-function mutants, but rather increased (Segref et al., 2014); however, the multi-omics analysis presented here suggests a general reduction of mitochondrial respiration, glycolysis and TCA cycle (Figure 22A). This effect might derive from a regulatory adaptation of the *ivd-1* loss-of-function mutants which possibly includes the transcriptional downregulation of proteasome subunits and other UPS components to remodel the proteasome's substrate

specificity (Figure 20). The putative stress response activated by impaired IVD-1 is reversed by *bcat-1(hh58)* mutation, which, in turn, restores transcriptional regulation of proteasome subunits as well as glycolytic genes (Figure 20B and 22A).

4.3 BCAA metabolism regulates UPS specificity

BCAA metabolic alterations regulate the expression of UPS components, including proteasome subunits of the 19S regulatory particle (Figure 20B), possibly resulting in specialized proteasome compositions, which might specifically degrade alternative substrates and protect specific proteins from conventional degradation. In line with this hypothesis, the UbV-GFP reporter proved to be a specialized UPS substrate and not an indicator for general UPS activity, which can be more reliably monitored through immunoblots of total ubiquitylated proteins (Figure 5A). Proteolytic activity of the proteasome and general ubiquitylation were not affected in *ivd-1* loss-of-function mutants (Segref et al., 2014), supporting the hypothesis that the UbV-GFP accumulation in *ivd-1* loss-of-function mutants derive by changed substrate specificity rather than general UPS impairment. Accordingly, the amino acid level of *ivd-1(tm6784)* mutants was comparable to wild-type (Figure 22B), suggesting that a sufficient amount of amino acids is efficiently recycled by the proteasome (Suraweera et al., 2012).

Recently, a study reported the reversible regulation of the proteasome assembly and activity in response to impaired mitochondrial respiration (Meul et al., 2020). Confirming the absence of oxidative stress, it was demonstrated that aspartate or pyruvate supplementation was sufficient to restore proteasome capacity via mTOR. Interestingly, the RNAi screen I conducted identified a role of pyruvate dehydrogenases in UPS regulation. Pyruvate dehydrogenases were also downregulated in *ivd-1(tm6784)* mutants (Figure 22A), suggesting a common metabolic adaptation, that might underlie the observed UPS regulation. However, *bcat-1(hh58)* further reduced the transcription of pyruvate dehydrogenases, instead of rescuing the expression, suggesting that the metabolic stress induced by depletion of pyruvate dehydrogenases influences the UPS activity in a distinct process. According to the metabolomics data I presented here, aspartate was stable in all mutants (Figure 22B), supporting the idea that the UPS

regulation observed upon altered BCAA metabolism follows a distinct pathway, excluding the involvement of pyruvate dehydrogenases (Meul et al., 2020).

Among the regulated subunits (Figure 20B), RPN-6 has been reported to be crucial for proteasome activity, proteostasis, and longevity (Vilchez et al., 2014). Moreover, *rpn-6.1* overexpression could suppress the proteolytic defects of *ivd-1(hh56)* loss-of-function mutants (Segref et al., 2014), confirming an important role of RPN-6.1 in the regulation of UPS activity upon BCAA metabolic stress. Alternatively, the UPS regulation could derive from post-translational protein modifications. 110 co- and post-translational modifications have been identified on the yeast 26S proteasome (Kikuchi et al., 2010); however, many have not been functionally elucidated yet. As alternative to the direct modification of UPS components, the already mentioned post-translational acylation triggered by IVA might modify UPS components or external components that directly or indirectly influence the regulation of ubiquitin-dependent proteolysis.

4.4 *C. elegans* model system to study the physiological roles of BCAA metabolism

Along with general *bcat-1* knock-down by RNAi or *bcat-1(hh56)/+*, the *bcat-1(hh58)* mutation represents a promising *C. elegans* model for the study of the multiple physiological roles of BCAA metabolism. *C. elegans* was recently proposed as part of a powerful integrative screening approach to identify molecular candidates causally linked with human pathological states. This screen identified *bcat-1* as a central player in neuronal functionality, in line with decreased BCAT1 expression in Parkinson's disease patients' brains (Mor et al., 2020; Yao et al., 2018). Similarly, and in line with its pivotal role in brain metabolism (Hull et al., 2015b; Sperringer et al., 2017), both BCAT human paralogs have been found to be elevated in the brains of Alzheimer's disease patients (Hull et al., 2015a). Intriguingly, neuron-specific *bcat-1(RNAi)* (Mor et al., 2020) induces a hyperactive metabolic state; whereas I observed general transcriptional downregulation of genes involved in mitochondrial metabolism upon *bcat-1(hh58)*, further supporting the idea that BCAT-1 has multiple tissue-specific physiological functions that need further characterization. According to my phylogenetic analysis, BCAT-1 is the progenitor of both

mammalian isoforms, the cytosolic BCAT1 and the mitochondrial BCAT2 (Figure 13A). Retaining its protein function in the cytosol, *bcat-1(hh58)*, might resemble the mammalian BCAT2 knock-out, representing a suitable model system to resolve how BCAT compartmentalization affects organismal physiology. In line with this hypothesis, BCAT2 knock-out mice are characterized by elevated energy expenditure and proteolysis (She et al., 2007). Moreover, human BCAT2 deficiency, an ultra-rare condition, causes elevated BCAAs in plasma and may be associated with developmental delay and autism (Knerr et al., 2019; Wang et al., 2015).

4.5 Disease relevance and possible novel therapies

Previous work conducted in our laboratory already identified the UPS machinery as a potential target to complement available therapies for isovaleric acidemia (Manoli and Venditti, 2016; Segref et al., 2014; Villani et al., 2017). Direct involvement of isovaleric acid in UPS regulation and enhanced protein aggregation further support the idea that proteostasis loss is causally linked with isovaleric acidemia pathology. These new data additionally highlight an opposing role of BCAT-1 in proteostasis regulation, introducing the BCAA transamination reaction as a potential therapeutic target. The progressive decline in quality control mechanism occurring during physiological aging or induced by inborn genetic mutations is a major trigger for the accumulation of misfolded proteins. Through exposure of hydrophobic amino acid residues, misfolded proteins have the potential to form toxic aggregates, which represent both cause and consequence of proteostasis loss (Balch et al., 2008). Moreover, intrinsically disordered regions, which were predicted to be present in around half of all mammalian proteins (Dunker et al., 2008), can trigger the formation of toxic aggregates associated with neurodegenerative pathologies such as Alzheimer's and Parkinson's disease. The identified connection between IVA and increased aggregation of the metastable protein Q40::YFP (Figure 25) suggests a general decline of the organismal protein quality control pathways, which, together with reduced ubiquitin-dependent degradation, leads to proteostasis collapse, therefore potentially promoting neurodegeneration.

Similarly, defects in the BCAA metabolism has been connected with aging-related

diseases and neurodegeneration (Arany and Neinast, 2018; Manoli and Venditti, 2016; Neinast et al., 2019; Peng et al., 2020; Siddik and Shin, 2019; Sperringer et al., 2017). Moreover, as proteasome inhibitors are clinically administered to treat certain types of cancer (Grigoreva et al., 2015; Nalepa and Wade Harper, 2003), inhibition of BCAT1 and BCAT2 has been recently proposed for the treatment of melanomas and pancreatic ductal adenocarcinoma, respectively (Lei et al., 2020; Li et al., 2020; Zhang et al., 2021). My study highlights a complementary role of proteostasis and BCAA metabolism in the maintenance of human health, suggesting that combined treatments targeting both pathways might be beneficial against possible drug resistance frequently developed by cancerous cells. Although a link was already clear, recent studies highlighted the numerous connections between metabolism and organismal proteostasis, indicating the relevance of identifying common molecular strategies to better understand pathological states and foster the development of new medical therapies (Ottens et al., 2021). In conclusion, the reported data confirm the involvement of BCAA metabolism in the regulation of proteostasis, including a direct role of increased intermediate metabolites, such as IVA. Considering the crucial role of proteostasis and BCAA metabolism in human health, this study might be relevant for the development of clinical interventions to treat organic aciduria, cardiovascular diseases, diabetes, neurodegenerative disorders, and cancer.

4.6 Outlook

The results obtained during this project provide a promising new direction with regard to the physiological consequences of metabolic impairments and the impact on organismal proteostasis. However, additional investigation is required to elucidate the molecular mechanism underlying the effects on proteostasis by altered BCAA metabolism. Particularly, critical points that should be further addressed are: (I) the *bcat-1* evolutionary conservation, (II) the nature of the *bcat-1(hh58)* mutation and its biochemistry, (III) the signal transduction that links metabolic impairments with the UPS regulation and its possible conservation in mammals.

The essentiality of BCAT-1 indicates that the BCAA transamination is required for

organismal survival and that its absence cannot be compensated by other proteins, although a *bcat-1* paralog (Y44A6D.5) is predicted in *C. elegans* by sequence homology. Investigating the role of Y44A6D.5 might be interesting to elucidate the specific roles of both BCAT enzymes and compare them with the evolutionary relatives in mammals. Phylogenetic analysis revealed that both BCAT-1 and Y44A6D.5 are predicted ancestors of both mammalian homologs proteins. However, sequence homology is higher for BCAT-1, suggesting, together with the *bcat-1* essentiality, that Y44A6D.5 might have evolved specialized roles in *C. elegans*, diverging from the other homologs (Table 2).

Table 2 *C. elegans* BCATs compared with *H. sapiens* BCATs

Pairwise alignment		Identical positions	Similar positions	Identity
<i>C. elegans</i>	<i>H. sapiens</i>			
BCAT-1	BCAT1	189	125	45.32%
BCAT-1	BCAT2	183	130	43.99%
Y44A6D.5	BCAT1	165	129	41.66%
Y44A6D.5	BCAT2	166	122	41.191%

Further experiments are required to get more information about the nature of the *bcat-1(hh58)* mutation. As already mentioned, hypothetical translation of a truncated protein would cause a disruption of the predicted N-terminal mitochondrial targeting sequence. In this possible scenario, BCAT-1 would still be functionally active but restricted to the cytosol only. To confirm the production of a truncated BCAT-1 protein lacking the first 20 amino acids, I started to design a construct to express the mutated BCAT-1 (BCAT-1*) according to the sequence of the CRISPR-Cas9-generated *hh58* allele. To see if the PSC is indeed causing translation from the alternative start codon residing downstream,

the BCAT-1* protein will be tagged both N-terminally and C-terminally. When expressing this construct under the *bcat-1* promoter in *C. elegans*, it will be possible to detect on Western blot if only the C-terminal tag is attached to the transcribed protein. As control, the same type of construct but with wild-type *bcat-1* gene sequence should confirm that both N-terminal and C-terminal fused tags are co-translated with the BCAT-1 protein. If this system confirms the proposed hypothesis, this strategy will be also valid to study tissue and sub-cellular localization of the BCAT-1* produced by the *bcat-1(hh58)* allele and assess if the downstream ATG represents an alternative start codon, initiating translation also in the wild-type allele, possibly in response to changing cellular conditions. Recombinant expression of BCAT-1* would also be interesting to measure its enzymatic activity *in vitro* and compare it with BCAT-1 wild-type.

The UPS regulation upon *ivd-1* loss-of-function was confirmed in fibroblasts derived from isovaleric acidemia patients, revealing that the severity of the symptoms was reflected by an increased stabilization of expressed UPS substrates (Segref et al., 2014). Depletion of either BCAT1 or BCAT2 in those fibroblasts would verify if the *bcat-1(hh58)* suppression of *ivd-1(tm6784)* observed in *C. elegans* is conserved in humans and elucidate the evolutionary connection between nematode and human BCATs. To investigate the physiological role of IVA in a mammalian system and its connection with proteostasis maintenance, IVA can be directly supplemented to wild-type cell lines transfected with proteostasis-related substrates. By selecting different types of cell lines, it would also be possible to explore alternative regulation routes of the BCAA metabolism depending on specific cellular environments. In case IVA can regulate proteostasis also in mammalian cells, it will be important to measure the transcriptional levels of UPS components and comparing them to the homologues that were reported to be regulated in my multi-omics analysis (Figure 20B). Since carnitine is therapeutically administered to treat isovaleric acidemia (Knerr et al., 2012; Manoli and Venditti, 2016), by supplementing this compound both in *C. elegans* and mammalian cells it would be possible to elucidate if carnitine can restore normal proteostasis by detoxifying the cells from elevated IVA. As *rpn-6.1* overexpression can, at least partially, restore the proteolytic capacity (Segref et al., 2014), overexpression of other proteasome subunit could also contribute to the recovery of proteolytic defects induced by IVA. To investigate the signal transduction connecting the

BCAA metabolism with the regulation of the UPS, the role of *hsf-1* and *skn-1* should be further analyzed both in *C. elegans* and in mammalian cells. Finally, a screening to identify other transcription factors involved in the UPS regulation upon metabolic changes, and possibly regulated by IVA levels, could be conducted in *C. elegans* and then validated with mammalian homologs. This regulation might be relevant for metabolic redirection of transcriptional PQC programs beyond BCAA.

5 Materials and Methods

5.1 *C. elegans* techniques

5.1.1 Solutions and reagents

Solution	Composition
M9 buffer	20 mM KH ₂ PO ₄ 40 mM Na ₂ HPO ₄ 80 mM NaCl 1 mM MgSO ₄
Nematode Growth medium (NGM) agar	0,25 % (w/v) bacto-peptone 0,3 % (w/v) NaCl 1,7 % (w/v) serva agar 1 mM CaCl ₂ 1 mM MgSO ₄ 5 µg/ml cholesterol 25 mM KPO ₄ buffer Nystatin 25 units/ml In case or RNAi: 100 µg/ml ampicillin (sterile filtered) 2 mM IPTG
bleaching solution	250 mM KOH 1.4 % - 1.7 % NaOCl
Lysogeny broth medium (LB)	1 % (w/v) bacto-pepton 0,5 % (w/v) yeast extract 1 % (w/v) NaCl adjusted to pH 7,5 sterilized by autoclaving ampicillin 100 µg/ml (sterile filtered)
LB agar	LB supplemented with 1,5 % (w/v) agar sterilized by autoclaving ampicillin 100 µg/ml tetracycline 12.5 µg/ml (sterile filtered)
antimycin A	Sigma-Aldrich, Cat.# A8674
Isovaleric acid	Sigma-Aldrich, Cat.# 129542
Bortezomib	Sigma-Aldrich, Cat. # 179324-69-7

5.1.2 Strains and cultivation methods

C. elegans strains were cultured according to standard methods (Brenner, 1974; Stiernagle, 2006), at 20°C, on nematode growth medium (NGM) agar plates seeded with OP50 *E. coli* as food source. All original strains derive from the Bristol N2 strain and are reported in Table 3. Derivative strains obtained by crossing are reported in Appendix 1.

Table 3

Identifier	Genotype	Origin
SJ4100	<i>zcls13[hsp-6p::GFP]V</i>	D. Ron
GR2245	<i>skn-1(mg570) IV</i>	G. Ruvkun
FX06784	<i>ivd-1(tm6784) IV</i>	National BioResource Project (NBRP)
PP838	<i>hecd-1 (tm2371) IV</i>	National BioResource Project (NBRP)
TM4853	<i>acs-19(4853)</i>	National BioResource Project (NBRP)
MIR23	<i>risls3 [K02A4.1p::K02A4.1::GFP + unc-119(+)]</i>	Caenorhabditis Genetics Center (CGC)
FX30253	<i>tmC24 [F23D12.4(tmIs1233) unc-9(tm9718)] X; tmEx4950 [unc-9(+) + vha-6p::GFP]</i>	Caenorhabditis Genetics Center (CGC)
PP563	<i>unc-119(ed4) hhls64 [unc-119(+); sur-5p::UbiV-GFP]III</i>	A. Segref, our lab
PP607	<i>hhls72[unc-119(+); sur-5::mCherry], hhls64 [unc-119(+); sur-5::UbiV-GFP]III</i>	A. Segref, our lab
PP556	<i>unc-119(ed4)III; hhls57 [unc-119(+); sur-5::GFP]</i>	A. Segref, our lab
PP545	<i>unc-119(ed4)III; hhls53 [unc-119(+); sur-5::^{K29/48R}-UbiV-GFP]</i>	A. Segref, our lab
PP1263	<i>hhls64 [unc-119(+); sur-5::UbiV-GFP]III; C36A4.9(hh5)III</i>	A. Segref, our lab
PP1264	<i>hhls64 [unc-119(+); sur-5::UbiV-GFP]III; ivd-1(hh6)IV</i>	A. Segref, our lab
PP3101	<i>bcat-1 (hh58) X</i>	This study
PP3387	<i>bcat-1 (hh56)/tmC24 [F23D12.4(tmIs1233) unc-9(tm9718)] X</i>	This study

5.1.3 Strain generation by crossing

To combine mutations and transgenes, 2-4 hermaphrodites were normally crossed with wild-type males, then heterozygous F1 males were crossed with hermaphrodites of a second strain. Males were generated after exposure of L4 worms to 30°C for 5 to 6 hours. To reduce effects caused by genetic backgrounds, all strains were outcrossed at least twice and whenever possible all mutant strains, including wild-type (WT), analyzed in a single experiment were isolated from the same cross. Details about all crossings and obtained strains are reported in Appendix 1.

5.1.4 Strain generation by CRISPR-Cas9

Mutation of *bcat-1* was conducted through CRISPR-Cas9, following the procedure reported in Paix et al., 2017. In brief, *dpy-10* co-conversion strategy allows to screen putative mutants avoiding a specific genetic background (Arribere et al., 2014). To get two independent loss-of-function alleles, two guide RNAs (crRNA) were designed to introduce a restriction site for NheI that contains TAG, serving as premature stop codon in the first exon of the coding sequence, in addition to a frame shift. To increase the probability of success, the guide RNAs (crRNA) were selected combining outputs of the two online tools CHOPCHOP (version 2) and Spacer Scoring for CRISPR (SSC) (Labun et al., 2016; Xu et al., 2015) and guidelines reported by Paix et al., 2017. Universal structural RNA (tracrRNA), *dpy-10* and *bcat-1* crRNAs, single-stranded DNA oligonucleotide (ssODN) template for the homologous recombination, and Cas9 nuclease were supplemented with HEPES and KCl. The obtained injection mix (Table 4) was centrifuged at full speed in a tabletop centrifuge and supernatant was injected with the aid of a FemtoJet (Eppendorf) in the gonad of several young adult worms immobilized with Holocarbon oil on a dried 2% agarose pad prepared on microscope slides several days in advance and stored at room temperature. After multiple microinjections, worms were rehydrated with a drop of M9 and gently transferred to OP50-seeded growth plates to recover. After 4/5 days, adult worms displaying either roller or dumpy phenotypes were isolated and let laying eggs for another day before genotyping to identify *bcat-1* mutant alleles. After PCR amplification of the interested *bcat-1* coding region, NheI restriction digestion (New England BioLabs) served to identify integration of the premature stop codon. Selected isolates were confirmed by sequencing and propagated avoiding dumpy and roller worms to exclude *dpy-10* mutations. In case of *bcat-1(hh56)*, heterozygous worms were isolated and subsequently crossed with FX30253 balancer strain to maintain heterozygous *bcat-1(hh56)/+* and outcrossed 4 times. *bcat-1(hh58)* was outcrossed 6 times. Crossing details, oligonucleotides used for genotyping and for CRISPR-Cas9 editing are reported respectively in Appendix 1, 2, and 3.

Table 4 CRISPR-Cas9 injection mix

Component	Concentration
Cas9 (NEB)	1 μ M
tracrRNA	0.0425 mM
dpy-10(cn64) crRNA	0.012 mM
dpy-10 ssODN	0.44 μ M
target crRNA	0.03 mM
ssODN repair template	0.5 μ M
HEPES	7.5 mM
KCl	25 mM

5.1.5 Population synchronization

Unless otherwise stated, all experimental analysis was performed on day 1 adult worms, synchronized by egg-prep (Stiernagle, 2006). In brief, worms were washed off the plates with M9, then bleached with bleaching solution and, after 3 washing steps with M9, the obtained eggs were seeded on culture plate or starved in M9 overnight to have a more synchronous population. Estimation of the number of eggs or L1 larvae was done with 1 μ l drop of M9 in triplicates in order to seed appropriate amounts of worms in each plate, considering lethality and fertility defects of each mutant strains. Except for experiments reported in Figure 5-10, all other experiments were conducted without the overnight starvation to reduce excessive stress and the possible secondary effects that starvation might have on metabolism. In case of developmental delay, either synchronization or collection was adapted according to the quantified average generation time and by optical inspection to confirm that worms reached the egg-bearing adult stage. In Figure 27 the alternative synchronization to have day 1 adult worms at the same time is summarized.

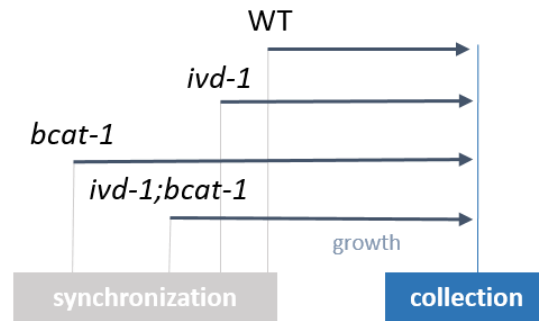


Figure 27 Synchronization of strains with developmental delay

5.1.6 Gene knock-down by RNAi feeding

RNA interference (RNAi) was performed following the standard feeding method (Kamath et al., 2001). In brief, HT115(DE3) bacteria were grown in LB medium supplemented with 0.1 mg/ml ampicillin overnight, diluted to an optical density (OD)₆₀₀ of 0.1 the following day and grown to a maximum OD₆₀₀ of 0.9. dsRNA expression was induced by adding IPTG to a final concentration of 2 mM for 30-60 min shaking at 37°C. Bacteria were seeded onto growth media NGM plates containing 2 mM IPTG and 0.1 mg/ml ampicillin. As control, bacteria expressing the empty vector pPD129.36 were used. *acs-19*, *ivd-1* or *hecd-1* which are known to accumulate the UbV-GFP (Segref et al., 2014), served as positive controls for RNAi activation. Alternatively, RNAi efficacy was validated with RT-PCR. Synchronized eggs or overnight starved L1 larvae were homogenously transferred on the seeded RNAi plates and incubated at 20°C until worm reached adult stage for live imaging and/or collection for Western blotting and/or RNA extraction.

5.1.7 Targeted metabolic RNAi screen

A list of genes related to the metabolic function of IVD-1 or ACS-19, involved in the mitochondrial respiration or mitochondrial transporters were selected using KEGG (Kanehisa et al., 2016) as reference, integrating with related studies (Arda et al., 2010; Yilmaz and Walhout, 2014). HT115 bacterial clones inducibly expressing dsRNA targeting the respective genes for RNAi silencing were isolated from Ahringer or ORFeomeWS112 libraries (Geneservice Ltd, available via Source BioScience) and validated by plasmid

isolation and partial sequencing. 71 genes were finally targeted for RNAi in the two worms strains SJ4100 (*hsp-6p::GFP*) and PP563 (*sur-5p::UbV-GFP*). The procedure was repeated in two independent experiments, with some overlap of targeted genes. Complete list of all targeted genes and GFP intensity are reported in Appendix 6.

5.1.8 Embryonic lethality quantification

To assess the lethality penetrance of the *bcat-1(hh56)* mutation, heterozygous *bcat-1(hh56)/tmC24* worms isolated from two independent lines were analyzed. 20 L4 larvae were singled from each line and removed from plates after 2 hours, unhatched eggs were immediately counted, while viable progeny was quantified after 3 days, distinguishing for phenotypically wild-type from Unc, which indicate two copies of the balancer *tmC24*. Dead embryos were obtained by subtracting the total number of viable progeny from the total number of laid eggs. All phenotypically wild-type larvae were confirmed to be heterozygous for *bcat-1(hh56)* by genotyping. Worms that were not alive when the progeny was quantified were censored. Proportions of unhatched eggs, phenotypically wild type and Unc larvae are reported in the graph.

The same procedure was applied for *bcat-1(hh58)* and *ivd-1(tm6784)* single and double mutants except that the single adult worms were left 4 hours on plates to lay eggs. For each strain 10 adult worms were singled, the total number of eggs counted after having removed the adults and viable larvae were counted 3 days after. Worms that were not alive when the progeny was quantified were censored.

5.1.9 Generation time quantification

The generation time or time to reach adulthood was quantified as the time needed from egg to reach adulthood. Adult worms were let laying eggs for 4 hours, after 2 days, 20 to 25 larvae were isolated from the progeny and monitored regularly to note the time when the first progeny eggs were laid. 2 experimental replicates were pooled together to have minimum 34 technical replicates for each strain, after censoring worms that died before reaching adulthood.

In case of IVA supplementation, brightfield images of 5 independent plates for each condition were captured after 3 days since worm synchronization by egg-prep and all developmental stages present in each image were quantified using the Fiji Cell counter plugin. The number of worms captured in a single image varied from 43 to 184.

5.1.10 Viable progeny quantification

To quantify the total viable progeny, 10-20 L4 larvae were singled for each strain and transferred every day. The total number of viable progenies was obtained summing up the number of viable worms present in each plate after the parental worm was transferred. Data from 2 independent experiments were pooled to have a minimum of 24 replicates after censoring parental worms that died before laying the entire progeny.

5.1.11 Chemical supplementation

For bortezomib supplementation, 50 mM stock solution was prepared in DMSO and then diluted in NGM before pouring the plates to have a final concentration of 10 μ M. Equal amount of DMSO was used as control.

For antimycin A supplementation, 10 mM stock solution was prepared in ethanol and serially diluted 1:1. Each stock solution was equally diluted in the bacteria suspension before seeding the RNAi NGM plates to have final concentrations of 1 μ M, 500 nM, 250 nM and 125 nM. Equal amount of water was used as control.

For IVA supplementation, 25x stock solutions of IVA were prepared in H₂O and poured on NGM plates seeded with OP50 to reach a final concentration of 3 or 6 mM, H₂O served as control. Unaltered pH of the growth plates was assessed by submerging a pH test strip into the agar.

5.2 Molecular biology

5.2.1 Solutions and reagents

Genotyping	
Single worm lysis buffer (SWLB)	50 mM KCl 10 mM Tris (pH 8.3) 2.5 mM MgCl ₂ 0.45 % (v/v) Tween 20 0.01 % gelatin H ₂ O add 100 ml sterilized by autoclaving before use add Proteinase K (50 µg/µl)
OneTaq QuickLoad (2X)	New England BioLabs, Cat. #M0482
NheI HF	New England BioLabs, Cat. # R3131
DNA loading dye (6X)	4 g Saccharose 2 µg Xylene cyanol Fill to 10 ml with ddH ₂ O Filtrate (0.2 µm)
TAE buffer	40 mM TRIS 1,4 % (v/v) acetic acid 1 mM EDTA pH adjusted to 8,5
Western Blot Analysis	
RIPA buffer	25 mM Tris HCl pH7.6 150 mM NaCl 1% Triton X-100 1 mM EDTA 1% sodium deoxycholate 1% SDS 1x protease inhibitor cocktail Roche
SDS loading buffer (2x)	0.018 g bromphenol blue Filtrate (0.2 µm) 3 ml (50 µl/ml) β-mercaptoethanol Fill to 60 ml with ddH ₂ O Freeze at -20 °C
MES buffer	97.8g MES 60.6 g Tris 10 g SDS 3 g EDTA Fill to 0.5 l with ddH ₂ O Adjust pH to 7.3
NuPAGE® Transfer Buffer	ThermoFischer Scientific

Blotting buffer	10 % Methanol 10 % NuPage transfer buffer (20x)
PBS (10X)	2.4 g KH ₂ PO ₄ 80 g NaCl 2 g KCl Fill to 1 l with ddH ₂ O Adjust pH with 0.1 M NaOH Autoclave
PBST (1X)	PBS + 0.01% Tween-20
Blocking solution	3% powder milk in PBST

5.2.2 Genotyping

Single worms were lysed in 10 µl SWLB for 1 hour at 65°C, followed by heat-inactivation by proteinase K at 95 °C for 15 minutes. The polymerase chain reaction (PCR) amplification was conducted adding 2 µl of the lysate the reaction mix (Table 5), following the standard program reported in Table 6, unless otherwise stated in Appendix 2, where also oligonucleotide sequences and expected size of the bands are reported. Amplicons were separated with gel electrophoresis on 1% agarose (TAE) supplemented with GelRed™ (Biotium). A DNA standard marker (GeneRuler 1kb Plus, Fermentas) was used as reference. In case of point mutations primers were designed with the help of the online tool PRIMER1 (<http://primer1.soton.ac.uk/primer1.html>) (Collins and Ke, 2012), following the ARMS-PCR strategy (Ye et al., 2001). Restriction fragment length polymorphism (RFLP) PCR was applied to identify CRISPR-Cas9 edited worms, since the introduced PSC contained a restriction site for NheI. After amplification with TH3383 and TH3384, enzymatic digestion was conducted adding 0.3 µl of NheI and CutSmart buffer (New England BioLabs) to each reaction tube and incubated at 37°C for at least 1 hour.

Table 5 Master mix for genotyping PCR, 1 reaction

OneTaq Quick load (NEB) 2x	7.5 µl
primers (10 µM)	0.3 µl
H ₂ O 2P	4.9 µl
3P	4.6 µl
4P	4.3 µl

Table 6 PCR genotyping standard program

Denaturing	94°C	5 min	32 cycles
	94°C	30 sec	
Annealing	45°C-68°C	20 sec	
Elongation	68°C	50 sec- 1min	
	68°C	5 min	
	10°C	hold	

Oligonucleotides were purchased by Metabion. Sequences and identification ID are reported in the Appendix 2 together with details about the relative genotyping conditions.

5.2.3 Western blot

Synchronized worms by egg-prep were harvested at day 1 of adulthood after washing with M9 at least twice to remove bacteria and progeny eggs. Alternatively, to have the same amounts of worms in each tube, worms were picked in M9, which was removed after settling. Worm pellets were flash-frozen in liquid nitrogen and stored at -80°C. After thawing in ice, worm pellets were re-suspended in RIPA buffer. Protein content was measured by Pierce BCA protein assay (ThermoFisher Scientific) before sonication. In case of manual picking, worms were re-suspended in SDS loading buffer and sonicated. Lysates were boiled at 95°C for 5 min and then centrifuged at 18000 x g for 15 min at 4°C. After 5 min of 95°C boiling, supernatant containing either 5 µg of quantified protein supplemented with SDS loading buffer or the equivalent volume of 20 picked worms was loaded on Bis-Tris 4-12% polyacrilamide gels for electrophoresis. Proteins were transferred to nitrocellulose membranes (Amersham Protran) with semi-dry blotting system (Bio-Rad, Trans-Blot Turbo) using NuPAGE transfer buffer (ThermoFischer Scientific). Membranes were blocked with 3% milk (in PBS + 0.1% Tween 20) and incubated with the primary antibodies overnight at 4°C in RotiBlock (Carl Roth). Incubation with fluorescently labelled secondary antibodies was done at room temperature for 1 hour, before detection with Li-Cor Odyssey scanner. Exceptionally, for the western blot reported in Figure 5C chemiluminescence with ECL secondary antibody was detected, due to higher sensitivity. Image Studio Lite (version 5.2) was used to import detected blots with Oyssey system while Image Lab (version 6.0.0) was used for the ECL system. Antibodies

and relative dilutions are reported in Table 7.

Table 7 Antibodies

I Antibody	II Antibody
Living Colors A.v. GFP Monoclonal Antibody [JL-8] Clontech Cat. # 632380 <i>Dilution 1:7000</i>	IRDye® 800CW Donkey anti-Mouse IgG Secondary Antibody Li-Cor Cat. # 926-32212; RRID AB_621847 <i>Diluton 1:15000</i>
Mouse monoclonal RFP antibody [6G6] Chromotek Cat. # 6g6-100; RRID: AB_2631395 <i>Dilution 1:5000</i>	IRDye® 680RD Donkey anti-Rabbit IgG Secondary Antibody Li-Cor Cat. # 926-68073; RRID: AB_10954442 <i>Dilution 1:15000</i>
Rabbit monoclonal alpha Tubulin antibody [EP1332Y] Abcam Cat. # ab52866; RRID: AB_869989 <i>Dilution 1:7000</i>	

5.2.4 RNA extraction

Synchronized worms by egg prep were harvested at day 1 of adulthood after washing with M9 at least twice to remove bacteria. Worm pellets were flash-frozen in liquid nitrogen and stored at -80°C. To extract total RNA, 1 ml TRIzol (Ambion) was added to the worm pellets, together with 200 µl zirconia beads and homogenization was conducted with Precellys 24-Dual cell homogenizer (Peqlab). After addition of 1-bromo-3-chloropropane, mixing and phase separation by centrifugation, aqueous supernatant was mixed with the same volume of 70% ethanol and total RNA was isolated with Quiagen RNeasy Mini kit following the manufacturer's instructions.

5.2.5 qRT-PCR

Using High-Capacity cDNA Reverse Transcription Kit (Applied Biosystems), 1500 ng of isolated RNA was retro-transcribed to cDNA. Gene expression levels were measured via quantitative real time PCR (qRT-PCR) with Bio-Rad CFX96 Real-Time PCR Detection System and the Luna Universal qPCR Master Mix (New England Biolabs), following the manufacturer instructions regarding concentrations and PCR program. Quantification

cycles (Cq) were obtained by the Bio-Rad CFX Manager 3.1 software and subsequently analyzed with Rstudio to calculate the fold changes: $2^{-\Delta\Delta Cq}$ as described previously (Bustin et al., 2009; Livak and Schmittgen, 2001). Actin served as internal control, primer efficiencies were checked by creation of a standard curve and retro-transcribed products lacking retrotranscriptase in the reaction was used as control to confirm absence of genomic DNA in the originally isolated RNA.

Table 8 qRT-PCR oligonucleotides

ID	Transcript	Sequence
TH3277	<i>skn-1b</i> Forward	CAACAGGTGGATCAACACGG
TH3278	<i>skn-1b</i> Reverse	AGGCGTAGTTGGATGTT GGG
TH3279	<i>skn-1a/c</i> Forward	GGCAAATTTGACCGAGATGCA
TH3280	<i>skn-1a/c</i> Reverse	GAACAAAGTCTCTGGTTGAGCA
TH3281	<i>skn-1a</i> Forward	AAGACGAAGACAGTGCTTCTC
TH3282	<i>skn-1a</i> Reverse	GTCGTCTCTTCTTCGTCGTC
TH3283	<i>skn-1a-c</i> Forward	ATTAAGCGAGTTGCAACAAGTG
TH3284	<i>skn-1a-c</i> Reverse	GACGAATCTTGCGAATCAACTG
TH3367	<i>ivd-1</i> Forward	TGGTCCATTGGGTCTCATGC
TH3368	<i>ivd-1</i> Reverse	CAATATCACAGGCGGCTTGC
TH3371	<i>bcat-1</i> Forward	ATCAAGGCTTATGGCCTCCG
TH3372	<i>bcat-1</i> Reverse	ACTGTCTCCAATCTGGCTGC

5.3 Microscope imaging

5.3.1 Live imaging

For visualization of UbV-GFP, 10-15 worms were picked and mounted on agar pads, immobilizing them with sodium azide as previously described (Shaham, 2006). Fluorescent and brightfield images of mounted immobilized worms were captured with Zeiss Axiozoom V16, equipped with Axiocam 506mono and ZEN 2.3 software. Fluorescent exposure times were always kept constant for every group of images compared. For the targeted metabolic RNAi screen, worm populations were imaged directly from plates, without mounting. Protein aggregation (conducted by Dr. Qiaochu Li) was visualized in GF78 strain expressing Q40::YFP in intestine (Mohri-Shiomi and Garsin, 2008). 1 or 2-day-old adults were placed on plates with or without IVA supplementation to lay eggs for 4 hours, and transgenic L4 animals were transferred to new plates. Animals

were then transferred every two days to new plates until aggregates quantification on day 6 of adulthood.

For the analysis of BCAT-1::GFP subcellular localization, confocal images of immobilized MIR23 worms stained with Mitotracker (ThermoFischer Scientific) were obtained with Zeiss Meta 710 confocal laser scanning microscope, with ZEN software 2009. Mitotracker staining was performed incubating for 2 hours synchronized adult worms on NGM plates seeded with heat-inactivated OP50 (95°C, 30 min) and supplemented with 10 μ M of Mitotracker DeepRed dissolved in DMSO, which was used as control to exclude morphological effects. Worms were then washed with M9 and incubated 2 hours on NGM plates seeded with heat-inactivated OP50, without Mitotracker stain.

5.3.2 Imaging quantification

For the RNAi screen qualitative manual quantification by scoring from 0 to 5 was compared with semi-automated integrated density quantification performed with an ImageJ macro (Appendix 5). The cumulative integrated density of all worms present in each image was divided by the total area covered by worms after background subtraction. The macro relies on user inputs, including background subtraction and threshold setting for both brightfield and fluorescent channels. Although more time-consuming than fully automated methods, the semi-automated method reported here represents a good compromise to have precise threshold and background subtraction integrated with automated fluorescence quantification. Although mostly resembling the manually assigned scores (Figure 10C), this method is more sensitive and less influenced by human bias, regardless of blindfolding, which was anyway applied for the manual quantification. The output raw data were imported in Rstudio and combined with the manually assigned scores. For each RNAi-targeted gene on the two strains SJ4100 (*hsp-6p::GFP*) and PP563 (*sur-5p::UbV-GFP*), the GFP manual intensity was normalized on the respective empty control by subtraction, whereas the automated GFP integrated density/worm area was divided by the empty control value and \log_2 transformed. Data were averaged for each RNAi target, since most had replicates, either coming from Ahringer and ORFeomeWS112 RNAi libraries, being present in both experimental replicates or both.

5.4 Multi-omics analysis

Synchronized worms by egg-prep were harvested at day 1 of adulthood after washing with M9 at least twice to remove bacteria. Worm pellets were split into 3 Eppendorf tubes (one for each omics) and flash-frozen with liquid nitrogen before storing at -80°C . 4 replicates were collected in independent experiments and following processing was conducted in parallel for each omics analysis.

For transcriptomics, Trizol was supplemented to worm pellets to extract RNA as described for qRT-PCR, 2 μg of RNA (50-200 $\text{ng}/\mu\text{l}$, $\text{OD}_{260/280} = 1.8\text{-}2.1$, $\text{OD}_{260/230} > 1.5$). Next generation sequencing was conducted by Cologne Center of Genetics (CCG; University of Cologne). Initial data analysis, including computation of fragments per kilobase of transcript per million (FPKMs), fold changes and relative adjusted P-values, was performed by Prerana Wagle from the CECAD Bioinformatics facility.

For proteomics, worm pellets were supplemented with urea buffer (8 M in 50 mM TEAB + 1x Roche protease inhibitor cocktail), sonicated, centrifuged for 15 min at 20000 x g and protein content was quantified with Pierce BCA protein assay (ThermoFisher Scientific). Samples were diluted to have 50 μg of proteins; DTT, and chloracetamide were added to a final concentration of 5 mM and 40 mM, respectively. Peptide digestion was conducted first with lysyl endopeptidase (Lys-C) and, after diluting the samples to a final urea concentration of 1.2 M with trypsin protease. Peptides were loaded with solvent A (0.1% formic acid in water) onto an in-house packed analytical column (50 cm — 75 μm I.D., filled with 2.7 μm Poroshell EC120 C18, Agilent). Mass-spectrometry analysis and initial data processing was conducted by Stefan Müller from the CECAD Proteomics facility using Spectronaut 13 (Bruderer et al., 2015). Protein quantification analysis was performed with the assistance of Stefan Müller using Perseus (version 1.6.7.0) (Tyanova et al., 2016), including \log_2 transformation, filtering for valid values in 4 out of 4 replicates in at least one strain, imputation of missing values from normal distribution and two-sample tests.

For metabolomics, worm lysates were processed and analyzed by Andrea Annibal from Antebi Lab (Max Planck Institute for Biology of Ageing, Cologne, Germany), including

sample preparation, processing generation of normalized intensities, fold changes and P-values.

5.5 Data processing, statistical analysis and bioinformatics

All graphs were generated with RStudio, reporting means and standard deviations, where not otherwise stated. Significant difference was calculated with R and reported in relation to the control condition by * for P-value ≤ 0.05 and ** for P-value ≤ 0.01 . In case of normally distributed data Tukey's Honest Significant Difference (HSD) was combined with one-way ANOVA, while for not normally distributed data pairwise comparisons were computed using Wilcoxon rank sum test with Bonferroni adjustment of P-values for multi-testing.

5.5.1 Software, databases, and online resources

Phenotype quantification, data visualization and statistical analysis were conducted with R in the RStudio environment. R packages and freely available online tools employed, as well as proprietary software are reported in Table 9.

Table 9

Software	Source or reference	Website link	Version
ImageJ	(Schindelin et al., 2012)	https://imagej.nih.gov/ij/	version 1.53c
Fiji Cell Counter plugin	https://github.com/fiji/Cell_Counter	https://imagej.net/plugins/cell-counter	
R	The R Foundation	https://www.r-project.org/	version 4.0.0 and 3.1.1
Rstudio	RStudio, PBC	https://www.rstudio.com/	version 1.2.5033
R collection of packages tidyverse	https://github.com/tidyverse	https://www.tidyverse.org	version 1.3.0
R package ggrepel	https://github.com/slowkow/ggrepel	https://www.rdocumentation.org/	version 0.8.2
R package ComplexHeatmaps	(Gu et al., 2016)	http://www.bioconductor.org/packages/devel/bioc/html/ComplexHeatmap.html	version 2.4.2
Perseus	(Tyanova et al., 2016)	https://maxquant.net/perseus/	version 1.6.7.0

Software	Source or reference	Website link	Version
Gimp	GNU Project https://www.gnu.org/	https://www.gimp.org/	version 2.8.18
Inkscape	The Inkscape Project	https://inkscape.org/	version 1.0.2
Pathview	(Luo et al., 2017)	https://pathview.uncc.edu/	
KEGG	(Kanehisa et al., 2016)	https://www.genome.jp/kegg/	
WormPaths	(Walker et al., 2021; Yilmaz and Walhout, 2016)	http://wormflux.umassmed.edu/	
CHOPCHOP	(Labun et al., 2016)	http://chopchop.cbu.uib.no/	
Spacer Scoring for CRISPR (SSC)	(Xu et al., 2015)	http://crispr.dfci.harvard.edu/SSC/	
T-COFFEE EXPRESSO	(Di Tommaso et al., 2011)	http://tcoffee.crg.cat/apps/tcoffee/doi:expresso	version 11.00
PhyML	(Guindon et al., 2010)	http://www.atgc-montpellier.fr/phyml/	version 3.0
TargetP-2.0	(Armenteros et al., 2019)	http://www.cbs.dtu.dk/services/TargetP/	
Image Studio Lite	LI-COR, Inc.	https://www.licor.com/bio/	version 5.2.5
Bio-Rad CFX Manager	Bio-Rad Laboratories	https://www.bio-rad.com/	version 3.1

5.5.2 Subcellular localization prediction

BCAT-1 localization prediction to mitochondria was obtained with MitoProt, TargetP-2.0, and iPSORT computational tools available online (Armenteros et al., 2019; Bannai et al., 2002; Claros and Vincens, 1996).

5.5.3 Multi-omics data processing

The processed transcriptomics, proteomics and metabolomics datasets were analyzed with R (version 4.0.0), in Rstudio environment (version 1.2.5033). Data frame organization, filtering, Z-scores calculation and scatterplots were conducted with the aid of the tidyverse collection of packages and ggrepel, while heatmaps were generated using

the ComplexHeatmap package (Gu et al., 2016). To compare expression levels of transcripts and proteins of the respective gene, the two datasets were merged using the Wormbase IDs. Regulated transcripts, proteins or metabolites for the “*ivd-1* response” were filtered if all the following criteria were met:

P-value (*ivd-1(tm6784)*/WT) ≤ 0.05

P-value (*ivd-1(tm6784)*/*hecd-1(tm2371)*) ≤ 0.05

$\log_2(\text{ivd-1(tm6784)}/\text{WT})/\log_2(\text{ivd-1(tm6784)}/\text{hecd-1(tm2371)}) > 0$

P-value (*ivd-1(tm6784)*; *bcat-1(hh58)*/*ivd-1(tm6784)*) ≤ 0.05

$\log_2(\text{ivd-1(tm6784)}/\text{WT})/\log_2(\text{ivd-1(tm6784)}; \text{bcat-1(hh58)}/\text{ivd-1(tm6784)}) < 0$

$\log_2(\text{ivd-1(tm6784)}/\text{hecd-1(tm2371)})/\log_2(\text{ivd-1(tm6784)}; \text{bcat-1(hh58)}/\text{ivd-1(tm6784)}) < 0$

Regulated transcripts, proteins or metabolites for the “*bcat-1* response” were filtered if all the following criteria were met:

P-value (*bcat-1(hh58)*/WT) ≤ 0.05

P-value (*ivd-1(tm6784)*; *bcat-1(hh58)*/*ivd-1(tm6784)*) ≤ 0.05

$\log_2(\text{bcat-1(hh58)}/\text{WT})/\log_2(\text{ivd-1(tm6784)}; \text{bcat-1(hh58)}/\text{ivd-1(tm6784)}) > 0$

Except for the metabolomics data, P-values refer to adjusted P-values or Q-values.

KEGG (Kanehisa et al., 2016) and WormPaths (Walker et al., 2021; Yilmaz and Walhout, 2016) were used as reference for mapping genes and metabolites within the *C. elegans* metabolic network. The metabolic map reported in Figure 22 was extracted from multiple maps generated by Pathview (Luo et al., 2017), using a simplified dataset of transcripts and metabolites reporting the fold changes relative to *ivd-1(tm6784)*/WT (reported on the left) and *ivd-1(tm6784)*;*bcat-1(hh58)*/*ivd-1(tm6784)* (reported on the right) simplified by assigning 1 for significantly up-regulated, -1 for significantly downregulated and 0 for not significant changes.

5.5.4 Phylogenetic analysis

Protein sequences of BCAT-1 homologs were retrieved from Swiss-Prot records in the UniProt database (<https://www.uniprot.org/>), selecting few representative model animals: *E. coli*, *S. pombe*, *S. cerevisiae*, *C. elegans*, *M. musculus*, *R. norvegicus*, *H. sapiens*. The sequences were aligned with T-COFFEE EXPRESSO (Version 11.00) using default settings (Di Tommaso et al., 2011). To generate a phylogeny tree, aligned sequences in PHYLIP format were processed with the online tool PhyML (version 3.0) (Guindon et al., 2010), using the Smart Model Selection (SMS) heuristic method to select the best

combination of substitution matrix and model for rates across sites (Lefort et al., 2017), followed by non-parametric bootstrap analysis (100 bootstraps). The phylogenetic tree was visualized with PRESTO on the ATGC bioinformatics platform (<http://www.atgc-montpellier.fr/>). The same list of proteins was submitted as FASTA file to TargetP to identify predicted targeting peptides (Armenteros et al., 2019).

The pairwise alignment of BCAT human and nematode homologues was conducted on UniProt (<https://www.uniprot.org/>), with the alignment algorithm Clustal Omega (Madeira et al., 2019).

References

Adeva-Andany, M.M., Calvo-Castro, I., Fernández-Fernández, C., Donapetry-García, C., and Pedre-Piñeiro, A.M. (2017). Significance of L-carnitine for human health. *IUBMB Life* 69, 578–594.

Akutsu, M., Dikic, I., and Bremm, A. (2016). Ubiquitin chain diversity at a glance. *J Cell Sci* 129, 875–880.

Alam, M.T., Olin-Sandoval, V., Stincone, A., Keller, M.A., Zelezniak, A., Luisi, B.F., and Ralser, M. (2017). The self-inhibitory nature of metabolic networks and its alleviation through compartmentalization. *Nature Communications* 8, 1–13.

An, J.H., and Blackwell, T.K. (2003). SKN-1 links *C. elegans* mesendodermal specification to a conserved oxidative stress response. *Genes Dev.* 17, 1882–1893.

Anderson, K.A., Huynh, F.K., Fisher-Wellman, K., Stuart, J.D., Peterson, B.S., Douros, J.D., Wagner, G.R., Thompson, J.W., Madsen, A.S., Green, M.F., et al. (2017). SIRT4 Is a Lysine Deacylase that Controls Leucine Metabolism and Insulin Secretion. *Cell Metabolism* 25, 838-855.e15.

Andréasson, C., Ott, M., and Büttner, S. (2019). Mitochondria orchestrate proteostatic and metabolic stress responses. *EMBO Reports* 20.

Arany, Z., and Neinast, M. (2018). Branched Chain Amino Acids in Metabolic Disease. *Curr Diab Rep* 18, 76.

Arda, H.E., Taubert, S., MacNeil, L.T., Conine, C.C., Tsuda, B., Van Gilst, M., Sequerra, R., Doucette-Stamm, L., Yamamoto, K.R., and Walhout, A.J.M.M. (2010). Functional modularity of nuclear hormone receptors in a *Caenorhabditis elegans* metabolic gene regulatory network. *Molecular Systems Biology* 6, 367.

Armenteros, J.J.A., Salvatore, M., Emanuelsson, O., Winther, O., Heijne, G. von, Elofsson, A., and Nielsen, H. (2019). Detecting sequence signals in targeting peptides using deep learning. *Life Science Alliance* 2.

Arribere, J.A., Bell, R.T., Fu, B.X.H., Artiles, K.L., Hartman, P.S., and Fire, A.Z. (2014). Efficient Marker-Free Recovery of Custom Genetic Modifications with CRISPR/Cas9 in *Caenorhabditis elegans*. *Genetics* 198, 837–846.

Ashburner, M., and Bonner, J.J. (1979). The induction of gene activity in drosophila by heat shock. *Cell* 17, 241–254.

Babygirija, R., and Lamming, D.W. (2021). The regulation of healthspan and lifespan by dietary amino acids. *Transl Med Aging* 5, 17–30.

Balch, W.E., Morimoto, R.I., Dillin, A., and Kelly, J.W. (2008). Adapting Proteostasis for Disease Intervention. *Science* 319, 916–919.

Balchin, D., Hayer-Hartl, M., and Hartl, F.U. (2016). In vivo aspects of protein folding and quality control. *Science* 353, aac4354.

Bannai, H., Tamada, Y., Maruyama, O., Nakai, K., and Miyano, S. (2002). Extensive feature detection of N-terminal protein sorting signals. *Bioinformatics* 18, 298–305.

Bard, J.A.M., Goodall, E.A., Greene, E.R., Jonsson, E., Dong, K.C., and Martin, A. (2018). Structure and Function of the 26S Proteasome. *Annu. Rev. Biochem.* 87, 697–724.

Bar-Ziv, R., Frakes, A.E., Higuchi-Sanabria, R., Bolas, T., Frankino, P.A., Gildea, H.K., Metcalf, M.G., and Dillin, A. (2020). Measurements of Physiological Stress Responses in *C. Elegans*. *JoVE (Journal of Visualized Experiments)* e61001.

Biswas, D., Duffley, L., and Pulinilkunnil, T. (2019). Role of branched-chain amino acid–catabolizing enzymes in intertissue signaling, metabolic remodeling, and energy homeostasis. *The FASEB Journal* 33, 8711–8731.

Blackwell, T.K., Steinbaugh, M.J., Hourihan, J.M., Ewald, C.Y., and Isik, M. (2015). SKN-1/Nrf, stress responses, and aging in *Caenorhabditis elegans*. *Free Radical Biology and Medicine* 88, 290–301.

Boos, F., Krämer, L., Groh, C., Jung, F., Haberkant, P., Stein, F., Wollweber, F.,

Gackstatter, A., Zöller, E., van der Laan, M., et al. (2019). Mitochondrial protein-induced stress triggers a global adaptive transcriptional programme. *Nature Cell Biology* 21, 442–451.

Bowerman, B., Eaton, B.A., and Priess, J.R. (1992). *skn-1*, a maternally expressed gene required to specify the fate of ventral blastomeres in the early *C. elegans* embryo. *Cell* 68, 1061–1075.

Bragoszewski, P., Turek, M., and Chacinska, A. (2017). Control of mitochondrial biogenesis and function by the ubiquitin - Proteasome system. *Open Biology* 7.

Braun, R.J., and Westermann, B. (2017). With the Help of MOM: Mitochondrial Contributions to Cellular Quality Control. *Trends in Cell Biology* 27, 441–452.

Bruderer, R., Bernhardt, O.M., Gandhi, T., Miladinović, S.M., Cheng, L.-Y., Messner, S., Ehrenberger, T., Zanotelli, V., Butscheid, Y., Escher, C., et al. (2015). Extending the Limits of Quantitative Proteome Profiling with Data-Independent Acquisition and Application to Acetaminophen-Treated Three-Dimensional Liver Microtissues*[S]. *Molecular & Cellular Proteomics* 14, 1400–1410.

Bustin, S.A., Benes, V., Garson, J.A., Hellemans, J., Huggett, J., Kubista, M., Mueller, R., Nolan, T., Pfaffl, M.W., Shipley, G.L., et al. (2009). The MIQE Guidelines: Minimum Information for Publication of Quantitative Real-Time PCR Experiments. *Clin Chem* 55, 611–622.

Chinen, Y., Nakamura, S., Tamashiro, K., Sakamoto, O., Tashiro, K., Inokuchi, T., and Nakanishi, K. (2017). Isovaleric acidemia: Therapeutic response to supplementation with glycine, L-carnitine, or both in combination and a 10-year follow-up case study. *Molecular Genetics and Metabolism Reports* 11, 2–5.

Clague, M.J., Urbé, S., and Komander, D. (2019). Breaking the chains: deubiquitylating enzyme specificity begets function. *Nat Rev Mol Cell Biol* 20, 338–352.

Claros, M.G., and Vincens, P. (1996). Computational Method to Predict Mitochondrially Imported Proteins and their Targeting Sequences. *European Journal of Biochemistry* 241,

779–786.

Collins, A., and Ke, X. (2012). Primer1: Primer design Web service for Tetra-Primer ARMS-PCR. *The Open Bioinformatics Journal* 6, 55–58.

Collins, G.A., and Goldberg, A.L. (2017). The Logic of the 26S Proteasome. *Cell* 169, 792–806.

Costa-Mattioli, M., and Walter, P. (2020). The integrated stress response: From mechanism to disease. *Science* 368, eaat5314.

Coux, O., Tanaka, K., and Goldberg, A.L. (1996). STRUCTURE AND FUNCTIONS OF THE 20S AND 26S PROTEASOMES. *Annual Review of Biochemistry* 49.

Dederer, V., Khmelinskii, A., Huhn, A.G., Okreglak, V., Knop, M., and Lemberg, M.K. (2019). Cooperation of mitochondrial and ER factors in quality control of tail-anchored proteins. *ELife* 8, 1–23.

Dejima, K., Hori, S., Iwata, S., Suehiro, Y., Yoshina, S., Motohashi, T., and Mitani, S. (2018). An Aneuploidy-Free and Structurally Defined Balancer Chromosome Toolkit for *Caenorhabditis elegans*. *Cell Reports* 22, 232–241.

Deshaies, R.J., and Joazeiro, C.A.P. (2009). RING Domain E3 Ubiquitin Ligases. *Annu. Rev. Biochem.* 78, 399–434.

Di Tommaso, P., Moretti, S., Xenarios, I., Orobittg, M., Montanyola, A., Chang, J.-M., Taly, J.-F., and Notredame, C. (2011). T-Coffee: a web server for the multiple sequence alignment of protein and RNA sequences using structural information and homology extension. *Nucleic Acids Research* 39, W13–W17.

Dickinson, D.J., and Goldstein, B. (2016). CRISPR-based methods for *caenorhabditis elegans* genome engineering. *Genetics* 202, 885–901.

Dikic, I. (2017). Proteasomal and Autophagic Degradation Systems. *Annual Review of Biochemistry* 86, 193–224.

- Dohmen, R.J., Willers, I., and Marques, A.J. (2007). Biting the hand that feeds: Rpn4-dependent feedback regulation of proteasome function. *Biochimica et Biophysica Acta (BBA) - Molecular Cell Research* 1773, 1599–1604.
- Doudna, J.A., and Charpentier, E. (2014). The new frontier of genome engineering with CRISPR-Cas9. *Science* 346.
- Dunker, A.K., Silman, I., Uversky, V.N., and Sussman, J.L. (2008). Function and structure of inherently disordered proteins. *Current Opinion in Structural Biology* 18, 756–764.
- Eisenberg-Bord, M., and Schuldiner, M. (2017). Ground control to major TOM: mitochondria–nucleus communication. *The FEBS Journal* 284, 196–210.
- El Hindy, M., Hezwani, M., Corry, D., Hull, J., El Amraoui, F., Harris, M., Lee, C., Forshaw, T., Wilson, A., Mansbridge, A., et al. (2013). The Branched-Chain Aminotransferase Proteins: Novel Redox Chaperones for Protein Disulfide Isomerase—Implications in Alzheimer’s Disease. *Antioxidants & Redox Signaling* 20, 2497–2513.
- Escobar-Henriques, M., Altin, S., and Brave, F. den (2020). Interplay between the Ubiquitin Proteasome System and Mitochondria for Protein Homeostasis. *Curr Issues Mol Biol* 35, 35–58.
- Finley, D. (2009). Recognition and Processing of Ubiquitin-Protein Conjugates by the Proteasome. *Annu. Rev. Biochem.* 78, 477–513.
- Finley, D., Tanaka, K., Mann, C., Feldmann, H., Hochstrasser, M., Vierstra, R., Johnston, S., Hampton, R., Haber, J., McCusker, J., et al. (1998). Unified nomenclature for subunits of the *Saccharomyces cerevisiae* proteasome regulatory particle. *Trends in Biochemical Sciences* 23, 244–245.
- Fiorese, C.J., Schulz, A.M., Lin, Y.F., Rosin, N., Pellegrino, M.W., and Haynes, C.M. (2016). The Transcription Factor ATF5 Mediates a Mammalian Mitochondrial UPR. *Current Biology* 26, 2037–2043.
- Franz, A., Ackermann, L., and Hoppe, T. (2014). Create and preserve: Proteostasis in

development and aging is governed by Cdc48/p97/VCP. *Biochimica et Biophysica Acta - Molecular Cell Research* 1843, 205–215.

Franz, A., Kevei, E., and Hoppe, T. (2015). Double-edged alliance: Mitochondrial surveillance by the UPS and autophagy. *Current Opinion in Cell Biology* 37, 18–27.

Fuchs, S., Bundy, J.G., Davies, S.K., Viney, J.M., Swire, J.S., and Leroi, A.M. (2010). A metabolic signature of long life in *Caenorhabditis elegans*. *BMC Biology* 8, 14.

Fujimuro, M., Tanaka, K., Yokosawa, H., and Toh-e, A. (1998). Son1p is a component of the 26S proteasome of the yeast *Saccharomyces cerevisiae*. *FEBS Letters* 423, 149–154.

Glickman, M.H., and Ciechanover, A. (2002). The Ubiquitin-Proteasome Proteolytic Pathway: Destruction for the Sake of Construction. *Physiological Reviews* 82, 373–428.

Glynn, S.E. (2017). Multifunctional Mitochondrial AAA Proteases. *Frontiers in Molecular Biosciences* 4, 34.

Goberdhan, D.C.I., Wilson, C., and Harris, A.L. (2016). Amino Acid Sensing by mTORC1: Intracellular Transporters Mark the Spot. *Cell Metabolism* 23, 580–589.

Green, C.L., Lamming, D.W., and Fontana, L. (2021). Molecular mechanisms of dietary restriction promoting health and longevity. *Nat Rev Mol Cell Biol* 1–18.

Grigoreva, T.A., Tribulovich, V.G., Garabadzhiu, A.V., Melino, G., and Barlev, N.A. (2015). The 26S proteasome is a multifaceted target for anti-cancer therapies. *Oncotarget* 6, 24733–24749.

Grune, T., Catalgol, B., Licht, A., Ermak, G., Pickering, A.M., Ngo, J.K., and Davies, K.J.A. (2011). HSP70 mediates dissociation and reassociation of the 26S proteasome during adaptation to oxidative stress. *Free Radical Biology and Medicine* 51, 1355–1364.

Gu, Z., Eils, R., and Schlesner, M. (2016). Complex heatmaps reveal patterns and correlations in multidimensional genomic data. *Bioinformatics* 32, 2847–2849.

Guerriero, C.J., and Brodsky, J.L. (2012). The Delicate Balance Between Secreted

Protein Folding and Endoplasmic Reticulum-Associated Degradation in Human Physiology. *Physiological Reviews* 92, 537–576.

Guindon, S., Dufayard, J.-F., Lefort, V., Anisimova, M., Hordijk, W., and Gascuel, O. (2010). New Algorithms and Methods to Estimate Maximum-Likelihood Phylogenies: Assessing the Performance of PhyML 3.0. *Syst Biol* 59, 307–321.

Guo, X., Huang, X., and Chen, M.J. (2017). Reversible phosphorylation of the 26S proteasome. *Protein Cell* 8, 255–272.

Haakonsen, D.L., and Rape, M. (2019). Branching Out: Improved Signaling by Heterotypic Ubiquitin Chains. *Trends in Cell Biology* 29, 704–716.

Harris, M., El Hindy, M., Usmari-Moraes, M., Hudd, F., Shafei, M., Dong, M., Hezwani, M., Clark, P., House, M., Forshaw, T., et al. (2020). BCAT-induced autophagy regulates A β load through an interdependence of redox state and PKC phosphorylation-implications in Alzheimer's disease. *Free Radical Biology and Medicine* 152, 755–766.

Hartl, F.U., Bracher, A., and Hayer-Hartl, M. (2011). Molecular chaperones in protein folding and proteostasis. *Nature* 475, 324–332.

Haynes, C.M., Yang, Y., Blais, S.P., Neubert, T.A., and Ron, D. (2010). The matrix peptide exporter HAF-1 signals a mitochondrial unfolded protein response by activating the transcription factor ZC376.7 in *C. elegans*. *Mol Cell* 37, 529–540.

Heo, J.-M., and Rutter, J. (2011). Ubiquitin-dependent mitochondrial protein degradation. *International Journal of Biochemistry and Cell Biology* 43, 1422–1426.

Hipp, M.S., Kasturi, P., and Hartl, F.U. (2019). The proteostasis network and its decline in ageing. *Nat Rev Mol Cell Biol* 20, 421–435.

Holdorf, A.D., Higgins, D.P., Hart, A.C., Boag, P.R., Pazour, G.J., Walhout, A.J.M., and Walker, A.K. (2020). WormCat: An Online Tool for Annotation and Visualization of *Caenorhabditis elegans* Genome-Scale Data. *Genetics* 214, 279–294.

- Holeček, M. (2018). Branched-chain amino acids in health and disease: Metabolism, alterations in blood plasma, and as supplements. *Nutrition and Metabolism* 15, 1–12.
- Hoppe, T. (2005). Multiubiquitylation by E4 enzymes: ‘one size’ doesn’t fit all. *Trends in Biochemical Sciences* 30, 183–187.
- Hoppe, T., and Cohen, E. (2020). Organismal Protein Homeostasis Mechanisms. *Genetics* 215, 889–901.
- Houtkooper, R.H., Pirinen, E., and Auwerx, J. (2012). Sirtuins as regulators of metabolism and healthspan. *Nature Reviews Molecular Cell Biology* 13, 225–238.
- Hull, J., Patel, V., El Hindy, M., Lee, C., Odeleye, E., Hezwani, M., Love, S., Kehoe, P., Chalmers, K., and Conway, M. (2015a). Regional Increase in the Expression of the BCAT Proteins in Alzheimer’s Disease Brain: Implications in Glutamate Toxicity. *J Alzheimers Dis* 45, 891–905.
- Hull, J., Patel, V.B., Hutson, S.M., and Conway, M.E. (2015b). New insights into the role of the branched-chain aminotransferase proteins in the human brain. *Journal of Neuroscience Research* 93, 987–998.
- Itoh, T., Ito, T., Ohba, S., Sugiyama, N., Mizuguchi, K., Yamaguchi, S., and Kidouchi, K. (1996). Effect of Carnitine Administration on Glycine Metabolism in Patients with Isovaleric Acidemia: Significance of Acetylcarnitine Determination to Estimate the Proper Carnitine Dose. *The Tohoku Journal of Experimental Medicine* 179, 101–109.
- James, H.A., O’Neill, B.T., and Nair, K.S. (2017). Insulin Regulation of Proteostasis and Clinical Implications. *Cell Metabolism* 26, 310–323.
- Johnson, E.S., Ma, P.C.M., Ota, I.M., and Varshavsky, A. (1995). A Proteolytic Pathway That Recognizes Ubiquitin as a Degradation Signal. *Journal of Biological Chemistry* 270, 17442–17456.
- Jones, D., Crowe, E., Stevens, T.A., and Candido, E.P.M. (2001). Functional and phylogenetic analysis of the ubiquitylation system in *Caenorhabditis elegans*: ubiquitin-

conjugating enzymes, ubiquitin-activating enzymes, and ubiquitin-like proteins. *Genome Biology* 3, research0002.1.

Jovaisaite, V., and Auwerx, J. (2015). The mitochondrial unfolded protein response—synchronizing genomes. *Current Opinion in Cell Biology* 33, 74–81.

Kanehisa, M., Sato, Y., Kawashima, M., Furumichi, M., and Tanabe, M. (2016). KEGG as a reference resource for gene and protein annotation. *Nucleic Acids Research* 44, D457–D462.

Kaushik, S., and Cuervo, A.M. (2015). Proteostasis and aging. *Nat Med* 21, 1406–1415.

Keller, M.A., Piedrafita, G., and Ralser, M. (2015). The widespread role of non-enzymatic reactions in cellular metabolism. *Current Opinion in Biotechnology* 34, 153–161.

Kerscher, O., Felberbaum, R., and Hochstrasser, M. (2006). Modification of Proteins by Ubiquitin and Ubiquitin-Like Proteins. *Annu. Rev. Cell Dev. Biol.* 22, 159–180.

Kikuchi, J., Iwafune, Y., Akiyama, T., Okayama, A., Nakamura, H., Arakawa, N., Kimura, Y., and Hirano, H. (2010). Co- and post-translational modifications of the 26S proteasome in yeast. *PROTEOMICS* 10, 2769–2779.

Kim, R.S., Hasegawa, D., Goossens, N., Tsuchida, T., Athwal, V., Sun, X., Robinson, C.L., Bhattacharya, D., Chou, H.-I., Zhang, D.Y., et al. (2016). The XBP1 Arm of the Unfolded Protein Response Induces Fibrogenic Activity in Hepatic Stellate Cells Through Autophagy. *Scientific Reports* 6, 39342.

Kipreos, E. (2005). Ubiquitin-mediated pathways in *C. elegans*. *WormBook*.

Klaips, C.L., Jayaraj, G.G., and Hartl, F.U. (2018). Pathways of cellular proteostasis in aging and disease. *J Cell Biol* 217, 51–63.

Knerr, I., Weinhold, N., Vockley, J., and Gibson, K.M. (2012). Advances and challenges in the treatment of branched-chain amino/keto acid metabolic defects. *Journal of Inherited Metabolic Disease* 35, 29–40.

- Knerr, I., Colombo, R., Urquhart, J., Morais, A., Merinero, B., Oyarzabal, A., Pérez, B., Jones, S.A., Perveen, R., Preece, M.A., et al. (2019). Expanding the genetic and phenotypic spectrum of branched-chain amino acid transferase 2 deficiency. *Journal of Inherited Metabolic Disease* 42, 809–817.
- Koegl, M., Hoppe, T., Schlenker, S., Ulrich, H.D., Mayer, T.U., and Jentsch, S. (1999). A Novel Ubiquitination Factor, E4, Is Involved in Multiubiquitin Chain Assembly. *Cell* 96, 635–644.
- Koizumi, S., Irie, T., Hirayama, S., Sakurai, Y., Yashiroda, H., Naguro, I., Ichijo, H., Hamazaki, J., and Murata, S. (2016). The aspartyl protease DDI2 activates Nrf1 to compensate for proteasome dysfunction. *ELife* 5, e18357.
- Komander, D., and Rape, M. (2012). The Ubiquitin Code. *Annual Review of Biochemistry* 81, 203–229.
- Kriegenburg, F., Ellgaard, L., and Hartmann-Petersen, R. (2012). Molecular chaperones in targeting misfolded proteins for ubiquitin-dependent degradation. *The FEBS Journal* 279, 532–542.
- Kruegel, U., Robison, B., Dange, T., Kahlert, G., Delaney, J.R., Kotireddy, S., Tsuchiya, M., Tsuchiyama, S., Murakami, C.J., Schleit, J., et al. (2011). Elevated Proteasome Capacity Extends Replicative Lifespan in *Saccharomyces cerevisiae*. *PLOS Genetics* 7, e1002253.
- Kuhlbrodt, K., Mouysset, J., and Hoppe, T. (2005). Orchestra for assembly and fate of polyubiquitin chains. *Essays in Biochemistry* 41, 1–14.
- Labbadia, J., and Morimoto, R.I. (2015). The Biology of Proteostasis in Aging and Disease. *Annu. Rev. Biochem.* 84, 435–464.
- Labun, K., Montague, T.G., Gagnon, J.A., Thyme, S.B., and Valen, E. (2016). CHOPCHOP v2: a web tool for the next generation of CRISPR genome engineering. *Nucleic Acids Research* 44, W272–W276.

- Lavie, J., De Belvalet, H., Sonon, S., Ion, A.M., Dumon, E., Melser, S., Lacombe, D., Dupuy, J.W., Lalou, C., and Bénard, G. (2018). Ubiquitin-Dependent Degradation of Mitochondrial Proteins Regulates Energy Metabolism. *Cell Reports* 23, 2852–2863.
- Lefort, V., Longueville, J.-E., and Gascuel, O. (2017). SMS: Smart Model Selection in PhyML. *Molecular Biology and Evolution* 34, 2422–2424.
- Lehmann, G., Udasin, R.G., and Ciechanover, A. (2016). On the linkage between the ubiquitin-proteasome system and the mitochondria. *Biochemical and Biophysical Research Communications* 473, 80–86.
- Lehrbach, N.J., and Ruvkun, G. (2016). Proteasome dysfunction triggers activation of SKN-1A/Nrf1 by the aspartic protease DDI-1. *ELife* 5, 1–19.
- Lei, M.-Z., Li, X.-X., Zhang, Y., Li, J.-T., Zhang, F., Wang, Y.-P., Yin, M., Qu, J., and Lei, Q.-Y. (2020). Acetylation promotes BCAT2 degradation to suppress BCAA catabolism and pancreatic cancer growth. *Signal Transduct Target Ther* 5.
- Li, J.-T., Yin, M., Wang, D., Wang, J., Lei, M.-Z., Zhang, Y., Liu, Y., Zhang, L., Zou, S.-W., Hu, L.-P., et al. (2020). BCAT2-mediated BCAA catabolism is critical for development of pancreatic ductal adenocarcinoma. *Nature Cell Biology* 22, 167–174.
- Li, W., Bengtson, M.H., Ulbrich, A., Matsuda, A., Reddy, V.A., Orth, A., Chanda, S.K., Batalov, S., and Joazeiro, C.A.P. (2008). Genome-Wide and Functional Annotation of Human E3 Ubiquitin Ligases Identifies MULAN, a Mitochondrial E3 that Regulates the Organelle's Dynamics and Signaling. *PLOS ONE* 3, e1487.
- Lill, R., and Mühlenhoff, U. (2008). Maturation of Iron-Sulfur Proteins in Eukaryotes: Mechanisms, Connected Processes, and Diseases. *Annual Review of Biochemistry* 77, 669–700.
- Lindquist, S., and Craig, E.A. (1988). The Heat-Shock Proteins. *Annual Review of Genetics* 49.
- Liu, C., Liu, W., Ye, Y., and Li, W. (2017). Ufd2p synthesizes branched ubiquitin chains to

promote the degradation of substrates modified with atypical chains. *Nature Communications* 8.

Liu, Y., Samuel, B.S., Breen, P.C., and Ruvkun, G. (2014). *Caenorhabditis elegans* pathways that surveil and defend mitochondria. *Nature* 508, 406–410.

Livak, K.J., and Schmittgen, T.D. (2001). Analysis of relative gene expression data using real-time quantitative PCR and the 2(-Delta Delta C(T)) Method. *Methods (San Diego, Calif.)* 25, 402–408.

Livnat-Levanon, N., Kevei, E., Kleifeld, O., Krutauz, D., Segref, A., Rinaldi, T., Erpapazoglou, Z., Cohen, M., Reis, N., Hoppe, T., et al. (2014). Reversible 26S proteasome disassembly upon mitochondrial stress. *Cell Reports* 7, 1371–1380.

Luo, W., Pant, G., Bhavnasi, Y.K., Blanchard, S.G., Jr, and Brouwer, C. (2017). Pathview Web: user friendly pathway visualization and data integration. *Nucleic Acids Research* 45, W501–W508.

Lysenko, E.A., Vepkhvadze, T.F., Lednev, E.M., Vinogradova, O.L., and Popov, D.V. (2018). Branched-chain amino acids administration suppresses endurance exercise-related activation of ubiquitin proteasome signaling in trained human skeletal muscle. *Journal of Physiological Sciences* 68, 43–53.

Madeira, F., Park, Y.M., Lee, J., Buso, N., Gur, T., Madhusoodanan, N., Basutkar, P., Tivey, A.R.N., Potter, S.C., Finn, R.D., et al. (2019). The EMBL-EBI search and sequence analysis tools APIs in 2019. *Nucleic Acids Res* 47, W636–W641.

Mannhaupt, G., Schnall, R., Karpov, V., Vetter, I., and Feldmann, H. (1999). Rpn4p acts as a transcription factor by binding to PACE, a nonamer box found upstream of 26S proteasomal and other genes in yeast. *FEBS Letters* 450, 27–34.

Manoli, I., and Venditti, C.P. (2016). Disorders of branched chain amino acid metabolism. *Translational Science of Rare Diseases* 1, 91–110.

Mansfeld, J., Urban, N., Priebe, S., Groth, M., Frahm, C., Hartmann, N., Gebauer, J.,

- Ravichandran, M., Dommaschk, A., Schmeisser, S., et al. (2015). Branched-chain amino acid catabolism is a conserved regulator of physiological ageing. *Nat Commun* 6, 10043.
- Mårtensson, C.U., Priesnitz, C., Song, J., Ellenrieder, L., Doan, K.N., Boos, F., Floerchinger, A., Zufall, N., Oeljeklaus, S., Warscheid, B., et al. (2019). Mitochondrial protein translocation-associated degradation. *Nature* 569, 679–683.
- Martin, F.-P.J., Spanier, B., Collino, S., Montoliu, I., Kolmeder, C., Giesbertz, P., Affolter, M., Kussmann, M., Daniel, H., Kochhar, S., et al. (2011). Metabotyping of *Caenorhabditis elegans* and their Culture Media Revealed Unique Metabolic Phenotypes Associated to Amino Acid Deficiency and Insulin-Like Signaling. *J. Proteome Res.* 10, 990–1003.
- Martinus, R.D., Garth, G.P., Webster, T.L., Cartwright, P., Naylor, D.J., Høj, P.B., and Hoogenraad, N.J. (1996). Selective Induction of Mitochondrial Chaperones in Response to Loss of the Mitochondrial Genome. *European Journal of Biochemistry* 240, 98–103.
- Matsumoto, S., Nakatsukasa, K., Kakuta, C., Tamura, Y., Esaki, M., and Endo, T. (2019). Msp1 Clears Mistargeted Proteins by Facilitating Their Transfer from Mitochondria to the ER. *Molecular Cell* 1–15.
- Mayor, T., Sharon, M., and Glickman, M.H. (2016). Tuning the proteasome to brighten the end of the journey. *American Journal of Physiology - Cell Physiology* ajpcell.00198.2016.
- Mehrtash, A.B., and Hochstrasser, M. (2018). Ubiquitin-dependent protein degradation at the endoplasmic reticulum and nuclear envelope. *Seminars in Cell and Developmental Biology* 93, 111–124.
- Meissner, B., Rogalski, T., Viveiros, R., Warner, A., Plastino, L., Lorch, A., Granger, L., Segalat, L., and Moerman, D.G. (2011). Determining the Sub-Cellular Localization of Proteins within *Caenorhabditis elegans* Body Wall Muscle. *PLOS ONE* 6, e19937.
- Melber, A., and Haynes, C.M. (2018). UPR mt regulation and output: A stress response mediated by mitochondrial-nuclear communication. *Cell Research* 28, 281–295.
- Meul, T., Berschneider, K., Schmitt, S., Mayr, C.H., Mattner, L.F., Schiller, H.B., Yazgili,

A.S., Wang, X., Lukas, C., Schlessner, C., et al. (2020). Mitochondrial Regulation of the 26S Proteasome. *Cell Reports* 32, 108059.

Mohri-Shiomi, A., and Garsin, D.A. (2008). Insulin Signaling and the Heat Shock Response Modulate Protein Homeostasis in the *Caenorhabditis elegans* Intestine during Infection*. *Journal of Biological Chemistry* 283, 194–201.

Mor, D.E., Sohrabi, S., Kaletsky, R., Keyes, W., Tartici, A., Kalia, V., Miller, G.W., and Murphy, C.T. (2020). Metformin rescues Parkinson's disease phenotypes caused by hyperactive mitochondria. *PNAS*.

Morimoto, R. (1993). Cells in stress: transcriptional activation of heat shock genes. *Science* 259, 1409–1410.

Münch, C. (2018). The different axes of the mammalian mitochondrial unfolded protein response. *BMC Biol* 16.

Nakatogawa, H., Suzuki, K., Kamada, Y., and Ohsumi, Y. (2009). Dynamics and diversity in autophagy mechanisms: lessons from yeast. *Nat Rev Mol Cell Biol* 10, 458–467.

Nalepa, G., and Wade Harper, J. (2003). Therapeutic anti-cancer targets upstream of the proteasome. *Cancer Treatment Reviews* 29, 49–57.

Nargund, A.M., Pellegrino, M.W., Fiorese, C.J., Baker, B.M., and Haynes, C.M. (2012). Mitochondrial Import Efficiency of ATFS-1 Regulates Mitochondrial UPR Activation. *Science* 337, 587–590.

Neinast, M., Murashige, D., and Arany, Z. (2019). Branched Chain Amino Acids. *Annu. Rev. Physiol.* 81, 139–164.

Ohsumi, Y. (2014). Historical landmarks of autophagy research. *Cell Res* 24, 9–23.

Ottens, F., Franz, A., and Hoppe, T. (2021). Build-UPS and break-downs: metabolism impacts on proteostasis and aging. *Cell Death & Differentiation* 1–17.

Paix, A., Folkmann, A., and Seydoux, G. (2017). Precision genome editing using CRISPR-

- Cas9 and linear repair templates in *C. elegans*. *Methods* 121–122, 86–93.
- Pakos-Zebrucka, K., Koryga, I., Mnich, K., Ljubic, M., Samali, A., and Gorman, A.M. (2016). The integrated stress response. *EMBO Reports* 17, 1374–1395.
- Passmore, L.A., and Barford, D. (2004). Getting into position: the catalytic mechanisms of protein ubiquitylation. *Biochemical Journal* 379, 513–525.
- Peng, H., Wang, Y., and Luo, W. (2020). Multifaceted role of branched-chain amino acid metabolism in cancer. *Oncogene* 39, 6747–6756.
- Perrin-Vidoz, L., Sinilnikova, O.M., Stoppa-Lyonnet, D., Lenoir, G.M., and Mazoyer, S. (2002). The nonsense-mediated mRNA decay pathway triggers degradation of most BRCA1 mRNAs bearing premature termination codons. *Human Molecular Genetics* 11, 2805–2814.
- Phillips, M.J., and Voeltz, G.K. (2016). Structure and function of ER membrane contact sites with other organelles. *Nat Rev Mol Cell Biol* 17, 69–82.
- Piedrafita, G., Keller, M.A., and Ralser, M. (2015). The impact of non-enzymatic reactions and enzyme promiscuity on cellular metabolism during (Oxidative) stress conditions. *Biomolecules* 5, 2101–2122.
- Pilla, E., Schneider, K., and Bertolotti, A. (2017). Coping with Protein Quality Control Failure. *Annual Review of Cell and Developmental Biology* 33, 439–465.
- Pohl, C., and Dikic, I. (2019). Cellular quality control by the ubiquitin-proteasome system and autophagy. *Science* 366, 818–822.
- Quirós, P.M., Langer, T., and López-Otín, C. (2015). New roles for mitochondrial proteases in health, ageing and disease. *Nat Rev Mol Cell Biol* 16, 345–359.
- Ravanelli, S., den Brave, F., and Hoppe, T. (2020). Mitochondrial Quality Control Governed by Ubiquitin. *Front Cell Dev Biol* 8.
- Richter, K., Haslbeck, M., and Buchner, J. (2010). The Heat Shock Response: Life on the

Verge of Death. *Molecular Cell* 40, 253–266.

Ritossa, F. (1962). A new puffing pattern induced by temperature shock and DNP in drosophila. *Experientia* 18, 571–573.

Ron, D. (2002). Translational control in the endoplasmic reticulum stress response. *J Clin Invest* 110, 1383–1388.

Rousseau, A., and Bertolotti, A. (2016). An evolutionarily conserved pathway controls proteasome homeostasis. *Nature* 536, 184–189.

Rousseau, A., and Bertolotti, A. (2018). Regulation of proteasome assembly and activity in health and disease. *Nature Reviews Molecular Cell Biology* 19, 697–712.

Rual, J.-F., Ceron, J., Koreth, J., Hao, T., Nicot, A.-S., Hirozane-Kishikawa, T., Vandenhaute, J., Orkin, S.H., Hill, D.E., van den Heuvel, S., et al. (2004). Toward Improving *Caenorhabditis elegans* Phenome Mapping With an ORFeome-Based RNAi Library. *Genome Research* 14, 2162–2168.

Ruggiano, A., Foresti, O., and Carvalho, P. (2014). ER-associated degradation: Protein quality control and beyond. *J Cell Biol* 204, 869–879.

Ryu, K.-Y., Maehr, R., Gilchrist, C.A., Long, M.A., Bouley, D.M., Mueller, B., Ploegh, H.L., and Kopito, R.R. (2007). The mouse polyubiquitin gene UbC is essential for fetal liver development, cell-cycle progression and stress tolerance. *The EMBO Journal* 26, 2693–2706.

Salminen, A., and Kaarniranta, K. (2012). AMP-activated protein kinase (AMPK) controls the aging process via an integrated signaling network. *Ageing Research Reviews* 11, 230–241.

Satyal, S.H., Schmidt, E., Kitagawa, K., Sondheimer, N., Lindquist, S., Kramer, J.M., and Morimoto, R.I. (2000). Polyglutamine aggregates alter protein folding homeostasis in *Caenorhabditis elegans*. *PNAS* 97, 5750–5755.

- Sauer, R.T., and Baker, T.A. (2011). AAA+ Proteases: ATP-Fueled Machines of Protein Destruction. *Annu. Rev. Biochem.* *80*, 587–612.
- Saxton, R.A., and Sabatini, D.M. (2017). mTOR Signaling in Growth, Metabolism, and Disease. *Cell* *168*, 960–976.
- Schmidt, M., and Finley, D. (2014). Regulation of proteasome activity in health and disease. *Biochimica et Biophysica Acta - Molecular Cell Research* *1843*, 13–25.
- Schmidt, O., Pfanner, N., and Meisinger, C. (2010). Mitochondrial protein import: from proteomics to functional mechanisms. *Nat Rev Mol Cell Biol* *11*, 655–667.
- Schulman, B.A., and Wade Harper, J. (2009). Ubiquitin-like protein activation by E1 enzymes: the apex for downstream signalling pathways. *Nat Rev Mol Cell Biol* *10*, 319–331.
- Segref, A., Torres, S., and Hoppe, T. (2011). A screenable in vivo assay to study proteostasis networks in *Caenorhabditis elegans*. *Genetics* *187*, 1235–1240.
- Segref, A., Kevei, E., Pokrzywa, W., Schmeisser, K., Mansfeld, J., Livnat-Levanon, N., Ensenauer, R., Glickman, M.H., Ristow, M., and Hoppe, T. (2014). Pathogenesis of human mitochondrial diseases is modulated by reduced activity of the ubiquitin/proteasome system. *Cell Metabolism* *19*, 642–652.
- Shaham, S. (2006). Methods in cell biology. WormBook.
- She, P., Reid, T.M., Bronson, S.K., Vary, T.C., Hajnal, A., Lynch, C.J., and Hutson, S.M. (2007). Disruption of BCATm in Mice Leads to Increased Energy Expenditure Associated with the Activation of a Futile Protein Turnover Cycle. *Cell Metabolism* *6*, 181–194.
- Shpilka, T., and Haynes, C.M. (2018). The mitochondrial UPR: Mechanisms, physiological functions and implications in ageing. *Nature Reviews Molecular Cell Biology* *19*, 109–120.
- Siddik, M.A.B., and Shin, A.C. (2019). Recent Progress on Branched-Chain Amino Acids in Obesity, Diabetes, and Beyond. *Endocrinology and Metabolism* *34*, 234.

Sonenberg, N., and Hinnebusch, A.G. (2009). Regulation of Translation Initiation in Eukaryotes: Mechanisms and Biological Targets. *Cell* 136, 731–745.

Song, J., Herrmann, J.M., and Becker, T. (2021). Quality control of the mitochondrial proteome. *Nat Rev Mol Cell Biol* 22, 54–70.

Soultoukis, G.A., and Partridge, L. (2016). Dietary Protein, Metabolism, and Aging. *Annu Rev Biochem* 85, 5–34.

Sperringer, J.E., Addington, A., and Hutson, S.M. (2017). Branched-Chain Amino Acids and Brain Metabolism. *Neurochemical Research* 42, 1697–1709.

Suraweera, A., Münch, C., Hanssum, A., and Bertolotti, A. (2012). Failure of amino acid homeostasis causes cell death following proteasome inhibition. *Molecular Cell* 48, 242–253.

Toyokawa, Y., Koonthongkaew, J., and Takagi, H. (2021). An overview of branched-chain amino acid aminotransferases: functional differences between mitochondrial and cytosolic isozymes in yeast and human. *Appl Microbiol Biotechnol*.

Tsukada, M., and Ohsumi, Y. (1993). Isolation and characterization of autophagy-defective mutants of *Saccharomyces cerevisiae*. *FEBS Letters* 333, 169–174.

Valerio, A., D'Antona, G., and Nisoli, E. (2011). Branched-chain amino acids, mitochondrial biogenesis, and healthspan: an evolutionary perspective. *Aging (Albany NY)* 3, 464–478.

Vembar, S.S., and Brodsky, J.L. (2008). One step at a time: Endoplasmic reticulum-associated degradation. *Nature Reviews Molecular Cell Biology* 9, 944–957.

Vilchez, D., Saez, I., and Dillin, A. (2014). The role of protein clearance mechanisms in organismal ageing and age-related diseases. *Nature Communications* 5, 5659.

Villani, G.R., Gallo, G., Scolamiero, E., Salvatore, F., and Ruoppolo, M. (2017). “Classical organic acidurias”: diagnosis and pathogenesis. *Clin Exp Med* 17, 305–323.

- van Vliet, A.R., Verfaillie, T., and Agostinis, P. (2014). New functions of mitochondria associated membranes in cellular signaling. *Biochimica et Biophysica Acta (BBA) - Molecular Cell Research* 1843, 2253–2262.
- Wagner, G.R., Bhatt, D.P., O’Connell, T.M., Thompson, J.W., Dubois, L.G., Backos, D.S., Yang, H., Mitchell, G.A., Ilkayeva, O.R., Stevens, R.D., et al. (2017). A Class of Reactive Acyl-CoA Species Reveals the Non-enzymatic Origins of Protein Acylation. *Cell Metabolism* 25, 823-837.e8.
- Walker, M.D., Giese, G.E., Holdorf, A.D., Bhattacharya, S., Diot, C., García-González, A.P., Horowitz, B.B., Lee, Y.-U., Leland, T., Li, X., et al. (2021). WormPaths: *Caenorhabditis elegans* metabolic pathway annotation and visualization. *Genetics*.
- Walter, P., and Ron, D. (2011). The Unfolded Protein Response: From Stress Pathway to Homeostatic Regulation. *Science* 334, 1081–1086.
- Wang, X., Yen, J., Kaiser, P., and Huang, L. (2010). Regulation of the 26S Proteasome Complex During Oxidative Stress. *Sci. Signal.* 3, ra88–ra88.
- Wang, X.L., Li, C.J., Xing, Y., Yang, Y.H., and Jia, J.P. (2015). Hypervalinemia and hyperleucine-isoleucinemia caused by mutations in the branched-chain-amino-acid aminotransferase gene. *J Inherit Metab Dis* 38, 855–861.
- Wang, Y., Argiles-Castillo, D., Kane, E.I., Zhou, A., and Spratt, D.E. (2020). HECT E3 ubiquitin ligases – emerging insights into their biological roles and disease relevance. *Journal of Cell Science* 133.
- Weidberg, H., and Amon, A. (2018). MitoCPR—A surveillance pathway that protects mitochondria in response to protein import stress. *Science* 360.
- White, J.P. (2021). Amino Acid Trafficking and Skeletal Muscle Protein Synthesis: A Case of Supply and Demand. *Frontiers in Cell and Developmental Biology* 9, 1293.
- White, P.J., and Newgard, C.B. (2019). Branched-chain amino acids in disease. *Science* 363, 582–583.

- White, P.J., McGarrah, R.W., Herman, M.A., Bain, J.R., Shah, S.H., and Newgard, C.B. (2021). Insulin action, type 2 diabetes, and branched-chain amino acids: A two-way street. *Molecular Metabolism* 52, 101261.
- Wiedemann, N., and Pfanner, N. (2017). Mitochondrial Machineries for Protein Import and Assembly. *Annu. Rev. Biochem.* 86, 685–714.
- Wolfe, R.R. (2017). Branched-chain amino acids and muscle protein synthesis in humans: Myth or reality? *Journal of the International Society of Sports Nutrition* 14, 1–7.
- Wrobel, L., Topf, U., Bragoszewski, P., Wiese, S., Sztolsztener, M.E., Oeljeklaus, S., Varabyova, A., Lirski, M., Chroscicki, P., Mroczek, S., et al. (2015). Mistargeted mitochondrial proteins activate a proteostatic response in the cytosol. *Nature* 524, 485–488.
- Xie, Y., and Varshavsky, A. (2001). RPN4 is a ligand, substrate, and transcriptional regulator of the 26S proteasome: A negative feedback circuit. *PNAS* 98, 3056–3061.
- Xu, H., Xiao, T., Chen, C.-H., Li, W., Meyer, C.A., Wu, Q., Wu, D., Cong, L., Zhang, F., Liu, J.S., et al. (2015). Sequence determinants of improved CRISPR sgRNA design. *Genome Res.* 25, 1147–1157.
- Yao, V., Kaletsky, R., Keyes, W., Mor, D.E., Wong, A.K., Sohrabi, S., Murphy, C.T., and Troyanskaya, O.G. (2018). diseaseQUEST: An integrative tissue network approach to identify and test novel human disease genes. *Nature Biotechnology*.
- Ye, Y., and Rape, M. (2009). Building ubiquitin chains: E2 enzymes at work. *Nat Rev Mol Cell Biol* 10, 755–764.
- Ye, S., Dhillon, S., Ke, X., Collins, A.R., and Day, I.N.M. (2001). An efficient procedure for genotyping single nucleotide polymorphisms. *Nucleic Acids Res* 29, e88.
- Yilmaz, L.S., and Walhout, A.J.M. (2014). Worms, bacteria, and micronutrients: An elegant model of our diet. *Trends in Genetics* 30, 496–503.

Yilmaz, L.S., and Walhout, A.J.M. (2016). A *Caenorhabditis elegans* Genome-Scale Metabolic Network Model. *Cell Systems* 2, 297–311.

Yoneda, T., Benedetti, C., Urano, F., Clark, S.G., Harding, H.P., and Ron, D. (2004). Compartment-specific perturbation of protein handling activates genes encoding mitochondrial chaperones. *Journal of Cell Science* 117, 4055–4066.

Youle, R.J. (2019). Mitochondria—Striking a balance between host and endosymbiont. *Science* 365, eaaw9855.

Zhang, B., Xu, F., Wang, K., Liu, M., Li, J., Zhao, Q., Jiang, L., Zhang, Z., Li, Y., Chen, H., et al. (2021). BCAT1 knockdown-mediated suppression of melanoma cell proliferation and migration is associated with reduced oxidative phosphorylation. *Am J Cancer Res* 11, 2670–2683.

Zhao, J., Zhai, B., Gygi, S.P., and Goldberg, A.L. (2015). mTOR inhibition activates overall protein degradation by the ubiquitin proteasome system as well as by autophagy. *PNAS* 112, 15790–15797.

Zhao, Q., Wang, J., Levichkin, I.V., Stasinopoulos, S., Ryan, M.T., and Hoogenraad, N.J. (2002). A mitochondrial specific stress response in mammalian cells. *EMBO J* 21, 4411–4419.

Appendix

Appendix 1 Strains and Crosses in detail

Strain ID	Genotype	Cross details/origin	Experiment
PP2630	<i>hhls64[unc-119(+); sur-5::UbiV-GFP]III; skn-1(mg570)IV</i>	Obtained by crossing PP563 (males) with GR2245	qRT-PCR of <i>skn-1</i> isoforms
SJ4100	<i>zcls13[hsp-6::GFP]V</i>	D. Ron lab	RNAi metabolic screen
PP563	<i>unc-119(ed4) hhls64 [unc-119(+); sur-5p::UbV-GFP]III</i>	Our lab	RNAi metabolic screen
FX06784	<i>ivd-1(tm6784) IV</i>	National BioResource Project (NBRP)	Crosses
PP3071	<i>risls3 [K02A4.1p::K02A4.1::GFP + unc-119(+)]</i>	2x outcrossed MIR23	BCAT-1 localization
PP3105	<i>hhls64[unc-119(+); sur-5::UbiV-GFP]III; ivd-1(tm6784) IV</i>	Obtained by crossing PP563 (males) with 4x outcrossed FX06784, then F1 males crossed with PP563	Crosses
PP607	<i>hhls72[unc-119(+); sur-5p::mCherry]</i>	Our lab	UbV-GFP stabilization, IVA supplementation
FX30253	<i>tmC24 [F23D12.4(tmIs1233) unc-9(tm9718)] X; tmEx4950 [unc-9(+) + vha-6p::GFP]</i>	Caenorhabditis Genetics Center (CGC)	Crosses
PP3387; PP3387a	<i>bcat-1 (hh56)/tmC24 [F23D12.4(tmIs1233) unc-9(tm9718)] X</i>	<i>bcat-1 (hh56)/+</i> obtained by CRISPR-Cas9 crossed with 4x outcrossed FX30253 (males)	Lethality quantification
3515	<i>hhls64[unc-119(+); sur-5::UbiV-GFP] III; ivd-1(tm6784) IV; bcat-1 (hh56)/tmC24 [F23D12.4(tmIs1233) unc-9(tm9718)] X</i>	2x outcrossed PP3387 crossed with PP3104(males), then F1 hermaphrodites crossed with 4x outcrossed FX30253 (males)	UbV-GFP stabilization
3516	<i>hhls64[unc-119(+); sur-5::UbiV-GFP] III; bcat-1 (hh56)/tmC24 [F23D12.4(tmIs1233) unc-9(tm9718)] X</i>		
PP3101	<i>bcat-1 (hh58) X</i>	Outcrossed x4 <i>bcat-1(hh58)</i> generated by CRISPR-Cas9	
PP3102	<i>hhls64[unc-119(+); sur-5::UbiV-GFP] III</i>		
PP3104	<i>hhls64[unc-119(+); sur-5::UbiV-GFP]III; ivd-1(tm6784) IV</i>	N2 (males) crossed with PP3101, then F1 males crossed with PP3015	UbV-GFP stabilization, development and progeny quantification, IVA supplementation
PP3106	<i>hhls64[unc-119(+); sur-5::UbiV-GFP] III; bcat-1 (hh58) X</i>		
PP3108	<i>hhls64[unc-119(+); sur-5::UbiV-GFP] III; ivd-1(tm6784) IV; bcat-1 (hh58) X</i>		

PP3103	<i>wild type</i>		
PP3105	<i>ivd-1(tm6784) IV</i>		
PP3107	<i>bcat-1 (hh58) X</i>		
PP3109	<i>ivd-1(tm6784) IV; bcat-1 (hh58) X</i>		
PP3154	<i>hecd-1 (tm2371) IV</i>	N2 (males) crossed with 2x outcrossed <i>hecd-1 (tm2371)</i> , then F1 males crossed with PP3106 to get similar background as other strains for the omics analysis	omics analysis
PP3349	<i>risls3 [K02A4.1p::K02A4.1::GFP + unc-119(+)]; hhls67 [unc-119(+); sur-5::UbiV-GFP]</i>		
PP3350	<i>ivd-1(tm6784) IV; risls3 [K02A4.1p::K02A4.1::GFP + unc-119(+)]; hhls67 [unc-119(+); sur-5::UbiV-GFP]</i>	N2 (males) crossed with PP3071, then F1 males crossed with PP3108	UbV-GFP stabilization, development and progeny quantification
PP3351	<i>bcat-1 (hh58) X; risls3 [K02A4.1p::K02A4.1::GFP + unc-119(+)]; hhls67 [unc-119(+); sur-5::UbiV-GFP]</i>		
PP3352	<i>ivd-1(tm6784) IV; bcat-1 (hh58) X; risls3 [K02A4.1p::K02A4.1::GFP + unc-119(+)]; hhls67 [unc-119(+); sur-5::UbiV-GFP]</i>		
PP3390	<i>hhls64[unc-119(+); sur-5::UbiV-GFP] III; ivd-1(tm6784) IV; hhls72[unc-119(+); sur-5p::mCherry]</i>		
PP3391	<i>hhls64[unc-119(+); sur-5::UbiV-GFP] III; bcat-1 (hh58) X; hhls72[unc-119(+); sur-5p::mCherry]</i>		UbV-GFP stabilization, IVA supplementation
PP3392	<i>hhls64[unc-119(+); sur-5::UbiV-GFP] III; ivd-1(tm6784) IV; bcat-1 (hh58) X; hhls72[unc-119(+); sur-5p::mCherry]</i>		
PP3393	<i>hhls64[unc-119(+); sur-5::UbiV-GFP] III; hhls72[unc-119(+); sur-5p::mCherry]; risls3 [K02A4.1p::K02A4.1::GFP + unc-119(+)]</i>	PP563 (males) crossed with PP3352, then F1 males crossed with PP607	UbV-GFP stabilization
PP3394	<i>hhls64[unc-119(+); sur-5::UbiV-GFP] III; ivd-1(tm6784) IV; hhls72[unc-119(+); sur-5p::mCherry]; risls3 [K02A4.1p::K02A4.1::GFP + unc-119(+)]</i>		
PP3395	<i>hhls64[unc-119(+); sur-5::UbiV-GFP] III; bcat-1 (hh58) X; hhls72[unc-119(+); sur-5p::mCherry]; risls3 [K02A4.1p::K02A4.1::GFP + unc-119(+)]</i>		
PP3396	<i>hhls64[unc-119(+); sur-5::UbiV-GFP] III; ivd-1(tm6784) IV; bcat-1 (hh58) X; hhls72[unc-119(+); sur-5p::mCherry]; risls3 [K02A4.1p::K02A4.1::GFP + unc-119(+)]</i>		

Appendix 2 Genotyping oligonucleotides and PCR conditions

Allele/Transgene	PrimerID	Forward/Reverse WT/Mut	Forward	Genotype notes
<i>sur-5p::UbV-gfp</i>	TH969	Forward	TTTTGGTACCATGCAAATCTTCGTC AAAACGTTG	Ta:50°-55°C elong: 1min band: 1.2 kbp
	TH984	Reverse	CGTTAGTTAGTAGAACTCAG	
<i>hsp-6p::gfp</i>	TH930	Forward	CTACCTGTTCCATGGGTAAG	Ta: 50-62°C band: 500bp
	TH931	Reverse	CTCCATCTTCAATGTTGTGTC	
<i>acs-19(hh5)</i>	TH2757	Forward Mut	AAGGTATTCAACACACTACAGGTC	Ta: 62°C WT: 414bp M: 208bp ext: 578bp
	TH2750	Reverse Mut	CTAGAAGGAGTCGGATAAGTCG	
	TH2751	Reverse WT	GTAGGCGTACGTCATGTAACC	
	TH2752	Forward WT	GGTGGAACTTAAAACGAGTC	
<i>ivd-1(hh6)</i>	TH2753	Forward Mut	CCATTCAATACATACTTGTCTCC	Ta: 55°C WT:292bp M:189bp ext:437bp
	TH2754	Reverse Mut	GAAAGAAGTATCTCCAACGA	
	TH2755	Reverse WT	GTATGCTGACAAGATTGACAAG	
	TH2756	Forward WT	TTACTAATTTTTTCGGTAATGAC	
<i>skn-1(mg570)</i>	TH2955	Forward Mut	CGCTGACGGCGTGATGATCATT	Ta: 52-68°C WT:220bp M:103bp ext:286bp
	TH2956	Reverse WT	CCAGTCAGTCGATGGGCGGT	
	TH2957	Forward WT	CGAAAAGTCATGCTCTCCCGTGA	
	TH2958	Reverse Mut	CGCGAGTCCGTGTCCGAATATT	
<i>bcat-1</i> CRISPR-Cas9 (NheI)	TH3383	Forward	AATGTACTGCCTCCATCGGC	Ta: 50-65°C WT:467bp hh56: 177bp+290bp hh58: 230bp+230bp
	TH3384	Reverse	GGGTCCAATGGCTTGGTCTT	
<i>ivd-1(tm6784)</i>	TH2753	Forward WT	CCATTCAATACATACTTGTCTCC	Ta: 50-62°C WT: 437bp M:939bp
	TH2755	Reverse	GTATGCTGACAAGATTGACAAG	
	TH3507	Forward Mut	TCCATTCGCACAGATACACA	
<i>acs-19(tm4853)</i>	TH1873	Forward	CATCTACGATTCGAGATGCTC	Ta: 48-62°C WT: 777bp M:307bp
	TH1974	Reverse	CAATAACACGACCTTCAGC	
<i>bcat-1p::bcat-1::gfp</i>	TH3825	Forward	TTAATGACATTTCAGTACGGC	Ta:55-60°C elong: 1 min band: 1057bp
	TH984	Reverse	CGTTAGTTAGTAGAACTCAG	
<i>hecd-1(tm2371)</i>	TH1259	Forward WT	TTCAGAAGATTTGGAGGACC	Ta:50-58 WT: 440 bp M: 300 bp
	TH1260	Forward Mut	GGACTATCGTATAAATGCTGTGGG	
	TH3804	Reverse	TCATAATCCATTTTCAGAAATTCAGT	
<i>bcat-1(hh58)</i>	TH3511	Reverse WT	CGTGGAGCAACTCGCGACAG	WT:253bp M:84bp ext:310bp
	TH3512	Forward Mut	ATCCTGTCCAGCTAGCGCGA	
	TH3383	Forward	AATGTACTGCCTCCATCGGC	
	TH3372	Reverse	ACTGTCTCCAATCTGGCTGC	

Appendix 3 CRISPR-Cas9 oligonucleotides

Use	Sequence	Purchased by
universal tracrRNA	AACAGCAUAGCAAGUUAAAAUAAGGC UAGUCCGUUAUCAACUUGAAAAAGU GGCACCGAGUCGGUGCUUUUUUU	Dharmacon
<i>bcat-1(hh56)</i> crRNA	ugucuccaaucuggcugcgg	Dharmacon
<i>bcat-1(hh56)</i> ssODN	cttcaacctgtcggatcaaggcttatggcctccgGCT AGCCcagccagattggagacagtaccaagagagg aaatt	Metabion (HPLC purified)
<i>bcat-1(hh58)</i> crRNA	ugcguggagcaacucgcgac	Dharmacon
<i>bcat-1(hh58)</i> ssODN	ccagaaatacacacaataatgccagcaatcctgtcC AGCTAGCgcgagttgctccacgcaccttcaacctt gtcggat	Metabion (HPLC purified)
<i>dpy-10</i> crRNA	GCUACCAUAGGCACCACGAG	Dharmacon
<i>dpy-10</i> ssODN	CACTTGAACCTTCAATACGGCAAGATG AGAATGACTGGAAACCGTACCGCATG CGGTGCCTATGGTAGCGGAGCTTCAC ATGGCTTCAGACCAACAGCCTAT	Metabion (HPLC purified)

Appendix 4 ImageJ Macro for BCAT-1::GFP localization

```
//Measure of bcat-1::GFP area (green channel) inside Mitotracker-stained area (red channel)
```

```
//This macro selects the fluorescent area in the red channel and inside this area measures the fluorescence of the green channel
```

```
//General Settings
```

```
setOption("BlackBackground", true);
run("Set Measurements...", "area_fraction redirect=None decimal=3");
run("Bio-Formats Macro Extensions");
roiManager("reset");
```

```
//File selection
```

```
ChosenDir = getDirectory("Choose a directory");
```

```
ProcessFiles(ChosenDir);
```

```
function ProcessFiles(dir) {
```

```
    fileList = getFileList(dir);
    outputDirName = dir + "Analysis";
```

```
    //add new Analysis folder if already existing
    folderCount = 1;
```

```

while (File.exists(outputDirName)) {
outputDirName = dir + "Analysis-" + folderCount;
folderCount++;
}

outputDirPath = outputDirName + File.separator;
File.makeDirectory(outputDirName);

//run macro for every file .lsm found
for (file = 0; file < fileList.length; file++) {
    if (endsWith(fileList[file], ".lsm")) {

        Macro2(); //specified below

    }

    //uncomment to read through subfolders as well
    //else if (endsWith(fileList[file], "/" ) && !matches(fileList[file],
".*Analysis.*")) {
        //    ProcessFiles(dir + fileList[file]);
        //    }
    }

    saveAs("Results", outputDirPath + "Quantification.tsv");
    close("Results");
}

function Macro2() {

    Ext.openImagePlus(dir + fileList[file]);

    OriginalImageTitle = getTitle();
    red = "C2-" + OriginalImageTitle;
    green = "C1-" + OriginalImageTitle;
    binary = OriginalImageTitle + "_mito";
    run("Split Channels");

    //Select Mitotracker-stained area
    selectWindow(red);
    run("Duplicate...", "title=[" + binary + "]");
    run("Enhance Contrast...", "saturated=0.01 normalize");
    run("Convolved Background Subtraction", "convolution=Gaussian
radius=150");
    run("Auto Threshold", "method=Li white");
    run("Median...", "radius=1");
    run("Create Selection");
    roiManager("Add");
    //run("Measure");
    save(outputDirPath + red + ".png");
}

```

```

        close(red);
        close(binary);

        //measure GFP inside the Mitotracker-stained area
        selectWindow(green);
        waitForUser("Background subtraction", "Select an area in the background
\n and select OK"); //\n new line
        while (!is("area")) {
            waitForUser("Error", "You need to select an area to subtract
background");
        }
        backgroundIntensity = getValue("Mean");
        run("Select None");
        run("Subtract...", "value=" + backgroundIntensity);
            roiManager("Select", roiManager("count")-1);
            roiManager("Measure");
            roiManager("Set Color", "red");
            run("Add Selection...");
        save(outputDirPath + green + ".png");
        close(green);
        close(OriginalImageTitle);
    }

```

Appendix 5 ImageJ Macro for targeted metabolic RNAi screen

```

//Semi-automated quantification of fluorescent intensity normalized on worm area

//This macro selects and measures the area with worms from the brightfield channel
//and the integrated density of the GFP positive area in the green channel

//General Settings
run("Set Measurements...", "area mean standard modal min centroid center perimeter
bounding fit shape feret's integrated median skewness kurtosis area_fraction stack
display redirect=None decimal=3");
run("Bio-Formats Macro Extensions");
roiManager("reset");

//File selection
ChosenDir = getDirectory("Choose a directory");

ProcessFiles(ChosenDir);

function ProcessFiles(dir) {

    fileList = getFileList(dir);
    outputDirName = dir + "Analysis";

    //add new Analysis folder if already existing
    folderCount = 1;

```

```

while (File.exists(outputDirName)) {
outputDirName = dir + "Analysis-" + folderCount;
folderCount++;
}

outputDirPath = outputDirName + File.separator;
File.makeDirectory(outputDirName);

//run macro for every file .czi found
for (file = 0; file < fileList.length; file++) {
    if (endsWith(fileList[file], ".czi")) {

        Macrol(); //specified below

    }

    //uncomment to read through subfolders as well
    //else if (endsWith(fileList[file], "/") && !matches(fileList[file],
".*Analysis.*")) {
        //    ProcessFiles(dir + fileList[file]);
        //    }
    }

    saveAs("Results", outputDirPath + "Quantification.tsv");
    close("Results");
}

function Macrol() {
    Ext.openImagePlus(dir + fileList[file]);

    OriginalImageTitle = getTitle();
        bright = "C2-" + OriginalImageTitle;
        green = "C1-" + OriginalImageTitle;
        binary = OriginalImageTitle + "_bin";
        bin_green = OriginalImageTitle + "_binGFP";
        run("8-bit");
        resetMinAndMax();
        run("Split Channels");

        //Measure area with worms
        run("Duplicate...", "title=[" + binary + "]);
        selectWindow(binary);
        run("Pseudo flat field correction", "blurring=50 hide");
        run("Median...", "radius=20");
        run("Minimum...", "radius=10");
        run("Threshold...");
        setThreshold(0,100);
        waitForUser("Threshold", "Adjust threshold then press OK");
}

```

```

run("Convert to Mask");
run("EDM Binary Operations", "iterations=30 operation=close");
run("EDM Binary Operations", "iterations=10 operation=erode");
run("Create Selection");
roiManager("Add");
run("Measure");

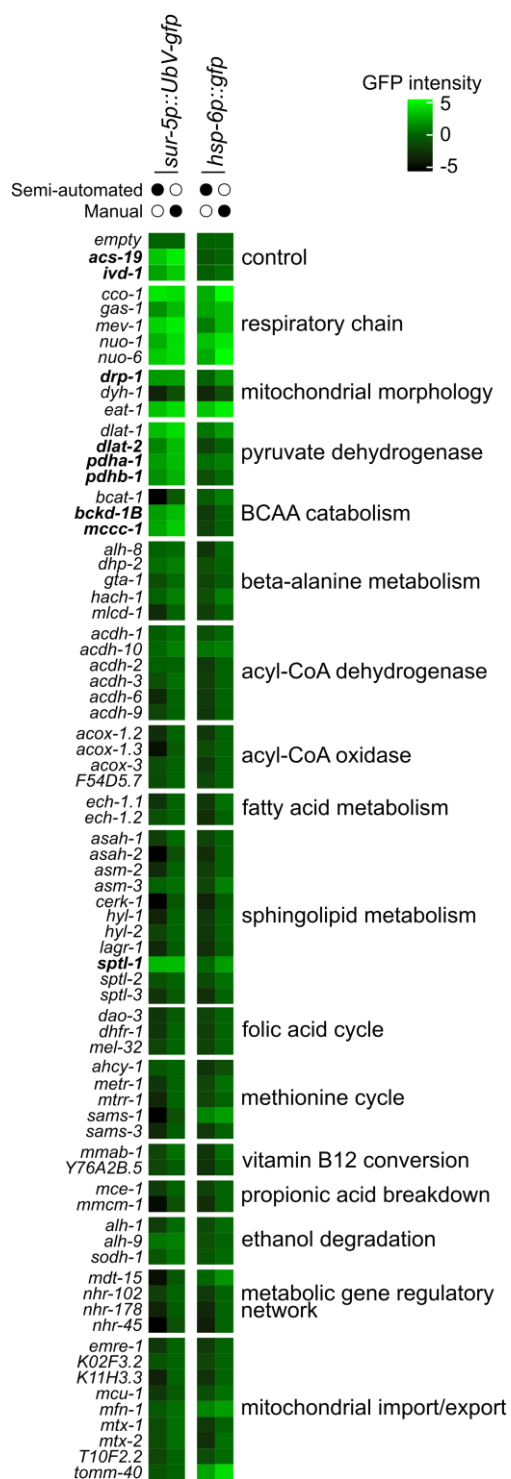
//save image with thresholded ROI
selectWindow(bright);
roiManager("Select", roiManager("count")-1);
roiManager("Set Color", "yellow");
run("Add Selection...");
save(outputDirPath + binary + ".png");
close(bright);
close(binary);

//measure GFP
selectWindow(green);
waitForUser("Background subtraction", "Select an area in the
background \n and select OK"); //\n new line
while (!is("area")) {
    waitForUser("Error", "You need to select an area to subtract
background");
}
backgroundIntensity = getValue("Mean");
run("Select None");
run("Subtract...", "value=" + backgroundIntensity);
run("Duplicate...", "title=[" + bin_green + "]");
run("Threshold...");
setThreshold(50,255);
waitForUser("Threshold", "Adjust threshold then press OK");
run("Convert to Mask");
run("EDM Binary Operations", "iterations=5 operation=close");
run("Create Selection");
roiManager("Add");
roiManager("Set Color", "red");
selectWindow(green);
roiManager("Select", roiManager("count")-1);
run("Measure");
run("Add Selection...");
save(outputDirPath + bin_green + ".png");

close(bin_green);
close(green);
close(OriginalImageTitle);
}

```

Appendix 6 Metabolic RNAi screen results



Declaration for the doctoral thesis / Erklärung zur Dissertation

„Hiermit versichere ich an Eides statt, dass ich die vorliegende Dissertation selbstständig und ohne die Benutzung anderer als der angegebenen Hilfsmittel und Literatur angefertigt habe. Alle Stellen, die wörtlich oder sinngemäß aus veröffentlichten und nicht veröffentlichten Werken dem Wortlaut oder dem Sinn nach entnommen wurden, sind als solche kenntlich gemacht. Ich versichere an Eides statt, dass diese Dissertation noch keiner anderen Fakultät oder Universität zur Prüfung vorgelegen hat; dass sie - abgesehen von unten angegebenen Teilpublikationen und eingebundenen Artikeln und Manuskripten - noch nicht veröffentlicht worden ist sowie, dass ich eine Veröffentlichung der Dissertation vor Abschluss der Promotion nicht ohne Genehmigung des Promotionsausschusses vornehmen werde. Die Bestimmungen dieser Ordnung sind mir bekannt. Darüber hinaus erkläre ich hiermit, dass ich die Ordnung zur Sicherung guter wissenschaftlicher Praxis und zum Umgang mit wissenschaftlichem Fehlverhalten der Universität zu Köln gelesen und sie bei der Durchführung der Dissertation zugrundeliegenden Arbeiten und der schriftlich verfassten Dissertation beachtet habe und verpflichte mich hiermit, die dort genannten Vorgaben bei allen wissenschaftlichen Tätigkeiten zu beachten und umzusetzen. Ich versichere, dass die eingereichte elektronische Fassung der eingereichten Druckfassung vollständig entspricht.“

Teilpublikationen:

Ravanelli, S., den Brave, F., and Hoppe, T. Mitochondrial Quality Control Governed by Ubiquitin. Front Cell Dev Biol. (2020).

Ravanelli, S., Li Q., Annibal A., Trifunovic A., Antebi A., Hoppe T. Reprograming of Proteasomal Degradation by Branched Chain Amino Acid Metabolism. Aging Cell. (2022).

Efstathiou S., Ottens F., Schütter L., Ravanelli S., Charmpilas N., Gutschmidt A., Le Pen J., Gehring N. H., Miska E. A., Bouças J., Hoppe T. ER-Associated RNA Silencing Promotes ER Quality Control. Nature Cell Biology. (2022).

Köln, 28.09.2022



Sonia Ravanelli

Curriculum vitae

Personal details	Sonia Ravanelli born on Mai 7th 1989, in Trento (Italy)
Education and Training	
<i>May 2016 – January 2022</i>	PhD student Thorsten Hoppe Lab <i>CECAD Research Center, Institute for Genetics University of Cologne (Cologne, Germany)</i>
<i>November 2014 – December 2015</i>	Student helper, Internship and Master Thesis Project Miltos Tsiantis Lab <i>Department of Comparative Development and Genetics Max Planck Institute for Plant Breeding Research (Cologne, Germany)</i>
<i>October 2013 – October 2015</i>	Master Course in Plant Sciences <i>Rhenish Friedrich Wilhelm University of Bonn (Bonn, Germany)</i>
<i>September 2008 – March 2012</i>	Undergraduate degree “Biomolecular Sciences and Technology” <i>University of Trento (Trento, Italy)</i>
University Entrance Qualification	
<i>September 2003 – June 2008</i>	Scientific High School, course of study in foreign languages <i>Liceo Scientifico Leonardo da Vinci (Trento, Italy)</i>